



**LIBRARY**  
**Michigan State**  
**University**

This is to certify that the

thesis entitled

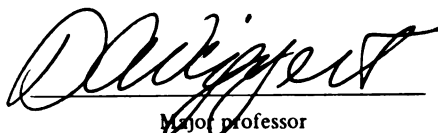
MULTIDIMENSIONAL TRANSPORT OF Pseudomonas stutzeri strain  
KC IN A MODEL AQUIFER SYSTEM: PREDICTING CT-REMEDIATION

presented by

Georgina Vidal-Gavilan

has been accepted towards fulfillment  
of the requirements for

Master of Science degree in Civil and Environmental  
Engineering



Major professor

Date July 6, 2000

**PLACE IN RETURN BOX** to remove this checkout from your record.  
**TO AVOID FINES** return on or before date due.  
**MAY BE RECALLED** with earlier due date if requested.

DATE DUE	DATE DUE	DATE DUE
OCT 16 2002		

***MULTIDIMENSIONAL TRANSPORT OF Pseudomonas stutzeri strain KC IN  
A MODEL AQUIFER SYSTEM: PREDICTING CT-REMEDIATION***

*By*

*Georgina Vidal-Gavilan*

*A THESIS*

*Submitted to  
Michigan State University  
in partial fulfillment of the requirements  
for the degree of*

*MASTER OF SCIENCE*

*Department of Civil and Environmental Engineering*

*2000*



## ABSTRACT

*Multidimensional transport of Pseudomonas stutzeri strain KC in a model aquifer system: Predicting CT-remediation*

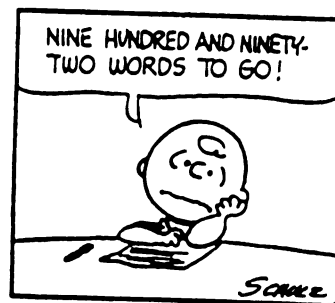
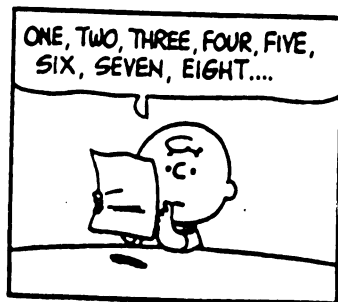
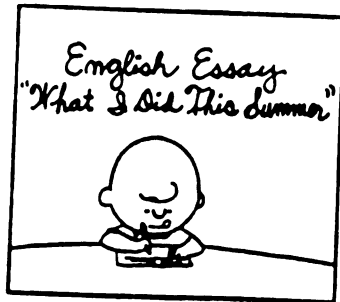
*by*

*Georgina Vidal-Gavilan*

A three-dimensional model aquifer was built to study the transport of *Pseudomonas stutzeri* strain KC during an inoculation event to remediate a CT-contaminated plume. Liquid-phase bacterial data was compared with tracer data to confirm the attachment of bacteria to the soil particles. Using the clean-bed filtration theory and the solids loading capacity, the amount of KC adhered to the soil was determined based on liquid phase biomass distribution. A three-dimensional gradient of tracer and biomass was observed to take place during the inoculation of strain KC, with concentrations decreasing at farther distances from the injection well. Hence, different biomass and nutrients availability is observed at several points of the 3D model.

Biomass and tracer distributions were subsequently used to predict CT remediation by strain KC that would occur in the model aquifer if its flow behavior can be simplified to be quasi-one-dimensional. A six-equation numerical model incorporating 6 variables (liquid phase CT, solid phase CT, liquid phase strain KC, solid phase strain KC, acetate and nitrate) was applied to obtain such predictions. Furthermore, an eight-equation model that considers the presence of native denitrifiers, was also developed to observe the CT-remediation and nutrient consumption under competition conditions. According to the predictions, different CT-removal efficiencies would be observed in different sections of the tank during the first two weeks of remediation activity. High CT degradation would be expected in locations near the injection point, where

more KC had been delivered. In addition, different nutrient consumption would occur in several locations of the aquifer, depending not only on the amount of KC present but also on the introduction of the native flora in the model and the values of the coefficients used. These would affect the availability of electron donor and electron acceptor for the denitrifying activity and could stimulate sulfate-reducing activity, and subsequent chloroform production, if the latter is depleted first. Model development, however, is needed to incorporate more realistic microbial kinetics and then confirm the findings.



## ACKNOWLEDGMENTS

I wouldn't be fair if I didn't mention that most of the data used in this thesis is a result of a team effort, by a group of people that worked to run the experiment in the 3D tank for this very first time. We all helped *babysitting* the tank, each and every day, which was sometimes frustrating. We got together to sample, which could take longer than otherwise thought due to the never-ending clogging problems. While we participated in the analytical procedures, the GC and the electrodes did most of the work. But most of all, we met several times to conduct the most interesting and imaginative discussions a researcher may experience during his or her life, barely sitting on a table but mostly surrounding the tank, as if this should provide us inspiration on how to carry out the next step. It was, after all, science and passion. And, moreover, entertaining.

And, of course, I wouldn't be fair if I didn't mention all these people, my research partners. So for them, Dr. Dybas, the bacteriologist, Dr. Zhao, the engineer, Emily King and Chris Ritchie, the working power, my heartfelt thanks.

I cannot forget, either, my advisor, Dr. Wiggert, who kept a close eye on my work and my imaginative mind, and whose comments and discussions resulted in a much more accurate document. If you are now able to read this paper, understand a major part of it and even find useful information, you can thank him.

And for the rest of you who assisted in some manner, because I'm sure I'm forgetting someone, please find yourself included in my extended acknowledgments. Perhaps you had a direct contribution to my work, and I'm thankful for that. Perhaps it was constructive criticism, at times bitter, but needed input. Maybe it was not as direct as it could have been, but this was also useful. But beyond all this, thanks for your smiles, and your company, which, after all, were more necessary. And for the others, because there are always *others*, ...

For people's dreams, life and happiness. Enjoy your time.

## TABLE OF CONTENTS

LIST OF TABLES.....	viii
LIST OF FIGURES.....	x
LIST OF SYMBOLS.....	xii
CHAPTER 1 – INTRODUCTION	
1.1 The Schoolcraft Project Hystory.....	1
1.2 Biostimulation vs. Bioaugmentation.....	2
1.3 Competition.....	3
1.4 CT-Remediation Activity by KC.....	4
1.5 Hypothesis and goals of study.....	6
CHAPTER 2 – A THREE DIMENSIONAL LAB-SCALE MODEL AQUIFER	
2.1 Materials.....	8
2.2 Construction of a Lab-Scale 3-dimensional Model Aquifer.....	9
2.3 Mixing Tank.....	15
2.4 Determination of Flow Patterns in the Model Aquifer.....	16
2.5 Soil Titration.....	20
2.6 Inoculation of P.KC.....	21
2.7 Methods of Data Acquisition.....	22
2.8 Analytical Methods.....	22
2.9 Methods of Data Interpolation.....	23
CHAPTER 3 – ANALYSIS OF DATA	
3.1 Breakthrough of Tracer.....	25
3.2 Breakthrough of CT.....	36
3.3 Soil Titration.....	42
3.4 Breakthrough and Distribution of P.KC.....	43
3.5 Liquid-solid Partitioning of P.KC.....	47
CHAPTER 4 – PREDICTION OF CT-REMOVAL EFFICIENCY	
4.1 Basis for Competition Between native flora and P.KC.....	52
4.2 Mass Balance Equations.....	52
4.3 Competition Equations.....	56
4.4 Numerical Simulation.....	59
4.5 One-dimensional Columns.....	61
4.6 Numerical Results.....	63
4.7 Feeding Events.....	72
4.8 Competition.....	77
4.9 Varying groundwater linear velocity and KC's yield for nitrate.....	81
4.10 Numerical Stability.....	85



## LIST OF TABLES

	Page
1. Integration of curve in Figure 19.....	48
2. Input parameters used in the mass balance equations.....	55
3. Initial and boundary conditions.....	61
A.1. First cross-flow tracer study. Liquid samples (bromide).....	95
A.2. First cross-flow tracer study. Flow rates.....	96
B.1. Vertical-flow tracer study. Liquid samples.....	97
C.1. CT sorption study. Liquid samples.....	99
C.2. CT sorption study. Flow rates.....	100
D.1. Liquid samples (cfu/ml) taken during the inoculation event.....	101
D.2. Liquid samples (cfu/ml) at the end of the inoculation event.....	102
D.3. Tracer samples taken during the inoculation event.....	103
D.4. Tracer samples taken at the end of the inoculation event.....	104
D.5. Tracer samples at the effluent during the inoculation.....	105
E.1. Starting conditions: Column 11.....	106
E.2. Starting conditions: Column 12.....	106
E.3. Starting conditions: Column 13.....	106
E.4. Starting conditions: Column 21.....	106
E.5. Starting conditions: Column 22.....	107
E.6. Starting conditions: Column 23.....	107
E.7. Starting conditions: Column 31.....	107
E.8. Starting conditions: Column 32.....	107
E.9. Starting conditions: Column 33.....	107
H.1. Bottom influent ports.....	120
H.2. Top effluent ports.....	120

H.3.	Cross-flow influent and effluent points.....	121
H.4.	Sampling ports.....	121



## LIST OF FIGURES

	Page
1. System schematics.....	10
2. Lab-scale model aquifer.....	11
3.a. Three-dimensional model aquifer dimensions and sampling ports.....	12
3.b. Vertical-flow influent and effluent points locations.....	13
3.c. Locations of sampling ports.....	14
4. Mixing tank.....	14
5. Schematics of flow directions in the 3D model aquifer.....	17
6. Bromide breakthrough at the cross-flow effluent.....	26
7. Profile of bromide breakthrough during the cross-flow tracer study.....	27
8. Inoculation bromide breakthrough at the cross-flow effluent.....	30
9. Bromide vertical profile.....	32
10. Bromide 3D vertical profile during vertical pumping.....	33
11. Bromide breakthrough at ports 911, 912, 913 and effluent.....	34
12. CT vertical profile.....	38
13. CT breakthrough.....	40
14. CT vertical 3D profile .....	41
15. Biomass breakthrough at ports 312, 322, 332, influent and effluent during inoculation.....	44
16. Bromide breakthrough at ports 312, 322, 332, influent and effluent during inoculation.....	44
17. Bromide and biomass breakthrough during inoculation.....	45
18. Biomass and bromide 3D distribution at the end of the inoculation.....	46
19. Biomass attached to the soil during inoculation.....	51
20. Solid-phase biomass distribution at the end of the inoculation.....	51

21.	One-dimensional columns in the model aquifer.....	62
22.	Predictions for column 12 using the 6-equation model.....	65
23.	Predictions for column 21 using the 6-equation model.....	66
24.	Predictions for column 33 using the 6-equation model.....	81
25.	CT-removal and biofilm establishment in column 12 using the 6-equation model.....	68
26.	CT-removal and biofilm establishment in column 21 using the 6-equation model.....	69
27.	CT-removal and biofilm establishment in column 33 using the 6-equation model.....	70
28.	Predictions for the first feeding event in column 12 using the 6-equation model.....	74
29.	Predictions for column 33 after the first feeding event using the 6-equation model.....	75
30.	Schematics of a three-hour feeding event.....	76
31.	Predictions for column 12 using the 8-equation competition model.....	78
32.	Predictions for column 21 using the 8-equation competition model.....	79
33.	Predictions for column 33 using the 8-equation competition model.....	80
34.	Predictions for column 33 using the 6-equation model and one-third of the linear groundwater velocity.....	82
35.	Predictions for column 33 using the 8-equation model and one-third of the linear groundwater velocity.....	83
36.	Predictions for column 33 using the 6 and 8-equation models and low $Y_{NI}$ .....	84
H.1.	Reference system used.....	120

## LIST OF SYMBOLS

symbol		units
$K_d$	distribution coefficient	kg/L
$K_{oc}$	water-octanol partitioning coefficient	
$f_{oc}$	fraction of organic carbon	dimensionless
$C$	concentration	ppb, ppm
$C_0$	influent concentration	ppb, ppm
$X$	biomass	cfu/ml
$h$	height tank	mm
$t$	time	min, hr
cfu	colony forming units	
CT	carbon tetrachloride	
$C_m$	model variable	
$i$	distance	cm
$C_{CT}$	concentration of carbon tetrachloride	$\mu\text{g/L}$
$C_A$	concentration of acetate	mg/L
$C_N$	concentration of nitrate	mg/L
$X_{KC}$	concentration of strain KC in the liquid phase	mg/L
$X'_{KC}$	concentration of strain KC in the solid phase	mg/L
AC	concentration of acetate	mg/L
NI	concentration of nitrate	mg/L
KCL	concentration of strain KC in the liquid phase	mg/L
KCS	concentration of strain KC in the solid phase	mg/L
NFL	concentration of native flora in the liquid phase	mg/L
NFS	concentration of native flora in the solid phase	mg/L

$b_{KC}$	KC decay rate	$\text{day}^{-1}$
$b_{NF}$	native flora decay rate	$\text{day}^{-1}$
$D$	dispersion coefficient	$\text{cm}^2/\text{day}$
$k'$	second-order rate coefficient	$\text{L}/\text{mg}\cdot\text{day}$
$\text{deg}$	second-order rate coefficient	$\text{L}/\text{mg}\cdot\text{day}$
$K_{CKC}$	strain KC attachment rate,	$\text{day}^{-1}$
$K_{YKC}$	strain KC detachment rate	$\text{day}^{-1}$
$K_{CNF}$	native flora attachment rate	$\text{day}^{-1}$
$K_{YNF}$	native flora detachment rate	$\text{day}^{-1}$
$K_{SKAC}$	strain KC acetate-half saturation coefficient,	$\text{mg}/\text{L}$
$K_{SKNI}$	strain KC nitrate-half saturation coefficient	$\text{mg}/\text{L}$
$K_{SNFAC}$	native flora acetate-half saturation coefficient	$\text{mg}/\text{L}$
$K_{SNFNI}$	native flora nitrate-half saturation coefficient	$\text{mg}/\text{L}$
$R$	retardation coefficient	dimensionless
$U$	linear velocity	$\text{cm}/\text{hr}, \text{cm}/\text{day}$
$\Theta$	porosity	dimensionless
$\rho$	soil bulk density	$\text{kg}/\text{L}$
$\mu_{MAX}$	strain KC maximum specific growth rate	$\text{day}^{-1}$
$\mu_{MAXNF}$	native flora maximum specific growth rate	$\text{day}^{-1}$
$\mu$	growth rate	$\text{day}^{-1}$
$Y_{KCAC}$	strain KC yield due to acetate, mg cells/mg acetate	$\text{mg cells}/\text{mg acetate}$
$Y_{KCNI}$	strain KC yield due to nitrate	$\text{mg cells}/\text{mg nitrate}$
$Y_{NFAC}$	native flora yield due to acetate	$\text{mg cells}/\text{mg acetate}$
$Y_{NFNI}$	native flora yield due to nitrate	$\text{mg cells}/\text{mg nitrate}$

CO	Courant number	dimensionless
$\alpha$	diffusion parameter	dimensionless
$\Delta t$	time step	day
$\Delta x$	distance step	cm
i	node or position	
k	time	day
L	length of the column	cm

## INTRODUCTION

### ***1.1 The Schoolcraft Project History***

A carbon tetrachloride-contaminated aquifer near Schoolcraft, Michigan, has been under investigation by the Michigan Department of Natural Resources (MDNR) since 1987. Contaminant plumes of this type have been associated with grain fumigation operations. The primary contaminant in this plume is carbon tetrachloride, but high levels of nitrate (60 mg/L) are also present, presumably as a result of farming operations. CT levels up to 400 µg/L are found in the groundwater near the center of the mass of the plume, with most samples showing concentrations ranging from 50 to 150 µg/L. A plan to remediate this plume was put forth by the MDNR in 1993. The proposed remedial action involved the extraction of the contaminated groundwater using a single recovery well. The extracted groundwater had to be treated on-site by air-stripping. The estimated duration of this remedial action was approximately 25 years (Halliburton NUS Environmental Corporation, 1991).

Also in 1987, a denitrifying bacterium that could degrade CT was isolated by Dr. Criddle while working on his Ph.D. at Stanford University. The bacterium was named *Pseudomonas* sp. strain KC, and was later identified as a member of the species *stutzeri*. Since its isolation, several physiology studies were conducted at MSU in order to characterize the biodegradation activity of *Pseudomonas stutzeri* st. KC. Furthermore, soil microcosms were built to study the feasibility of the application of KC to the field. Promising results with high CT-removals encouraged the application of KC for the remediation of the CT-contaminated plume (Dybas *et al.*, 1995; Mayotte *et al.*, 1996; Witt 1995 and 1998).

In 1993, MSU (Department of Environmental Engineering, Center for Microbial Ecology), The University of Michigan (Dr. M. Barcelona) and Golder Associates, became

involved in the remediation of Schoolcraft aquifer Plume A, the CT-contaminated plume. Bioremediation of Plume A by bioaugmentation with *Pseudomonas stutzeri* st. KC was chosen as a remediation alternative. The first pilot test at the Schoolcraft site was conducted in 1994. The test resulted in an average CT-removal of 68%, but some difficulty in the delivery of chemicals was experienced (Dybas *et al.*, 1998). Four years later, the team expanded to include MSU Departments of Geological Science and Chemical Engineering, Traverse Group, and EFX Systems. The full-scale operation started at Schoolcraft in 1988 and it has been fully operational since then, achieving CT-removals of 99% in most of the wells and an average removal of 95% (Dybas *et al.*, 2000. Hyndman *et al.*, 2000).

The pilot-scale project (Schoolcraft project, Plume A remediation) is approaching the end. During these 12 years of research, valuable information has been obtained about remediation activity, lab and field scale operations, delivery of chemicals, control of biological activity, etc. Several experiments have been conducted at both lab and field-scales. Modeling efforts to mathematically represent the biological process have been conducted as well. The system is ready for full-scale operation (to capture the whole width of the plume).

In order to increase the control over the system, though, there is need for optimizing the delivery of microbes to the subsurface. The objective of the on-going research efforts, and of this thesis, is to characterize the transport of strain KC during an inoculation event and to increase the understanding of the biological processes occurring in the aquifer between KC and indigenous flora.

## ***1.2 Biostimulation vs. Bioaugmentation***

When designing a bioremediation strategy, there are essentially two main options to choose from: *biostimulation* and *bioaugmentation*. Biostimulation involves enhancing the growth of indigenous microflora to stimulate the degradation of a given compound. Biostimulated organisms may or may not be able to degrade the targeted compound. In some cases, the

degradation pathway may include undesirable end products. Particularly in the case of Schoolcraft, the stimulation of the indigenous denitrifying populations does not degrade CT, whereas the stimulation of sulfate-reducing microorganisms promotes chloroform formation as a product of CT degradation.

On the other hand, bioaugmentation involves the introduction of a non-indigenous organism with the capacity to degrade a specific compound. Bioaugmentation offers the promise of increased control over transformation pathways and kinetics. However, bioaugmentation promotes competition between indigenous microflora and the organisms being introduced. This competition presents a challenge when attempting to initiate the degradation of a particular compound when adding a non-indigenous organism to the environment. To be effective, novel organisms introduced into the environment must be able to survive and compete with indigenous organisms. Nevertheless, to minimize the possibility of ecological disturbance, colonization should ideally be constrained. A possible solution is to create a temporary niche for the introduced organism (KC in this case). Alkalinity addition creates such a niche, by reducing the bioavailability of essential trace metals, such as iron, thereby favoring organisms with efficient trace metal scavenging systems (Tatara et al., 1993. Dybas et al., 1995). See section *1.4 CT-remediation activity by KC*.

### ***1.3 Competition***

Once favorable conditions for KC growth are created (pH adjustment) and KC is inoculated into the matrix, a succession between indigenous and non-indigenous microorganisms will take place based on competition. This may be for the nutrients that are added or for available trace metals and nutrients. According to the resource-based competition theory, when microbial strains compete for the same limiting nutrient in a continuous culture, only one strain will survive and all others will die out (Hansen and Hubbel, 1980). Experimental results have shown that two species were observed to coexist only if either (1) each was limited by a different resource and



met the theoretical criteria for coexistence, or (2) the species were limited by the same resource and did not differ significantly in their resource requirements (Tilman, 1981).

The basic Monod's kinetic parameters for competition between P.KC and native flora after the addition of acetate were experimentally determined using batch experiments (Knoll, 1994. Dybas *et al.*, 1995.). Both strain KC and the Schoolcraft groundwater flora exhibited similar biphasic growth patterns at an initial pH of 8.2. In each case, nitrate was first converted to nitrite, and nitrite was subsequently converted, presumably to NO, N<sub>2</sub>O, and N<sub>2</sub>. A critical difference between strain KC and Schoolcraft flora was in the observed yield. For the first phase of growth (nitrate to nitrite), the observed yield for strain KC was four times the observed yield for the Schoolcraft flora. This translated into a fourfold higher maximum specific growth rate for strain KC. A likely explanation for this yield difference is the competitiveness of strain KC under iron-limiting conditions. Dybas *et al.* (1995) have shown that strain KC produces a wide spectrum of iron-binding activities at pH 8.2.

For a single growth limiting substrate, competition theory predicts that the superior competitor will be the organism with the lowest resource requirement, as measured by the parameter R\* (Tilman, 1981). This parameter is identical to the parameter J of Hansen *et al.* (1980) and S<sub>min</sub> of Rittman and McCarty (1980). It is the minimum resource (substrate) level where growth balances decay, and is given by  $S_{min} = K_s (b/(\mu - b))$ , where b is the decay coefficient (d<sup>-1</sup>). When K<sub>s</sub> and b are similar for two competing populations, the critical factor affecting the competition is  $\mu$ . For KC, a low value would be expected for S<sub>min</sub> because of its high specific growth rate at moderate alkaline pH levels (Dybas *et al.*, 1995).

#### **1.4 CT-remediation activity by KC**

*Pseudomonas stutzeri* strain KC is a natural isolate derived from an aquifer in Seal Beach, California (Criddle *et al.*, 1990). Strain KC grows optimally at temperatures that are typical of aquifers (10-20°C), and is able to persist and compete in aquifer materials and soils (Lewis and

Crawford, 1993; and Tatara *et al.*, 1993). Under denitrifying conditions, strain KC rapidly transforms CT to carbon dioxide, formate and unidentified non-volatile end products without the production of chloroform (Dybas *et al.*, 1995), a common product of CT degradation that is also harmful and persistent in the environment. In order to allow the rapid transformation of CT by strain KC, an anoxic environment, an electron donor such as acetate, an electron acceptor such as nitrate, and iron-limiting conditions are needed (Criddle *et al.*, 1990; Lewis and Crawford, 1993; and Tatara *et al.*, 1993).

Numerous experiments have been completed to better understand the mechanism of CT transformation via bioaugmentation with strain KC. The results of these experiments indicate that CT transformation is influenced by the availability of iron. In iron-rich groundwater and soils inoculated with strain KC, CT transformation can be achieved by raising the pH of the groundwater and soil materials to 7.7-8.2, a range where ferric iron solubility is lowest (Stumm and Morgan, 1981). That seems to stimulate the production of a biomolecule by KC and its release to the environment. This biomolecule, which has been recently identified as 2,6-bispyridine thiocarboxylate (Lee *et al.*, 1999), may be linked to iron chelation. It can be produced under both oxic and anoxic conditions; however, the presence of oxygen totally avoids any reaction with C present in the environment. Under anoxic conditions, such as denitrifying conditions, the biomolecule reacts—fortuitously—with CT and is then deactivated, to be reactivated later at the cell membrane. The degradation of CT by KC is, hence, co-metabolic, and KC does not derive any energy from it.

The value of pH adjustment in creating a niche favorable for growth of strain KC is also associated with optimal growing conditions. At pH 8.2, strain KC shows its maximum growth and presents higher affinity for the substrate than the indigenous Schoolcraft flora. That gives strain KC a competitive advantage over the native flora.

### ***1.5 Hypothesis and goals of study***

It is believed that the biomass injected during an inoculation event is transported and deposited in the soil by adhesion to the solid particles. The biomass breakthrough observed during the inoculation of a solid matrix should, hence, be retarded relative to the transport of an ideal tracer. Several authors (Harvey, 1991. Martin *et al.*, 1992. Rijnaarts, *et al.*, 1996) have applied the clean-bed filtration theory to describe the deposition of bacteria in porous media, and modeled its behavior in terms of collector efficiency. Radabaugh, 1998, determined the basic filtration parameters for strain KC in Schoolcraft-material one-dimensional columns and determined its solids cell concentration at saturation (soil loading capacity). All these principles and data could be applied to estimate the amount of strain KC adhering to the soil particles during an inoculation event. It is expected that the 3-dimensional data for an ideal tracer together with biomass data from the liquid phase, obtained during the inoculation of a 3-dimensional lab-model aquifer, can provide a valid estimation of the amount of biomass (strain KC) in the soil. Both kinds of biomass, solid and liquid phase, will use the resources added and start building the biofence or bioactive zone that will degrade the CT.

Furthermore, it is hypothesized that not only the newly introduced organism but also the indigenous flora already existing at the site are responsible for the location and characteristics of the biofilm. That is, the starting biomass present at the reactive zone, or, in other words, the ratio between *Pseudomonas* sp. strain KC that is effectively introduced to the matrix and the native flora may affect the competition of the two kinds of organisms. Although the concentrations of KC that are used for inoculation have shown the capacity to carry out CT degradation in the presence of indigenous flora, the starting ratio between these two groups of microorganisms may have an effect on short and/or long term biofilm structure, and hence on reaction rates and nutrient consumption.

For these purposes, a 3-dimensional flow cell was built to simulate aquifer conditions in the lab. In addition to an inoculation event, tracer and sorption experiments were carried out to

characterize and study the multidimensional transport of chemicals and bacteria. The study of *Pseudomonas* sp. strain KC transport through the matrix will provide information about the concentration and gradient of microbes between pump and extraction wells. Modeling efforts, in conjunction with previously obtained data, will allow us to predict the effectiveness of *Pseudomonas* sp. strain KC degradation activity. The competition between KC and native flora will also be modeled and predicted, although no data are now available to confirm these last predictions.

In order to study and/or validate these hypotheses, the following goals will be addressed in this work:

- Characterize the transport of chemicals through a 3-dimensional-flow lab model aquifer.
- Follow and determine the biomass distribution that occurs during an inoculation event.
- Study the liquid-solid partitioning of strain KC after an inoculation event.
- Develop an understanding of biofilm development subsequent to the inoculation phase.
- Predict CT removal efficiencies in a 3-dimensional flow cell based on the transport and biomass distribution data obtained experimentally from the 3D cell.

## A 3-DIMENSIONAL LAB-SCALE MODEL AQUIFER: THE EXPERIMENT

### 2.1 Materials

Groundwater. Groundwater from a CT-contaminated aquifer in Schoolcraft, Michigan, was used in all experiments. Groundwater was obtained from a two-inch PVC well screened from 30 to 80 feet below the ground surface using a 10 gpm centrifugal pump. Groundwater was stored in 25-liter carboys at 4°C. All groundwater was nitrogen-stripped prior to its pumping into the aquifer system to remove any CT present (see Figure 1), and also deaired by bubbling nitrogen gas. Groundwater was kept at pH 7.4 by bubbling in carbon dioxide gas.

Organisms. *Pseudomonas* sp. strain KC (DSM deposit number 7136, ATCC deposit number 55595) was derived originally from aquifer solids from Seal Beach, California. It is kept cryogenically at -80°C in the laboratory.

Chemicals. Carbon tetrachloride (99% purity) was obtained from Aldrich Chemical Company, Milwaukee, Wisconsin. All other chemicals used were obtained from J.T. Baker, Phillipsburg, New Jersey. Trace metals solutions for KC growth were prepared in the lab to obtain the following concentrations: FeSO<sub>4</sub> 0.6 ppm, CuSO<sub>4</sub> 0.12 ppm, ZnSO<sub>4</sub> 0.29 ppm, NiCl 0.07 ppm, H<sub>3</sub>BO<sub>3</sub> 0.03 ppm, MnCl<sub>2</sub>·4H<sub>2</sub>O 0.4 ppm.

Media. The culture broth used for KC cultures was Nutrient Broth from DIFCO, Grayson, Georgia. The nutrient agar used for plates was R2A agar from DIFCO.

## ***2.2. Construction of a lab-scale 3-dimensional model aquifer***

A lab-scale complex system was built to model a sand-aquifer with the aim of obtaining data in three space dimensions. The model included not only the tank containing the aquifer material, but several side sets and pumping to provide flow to the system and regular addition of chemicals as needed. Figure 1 shows a schematic layout of the system. In order to help visualize its configuration, a picture of the system has been included in Figure 2.

The final design of the 3-dimensional model aquifer was the result of the modeling efforts conducted at the Department of Geological Sciences, Michigan State University. A stainless steel column was constructed to be 91.4-cm high and 61-cm diameter. There are 57 sampling ports located across the column, sampling at 9 different layers and 3 different depths, there being 9 sampling ports per odd-numbered layer and 3 sampling ports per even-numbered layer. Stainless steel 1/16" inch lines were placed at the holes to achieve these depths. An internal grid of stainless steel wires was also placed in the tank to keep the sampling lines in place during the packing process. There are 7 influent ports located at the bottom and 7 at the top as well (see Figure 3). Finally, there is a second injection point located at one side and its exit point at the other side; both are 30.5 cm high. They act as an injection/extraction well.

The model was built to mimic field conditions at a lab-scale with the main objective of obtaining 3-dimensional data of the biodegradation process. Two leak tests were performed prior to filling the tank with the solids. The tank was then wet-packed with aquifer materials obtained from the Schoolcraft aquifer and finally covered. Afterwards, all side systems were connected to the tank (groundwater pumping system, delivery system, overflow system, and cooling system. Figure 1). Metal piping was wrapped around the tank to allow the circulation of 8°C chilled water for cooling purposes. A plastic cover was also placed overlaying both the tank and the pipe to reduce heat transfer from the environment. The system was kept at 10-12°C to mimic field conditions.

**Figure 1.** System schematics.

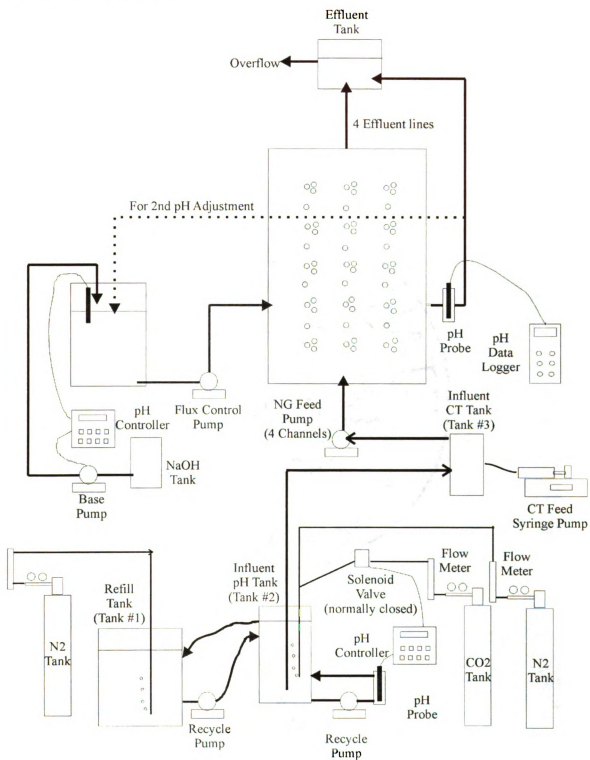


**Figure 2.** Lab-scale model aquifer.

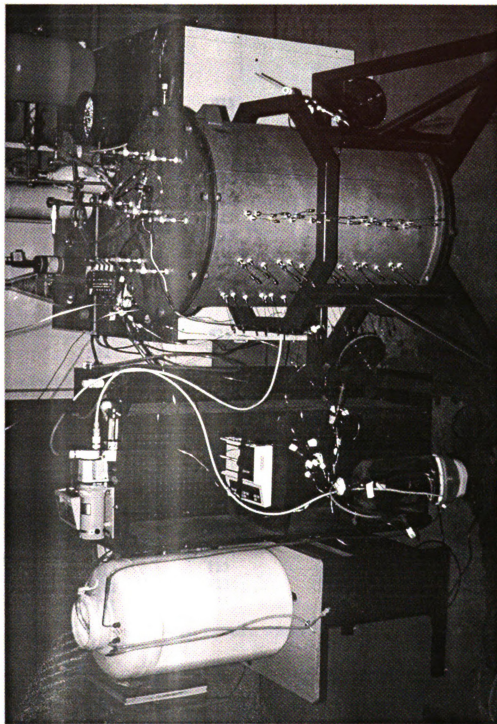




**Figure 3.a.** 3D model aquifer dimensions and sampling ports.

## Label for Sampling Ports of 3-D Flow Cell

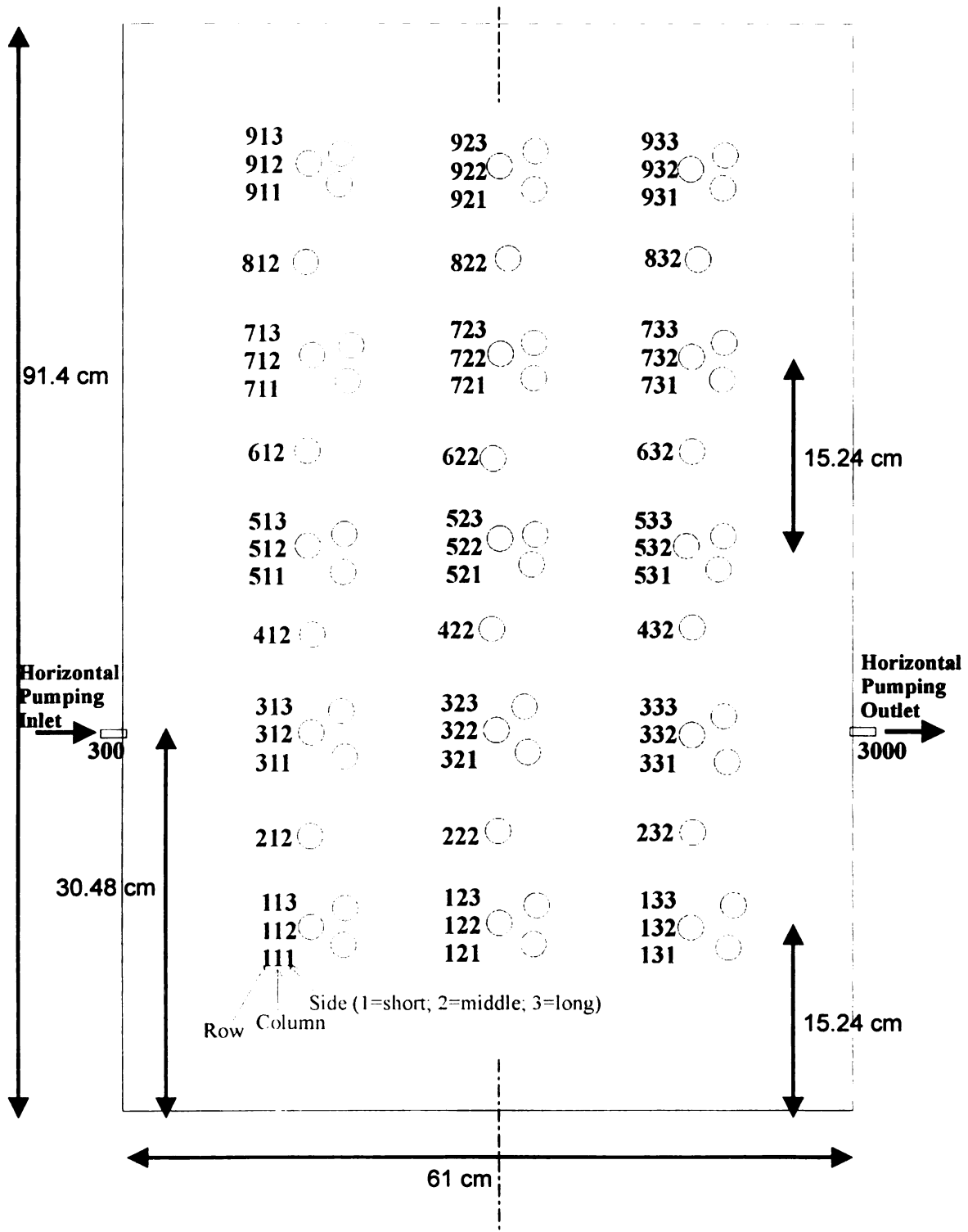
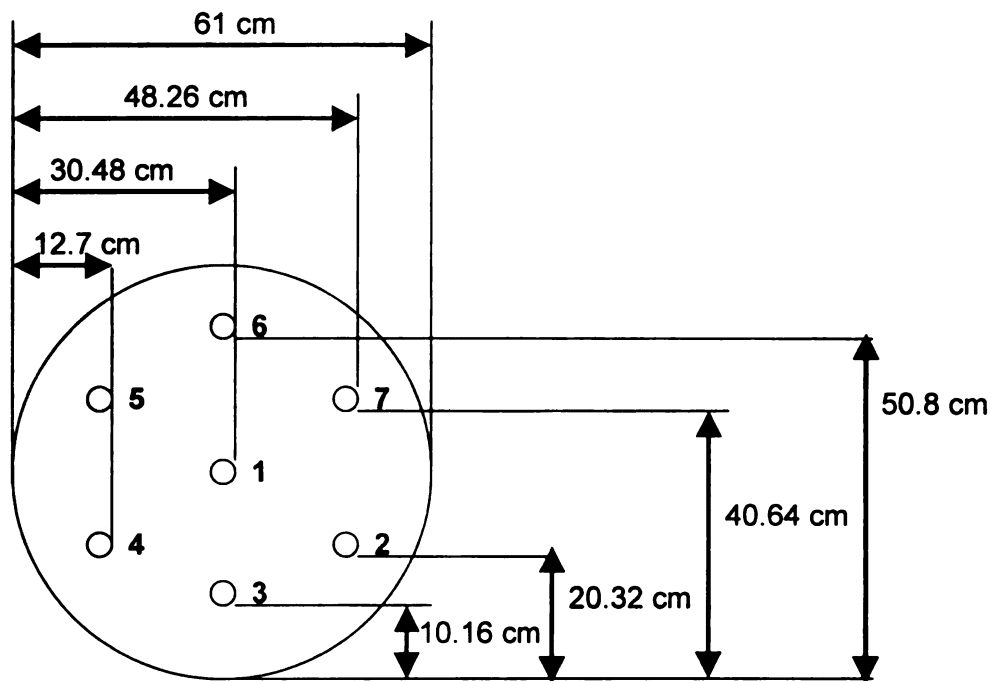
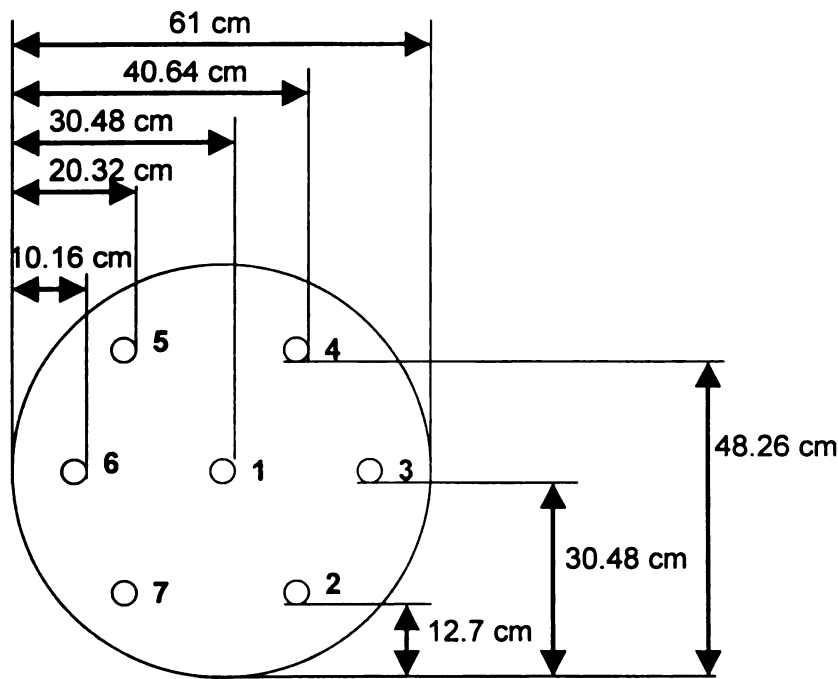


**Figure 3.b.** Locations of vertical-flow influent and effluent ports.



**BOTTOM INFLUENT POINTS**



**TOP EFFLUENT POINTS**

**Figure 3.c.** Locations of sampling ports.

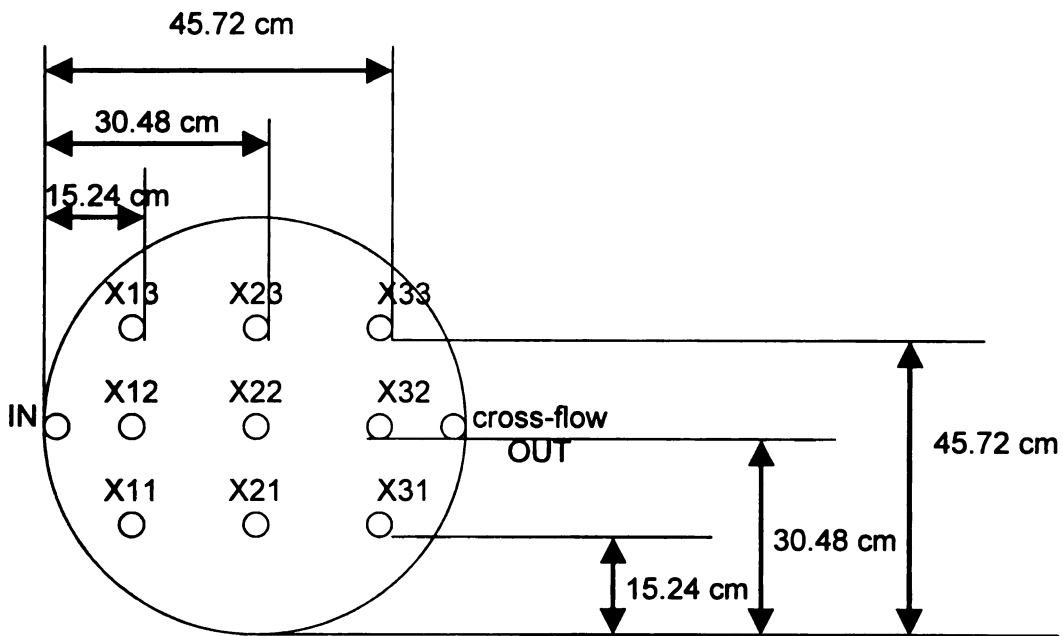
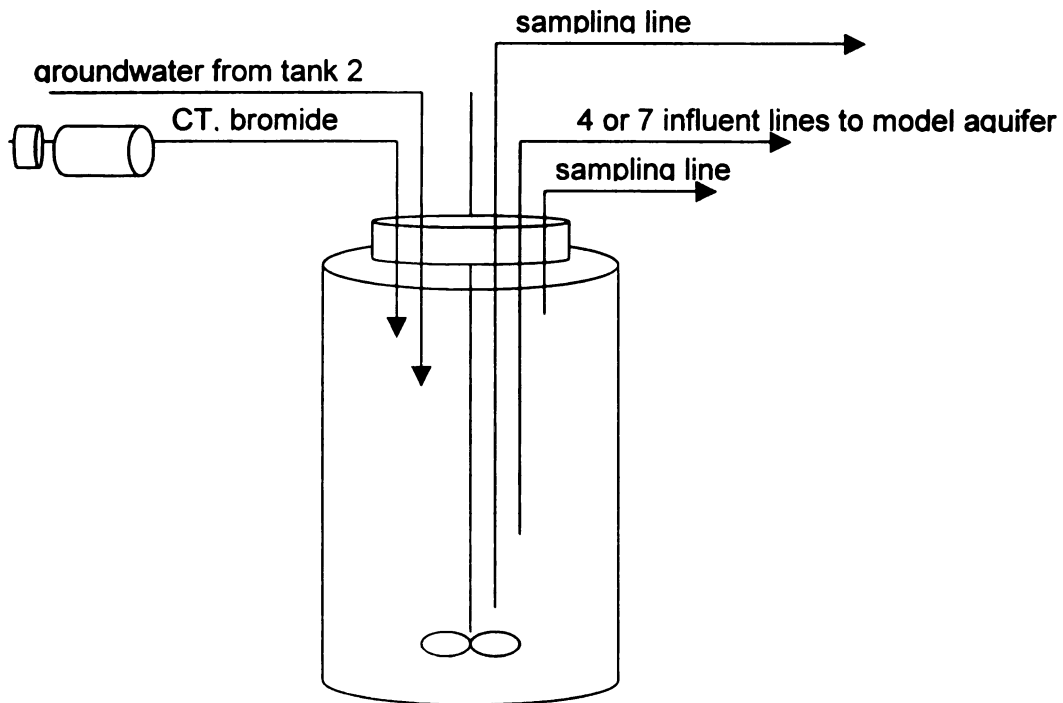


**Figure 4.** Mixing tank.



Groundwater pumping system. Groundwater is obtained from the Schoolcraft site, and is first nitrogen sparged to eliminate any CT present (refill tank, Figure 1). It is then pumped into the influent pH tank where N<sub>2</sub> is sparged again to deoxygenate it and thus achieve anoxic conditions, and the pH is adjusted to keep groundwater at the natural pH (7.2) by means of CO<sub>2</sub> (gas) and base. Overflow from tank 2 flows back to tank number 1 by gravity.

CT-free and pH-adjusted water is driven to the mixing tank, where a constant concentration of CT (50 ppb) is provided, and finally flows into the tank at a flow rate of 19 L/day to provide a natural gradient velocity of 14.8 cm/day, or at 56 L/day to achieve three times natural gradient velocity. Groundwater flows up vertically to assure full saturation of the aquifer. Although seven influent and seven effluent ports were originally placed at the bottom and at the top of the column, just four at each location were used for this experiment (numbers 1, 2, 4 and 6. See Figure 3.b). The four effluent lines converge into a constant head reservoir located 15 cm above the top of the tank that discharges out of the system.

A cross-flow is intermittently set at 16.6 L/h to simulate injection and withdrawal wells. Soil pH titration, inoculation and regular feeding events, in the same manner as they are done in the field, are conducted through this cross-flow well. Inoculation is carried out once at the beginning of the experiment and activity is sustained by weekly additions of acetate and phosphate through the delivery system injection point. However, no feeding event is reported in this document. During the inoculation event, samples were taken from the closer sampling ports, and analyzed for both bacteria and tracer, with the immediate goal of studying bacterial transport.

### **2.3 Mixing tank**

In order to provide a constant concentration of CT and tracer to the model aquifer column, minimizing losses and adsorption of CT, a mixing tank system was built to pump Schoolcraft groundwater and CT-spiked Schoolcraft groundwater separately into the mixing reservoir, providing then a single influent flow to the 3-dimensional tank.

Schoolcraft deoxygenated and pH-adjusted groundwater (to pH 7.4) flows by gravity into the glass mixing tank, and is pumped out and into the model aquifer by a peristaltic pump providing a constant flow rate. Syringe pumps constantly pump bromide and/or CT solutions into the mixing tank to provide a steady-state concentration of chemicals according to the groundwater flow rate (Figure 4).

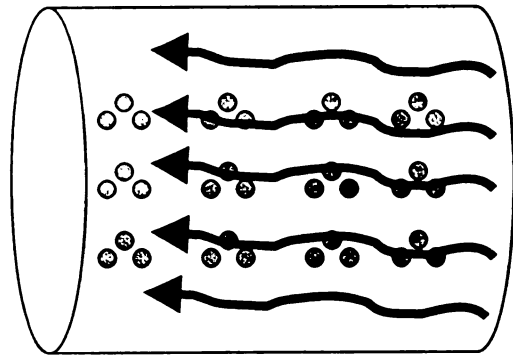
Two sampling lines enter the mixing tank at different heights. An electromagnetic stirrer located at the bottom continuously stirs the tank content. Before regular operation, the tank was filled with groundwater flowing by gravity and by venting to the atmosphere. Once the tank was filled, all ports were closed or connected to the water-flow lines and no opening was left to the atmosphere. The water volume is kept constant by flow of new groundwater into the tank, induced by the constant pumping of the peristaltic pump from the mixing tank to the column. During operation, however, problems were experienced on the influent line (gravity flowing groundwater line, from tank 2 to the mixing tank) and some variability was observed on the water volume of the mixing tank, creating variation in the model aquifer influent concentrations.

## ***2.4 Determination of flow patterns in the model aquifer***

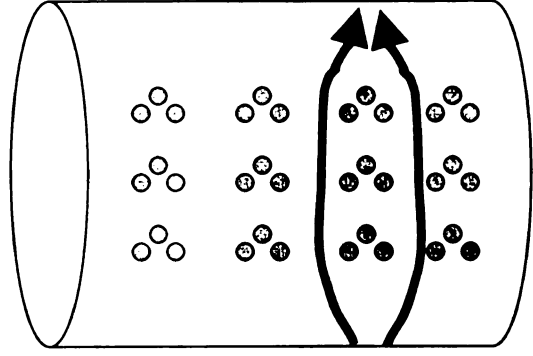
Horizontal flow conservative tracer study. Bromide (NaBr) was used as a conservative tracer to study the horizontal flow patterns that take place in the model aquifer when pumping through the side injection and extraction points. The major objective of this phase of the study was to observe the consistency of the flow patterns and to experimentally determine the time needed for breakthrough and saturation of tracer/substrates in the delivery zone.

Tracer solutions were prepared to provide an influent concentration of about 100 ppm NaBr. Four 25-liter carboys were needed to provide enough water for a 3-hour pumping event; tracer solutions from all carboys were mixed several times to achieve approximately the same concentration in all of them. The final concentration pumped into the column was of 114.5 ppm and was assumed constant during the duration of the study.

**Figure 5.** Flow directions in the 3D model aquifer.



**vertical flow: natural gradient**



**cross flow: pumping events**

Schoolcraft traced groundwater flowed horizontally through the model aquifer simulating a pumping event from an injection to an extraction well (e.g. Figure 5). A flow rate of approximately 280 ml/min was used for 3 hours, although some variation was observed ( $\pm 20$  ml/min). The vertical flow remained stopped during the cross flow (horizontal) pumping and was immediately restarted at the end of the experiment. Exit points at the top of the tank were also closed during the cross flow study.

Samples were periodically taken from the zone of influence of the cross flow pumping and analyzed using a bromide probe working off-line. The bromide data-logger was connected to the cross flow effluent during the pumping event to obtain breakthrough data.

Some problems were experienced when using the bromide probe. Consistent conductance readings were difficult to achieve using this probe, possibly indicating a faulty bromide probe. Hysteretic behavior could also cause some of the “abnormal” readings obtained. It should be noted that bromide electrodes are not designed for flow through use.

Vertical flow conservative tracer study. Bromide (NaBr) was used again as a conservative tracer to study the vertical flow patterns that take place in the model aquifer. The major objective of this exercise was to observe the consistency of the flow patterns and to experimentally determine the presence of major dead zones and/or differences in the aquifer, rather than to determine the physical parameters that control the movement of solutes through porous media (advection and hydrodynamic dispersion).

Tracer solutions were prepared to provide a constant influent concentration of about 80 ppm NaBr; three syringes injected the bromide solutions into the mixing tank at an overall flow rate of 1.5 ml/h (0.5 ml/h each). Although the mixing tank configuration had been successfully tested previously to starting the experiment, some variation in the concentrations was experienced during the vertical tracer study due a varying influent flow rate (water flowing from the mixing tank and into the aquifer).

Schoolcraft traced groundwater flowed up vertically through the model aquifer simulating natural gradient flow occurring at Schoolcraft aquifer (14.8 cm/day, determined by Halliburton NUS Environmental Corporation, 1991) and assuring fully-saturated conditions within the column (Fig. 5). A linear flow velocity of three times the natural ( $3 \times 14.8$  cm/day) was finally used for the tracer study. That was achieved by pumping through the aquifer at a flow rate of approximately 33 ml/min (assuming a column porosity of 37%).

Samples from all sampling ports were taken every 12 hours to obtain a vertical profile of concentrations throughout the column. When bromide breakthrough approached the top of the tank, sampling was intensified to obtain a complete breakthrough data set. All samples were analyzed using a bromide probe, operating off-line. Finally, a bromide probe was connected in-line to the aquifer effluent to obtain periodic data of the overall breakthrough at the averaged effluent. As occurred during the vertical flow tracer study, baseline drift of the bromide probe created some problems for data interpretation.

CT saturation experiment. Upon completion of the model aquifer column and cross flow tracer studies, CT-spiked groundwater was pumped into the column using vertical flow. Groundwater was also spiked with bromide since both experiments (vertical conservative tracer study and CT saturation) were conducted simultaneously. A syringe pump with concentrated CT solution pumped into the mixing tank at 0.5 ml/h. The CT concentration of the effluent from the mixing tank was analyzed periodically for the 10 days that the sorption experiment lasted, and intended to be constant at around 50 ppb. However, a noticeable variation was obtained in this concentration due to some problems experienced in the mixing tank.

As in the vertical tracer study, groundwater flowed through the model aquifer at an average flow rate of 33 ml/min. Samples were periodically taken to obtain vertical profile concentrations and breakthroughs and analyzed by gas chromatography.



For this model aquifer, it was assumed that CT was distributed amongst the solid and solution phases. Organic contaminants transported by groundwater are distributed between four phases: gas phase, solid phase, solution phase and pure chemical phase. Henry's Law governs the extent to which an organic compound will exist in the vapor phase. Extremely small air pockets may have existed in certain areas of the column; however, the effects of such occurrences would be minor. On the other hand, the low CT concentrations used would have avoided the formation of pure CT phases (non-aqueous liquid phases or NAPL's), common when solubility limits are approached or reached. Therefore, migration of CT through the Schoolcraft aquifer material column was assumed to exist only in the solid and solution phases. Studies (Schwarzenbach *et al.*, 1981) have shown that the degree of adsorption is proportional to a distribution coefficient,  $K_d$ . The distribution coefficient is defined as the following:

$$K_d = K_{oc} f_{oc} \quad (1)$$

where  $K_{oc}$  is the water-octanol partitioning coefficient and  $f_{oc}$  the fraction of organic carbon present in the solid matrix.

## **2.5 Soil titration.**

Schoolcraft groundwater is pumped vertically into the aquifer at its naturally-occurring pH of 7.2. In order to optimize the growth of KC, though, a pH of 8.2 is required. Hence, a pH 8.2 zone needs to be created prior to inoculation. As oncoming water crossing the inoculation/reactive zone has an original pH of 7.2, it will tend to decrease the pH of the reactive zone from 8.2 towards 7.2. In order to avoid this decrease, all pumping events must be carried out at pH 8.2, thus providing titration capacity to the soil.

The first soil titration in the aquifer column was conducted before the inoculation of *Pseudomonas* sp. strain KC. Groundwater at pH 8.2 was pumped cross-flow from the mixing tank for 16 hours at a flow rate of 300 ml/min, reproducing the soil-titration event in the field. A pH-data logger was connected into the cross flow effluent exit and values were recorded every 5 minutes. Vertical flow was stopped and vertical flow effluent points remained closed during the pumping. Water used for pH adjustment was groundwater from Schoolcraft, with a constant concentration of CT provided by the syringe pumps.

One week after inoculation, the pH had decreased in the reactive zone to values of 7 to 7.4. The soil matrix was titrated again for the second time to determine the total amount of base needed to fully titrate the soil to pH 8.2. Base-added groundwater was pumped using the same influent point (cross flow), for an overall period of 72 hours.

## **2.6 Inoculation of *P.KC*.**

Strain KC cells were obtained from cryogenically (-80°C) preserved cultures located within the laboratory and streaked in fresh nutrient agar plates, containing R2A media, and incubated at room temperature. KC cultures were obtained 6 days later by picking visible colonies and inoculating 5 ml of sterilized aerobic nutrient broth, which are dispensed into 25-ml flasks. Twenty-four hours later, the 5-ml aerobic cultures were transferred to larger Erlenmeyer flasks containing 250 ml of aerobic nutrient broth. Three 250-ml one-day old cultures were used to inoculate an aerobic 57-liter fermenter containing filter-sterilized Schoolcraft groundwater, amended with base (pH=8.2), acetate (800ppm), phosphate (10 ppm), and trace metals. In all liquid cultures, pH was manually kept at around pH 8.2 to avoid its increase up to toxic levels. Finally, bromide was also added to the fermenter for tracer purposes.

The 57-liter fermenter was connected to the cross-flow influent point by using a diaphragm pump. Inoculation of KC into the model aquifer lasted 3 hours at an approximate 290 ml/min-pumping rate. Liquid samples were periodically taken from the sampling ports located

within the main direction of the cross flow (312, 322 and 332) and also from influent and effluent lines, and analyzed for biomass and tracer. At the end of the inoculation, vertical flow was restored to the natural gradient linear flow velocity (14.8 cm/day) and cross flow was closed. Liquid samples were then obtained from rows 100, 300 and 500 and analyzed again for biomass and tracer.

## ***2.7 Methods of data acquisition (sampling)***

All liquid samples obtained from the model aquifer tank were withdrawn using a glass tuberculin syringe with a 1/16" stainless steel sampling line connecting to every sampling port. For bromide analysis purposes, samples were transferred to 20-ml glass vials and immediately analyzed, or transferred to Eppendorf tubes and stored at -4°C. For CT analysis purposes, samples of known amounts were transferred into the GC glass vial and immediately capped. After inoculation, 40µl of NaHSO<sub>4</sub> (40%) were added to CT samples to quench any bioreaction. Syringes were rinsed internally with methanol and deionized water between each sampling event.

Samples for determination of biomass concentration were dispensed into 20-ml sterile plastic tubes. A series of consecutive dilutions ( $10^{-1}$ ,  $10^{-2}$ ,  $10^{-3}$ ,  $10^{-4}$ ,  $10^{-5}$ , and  $10^{-6}$ ) were then made in test tubes containing sterile solutions of phosphate buffer. One-hundred microliters of all samples and dilutions were immediately transferred to R2A agar plates for quantification purposes. Plates were kept at room temperature for at least a week and then counted for colony forming units.

## ***2.8 Analytical Methods***

Bromide was analyzed by a Cole-Parmer bromide electrode connected to a Jenco model 6091 microcomputer pH-vision data logger (mV mode). External calibration curves were prepared with Schoolcraft groundwater.

Carbon tetrachloride was analyzed by removing samples of headspace gas above the liquid samples and detected by gas chromatography as described by Tatara *et al.* (1993). External calibration curves were prepared by the addition of a primary standard (3 ng of CT per  $\mu\text{l}$  of methanol) to secondary water solutions having the same gas/water ratio, ionic strength, and temperature as the assay samples to generate a 7-point calibration curve which bracketed the concentrations in assay samples. CT was assayed by an autosampler (AutoSystem A HS40, Perkin Elmer) with the following parameters: sample temperature 90°C; needle temperature 100°C; transfer temperature 100°C; pressure 40 psi; carrier gas 5 ml/min; GC cycle time 23.0 min; thermostat time 30.0 min; pressures. time 2.0 min; inject time 0.2 min; withdrawal time 0.2 min; vial venting ON; and sample shaker OFF. The gas chromatograph used was a Perkin-Elmer AutoSystem equipped with a capillary column (105m x 0.53mm 502.2MTx (Restek) capillary column) and an electron capture detector (ECD) with a nitrogen carrier. The method used started with an oven temperature of 45°C for 12 minutes and then increased to 200°C in 45°C/min ramp, to hold the temperature in 200°C for 2 more minutes.

Measurements of pH were made with a Jenco model 6091 pH meter and a Hanna Instruments pH probe.

Biomass concentrations were determined by plate counts on R2A agar dishes.

## **2.9 Methods of data interpolation**

A 3-dimensional numerical grid reproducing the lab-scale model aquifer was assembled by the Department of Geological Sciences, MSU. The model, a cylinder with same dimensions as the lab model, was used in this thesis to interpolate 3-dimenional data using the software package

GMS (Groundwater Modeling System, a groundwater modeling environment for MODFLOW, MODPATH, MT3D, FEMWATER, SEEP2D and RT3D, developed by the Brigham Young University, Utah).

*Color figures.* Some images in this thesis are presented in color.

## ANALYSIS OF DATA

### ***3.1 Breakthrough of tracer***

Horizontal flow conservative tracer study. Figure 6 shows the bromide breakthrough at the cross-flow effluent obtained during the first horizontal-flow conservative-tracer study. Graph-data was obtained by a bromide probe connected in line and recorded by a data logger.

The bromide front (50% breakthrough) occurred 160 minutes after the beginning of the experiment. The average pumping rate for the duration of the experiment was 280 ml/min (See Appendix A). Therefore, 44.8 liters of Schoolcraft groundwater were pumped from the beginning of the study and until the front reached the effluent point (at 160 minutes). This volume, nevertheless, was not measured but obtained by multiplying the flow-rate by the time of the pumping. At the end of the pumping event (180 minutes), approximately 50.4 liters of groundwater were cross-pumped (50% tank pore space), according to the average flow. However, the effluent never reached 100% breakthrough, but a maximum value of 80%. According to these values, conservative chemicals could be effectively transported across the column using a pumping rate of 280 ml/min for 3 hours. Nevertheless, lower concentrations could occur at the far end of the cross pumping (near the effluent point).

In addition to the effluent, samples were also obtained and analyzed from the sampling ports located throughout the lab column, enabling a 3-dimensional picture of the water movement to be obtained. Data was later incorporated into the 3-dimensional grid that represents the model aquifer and interpolated using universal kriging in GMS. Figure 7 shows the statistical interpolation of bromide data at 90, 120, 150 and 180 minutes after the beginning of the cross-flow pumping, in addition to the sampling ports raw data. These results are entirely based on

**Figure 6.** Bromide breakthrough at the cross-flow effluent.  
Bromide probe data logger connected in line to the effluent. Final level: 70%.

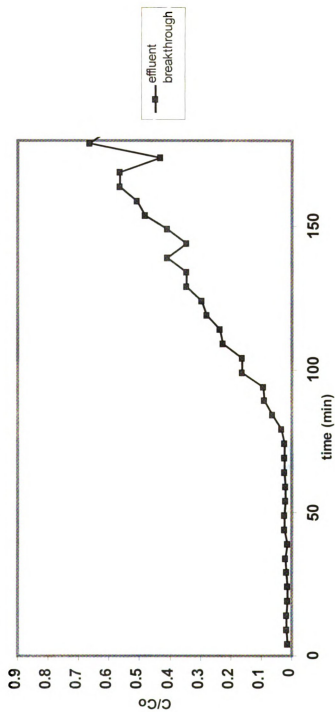
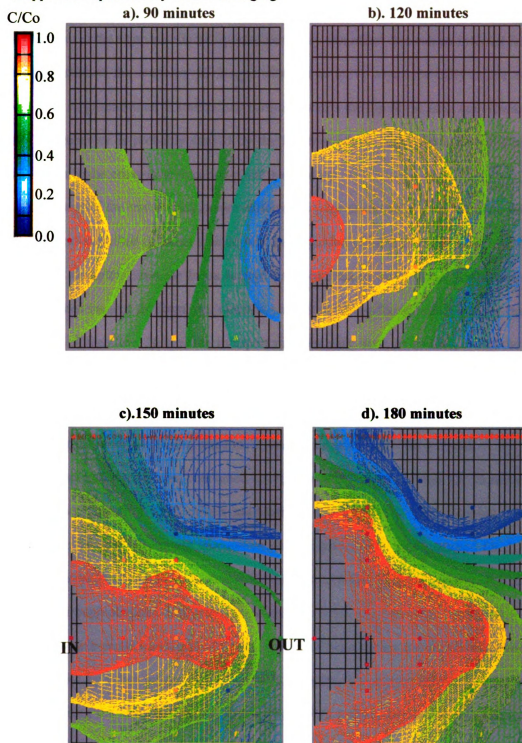


**Figure 7.** Profile of bromide breakthrough during the cross-flow tracer study, seen perpendicular to the surface. Cross-flow at 280 ml/min. Vertical flow stopped. Interpolation by universal kriging





statistics and model constraints (such as impermeable barriers, constant heads, etc.) were not considered. Thus, some illogical information on the obtained figures may exist. However, it can be seen how the front moves and expands with time: injected water moves horizontally towards the exit point but at the same time is transported vertically. An effect that can be inferred from the sequence of results is the tendency of the groundwater to move asymmetrically in the vertical direction. That is, groundwater is transported further towards the top of the tank than towards the bottom. This behavior is probably caused by the location of the aquifer boundaries, since the bottom is closer to the cross-flow injection point than the top.

At the end of the tracer study, major differences were observed in tracer vertical profiles. Thus, for vertical sampling columns located near the injection point and/or the main direction of the cross-flow, complete bromide breakthrough had occurred in more sampling ports than in sampling columns located far from the injection point (near the effluent point) and far from the main direction of the flow. Hence, the transport of chemicals, such as acetate, would be more effective near the influent point and would decrease in a non-ideal radial fashion. It is expected, then, that more acetate will be delivered in sampling column 12 than in column 33, and that may affect the biological processes taking place in different locations within the 3-D tank.

A second tracer study was conducted during the inoculation of strain KC to relate both kinds of transport (conservative chemicals and bacteria) directly. The average pumping rate used was 273 ml/min for the 180-minute inoculation event. Hence, 49 L were pumped for 3 hours. Again, this value was not measured but derived from calculations. Figure 8 presents the effluent bromide breakthrough obtained during the inoculation.

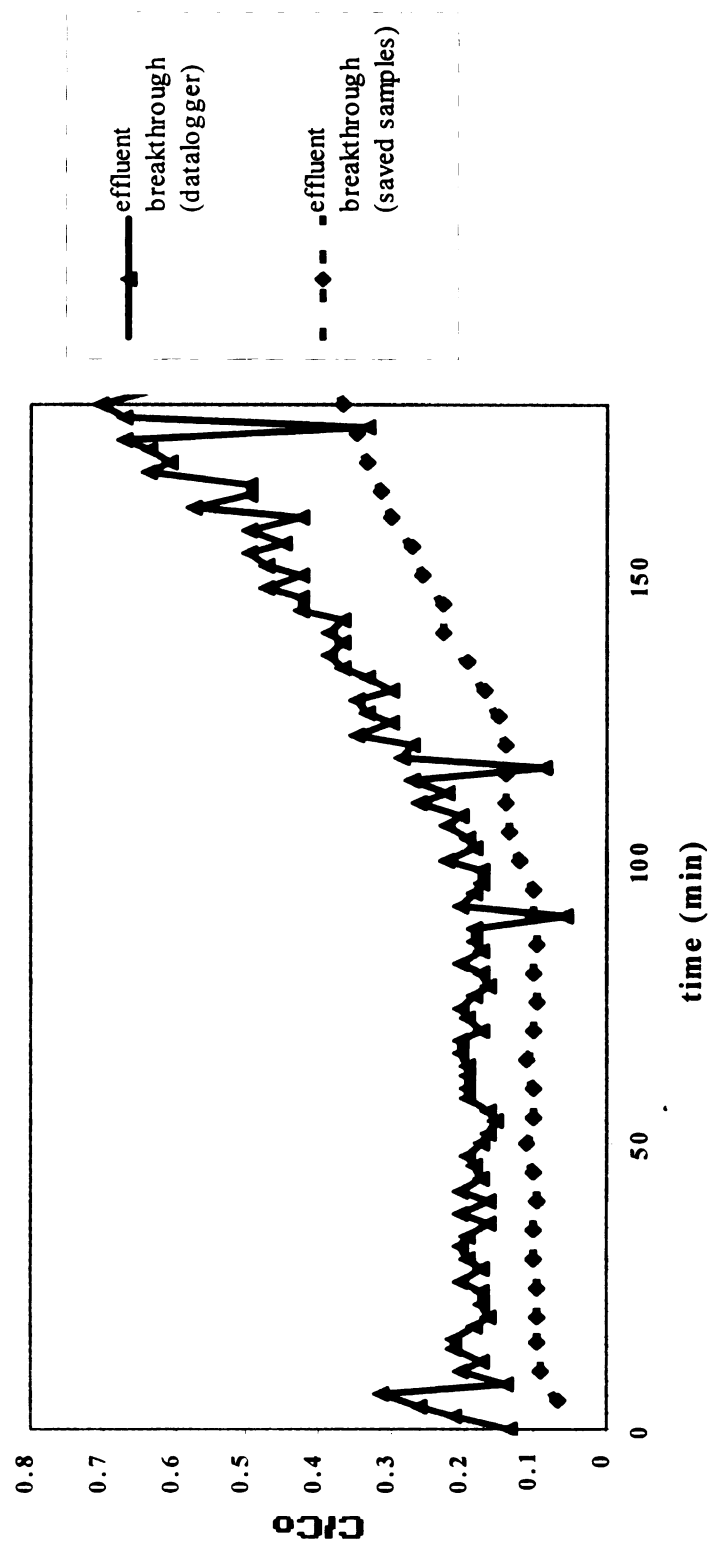
The bromide probe was connected in line to the effluent during the inoculation event and data was collected by a data logger. Simultaneously, samples were collected every 5 minutes and later analyzed using the same bromide probe working off line. Both sets of data are presented in Figure 8. Three major differences can be inferred from these two sets of data: (a) high background (noise) bromide levels present in the samples according to the data logger data, (b)

elevated bias levels in the data logger data, (c) lower bromide breakthrough from the saved samples.

The strong hysteretic behavior of the bromide probe and also its instability, makes the bromide electrode less appropriate for in line analysis. The probe was connected to the effluent right after the calibration curve was completed. This was done from low to high concentrations, which could explain why initial readings indicate the presence of bromide when theoretically it had not yet been transported. The lag time required for going from high to low readings, in addition to the inaccuracy of the bromide probe readings at low concentrations, could have generated this high noise in the initial samples. In order to get better readings, the probe needs to be recalibrated and cleaned often, and enough response-time has to be provided for analysis. On the other hand, the electrode is an unstable instrument. Readings (mV) change considerably with slight changes among the samples, and even when analyzing the same sample. Effects of this instability could be reduced by allowing again a longer response time. However, when working in line, these effects cannot be eliminated and may be reflected in the data. For all of these problems it is strongly recommended that one use the bromide probe off line and/or use a more stable method of analysis (ion chromatography for instance). The bromide probe was used in line to get an immediate impression of bromide breakthrough (i.e. whether 50 and 100% breakthrough were attained or not). However, it was later realized that those readings often lead to wrong conclusions.

At the end of the inoculation event (3 hours), 40% and 70% of bromide breakthrough was attained according to the saved samples analysis and the logger data, respectively. In both cases, the percentage was lower than the one obtained during the first cross-flow tracer study. Part of the difference could have been caused by the lower flow rate used during the inoculation event (273 ml/min versus 280 ml/min for the first tracer study). Clogging within the column and/or rearrangement of solid particles due to flowing water may have also caused different flow behavior.

**Figure 8.** Inoculation bromide breakthrough at the cross-flow effluent.  
Data from bromide electrode connected in line and from saved samples measured off-line.



Vertical flow conservative tracer study. Figure 9 shows the vertical profile of bromide concentration in the 3D model aquifer at 16 and 24 hours after starting the tracer injection. Data points represent the average of bromide concentrations at each layer (9 sampling ports per layer); standard deviations are given by the error bars. Absolute concentrations are presented rather than relative ones ( $C/C_0$ ) due the lack of a constant value at the influent. It is believed that this variability, though, does not affect the main results of this tracer study.

The bulk of tracer water moved vertically by the groundwater flow (advection), whereas the spreading concentrations at the front were caused by both mechanical dispersion and molecular diffusion. The bromide front (50% breakthrough) moved up 40 cm during the first 16 hours, and was transported to above half the height of the tank (approximately 56 cm) after 24 hours. That roughly represents a linear groundwater vertical velocity of 2.5 cm/hr for the first period (0-16 hours) and 2.0 cm/hr for the second (16 to 24 h), with an average velocity of 2.3 cm/hr for the first day. Some of the variability of the groundwater velocity was caused by the varying influent flow (measured at the effluent), due to clogging problems within the tank.

The port data were interpolated into the 3D grid and the results are presented in Figure 10. The bromide front advances fairly uniformly across the horizontal layers, with a slight tendency to move faster at the center of the tank. The location of the sampling ports in the tank could explain this trend. First, the column of sampling ports sampling in the center of the tank (column 22, Figure 3) is sampling the streamline that joins influent port 1 with effluent port 1, both also located in the center of their layer. Higher concentrations—faster breakthrough—could be expected in this section of the tank due to flow patterns that allow a vertical streamline to exist as the shortest streamline in the aquifer. All other streamlines within the aquifer would curve near the influent and effluent ports and thus would be longer than the center one. On the other hand, lower concentrations observed near the walls could be the result of statistical phenomena, due to the absence of sampling ports near the walls and thus longer distances from the wall to the scattered data points from which data is inferred. The interpolation process obtained by GMS

**Figure 9.a.** Bromide vertical profile at 16 hours of vertical pumping.  
 Nine readings (ports) per data point or layer,  $\pm$  standard deviation.

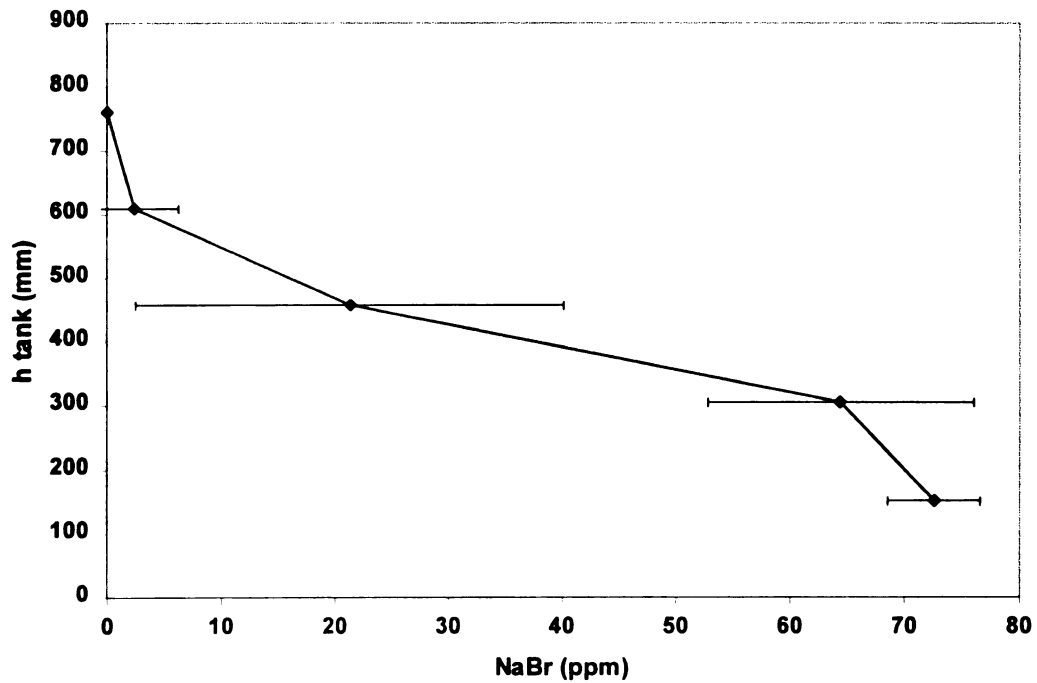


**Figure 9.b.** Bromide vertical profile at 24 hours of vertical pumping.  
 Nine readings (ports) per data point or layer,  $\pm$  standard deviation.

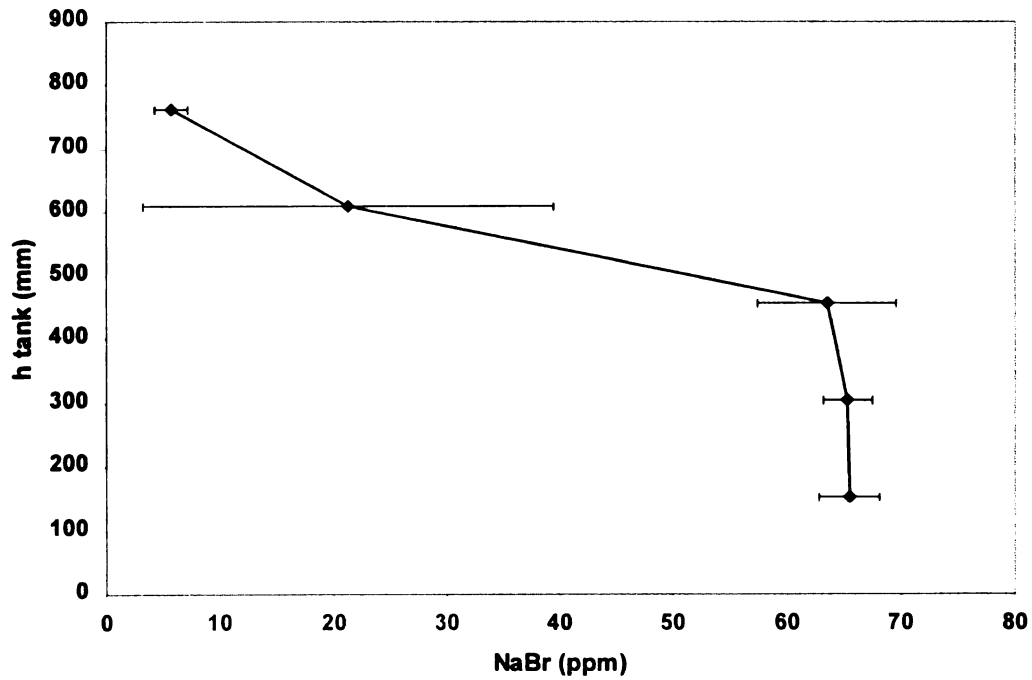
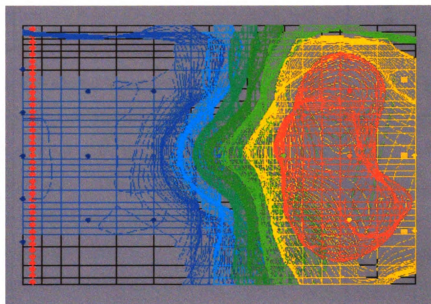




**Figure 10.** Bromide 3D vertical profile during vertical pumping, seen normal to the surface. Scattered data measured by bromide electrode. Interpolation into the 3D numerical grid by GMS (kriging).

a). 16 hours



b). 24 hours

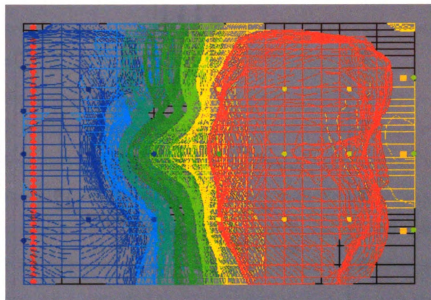
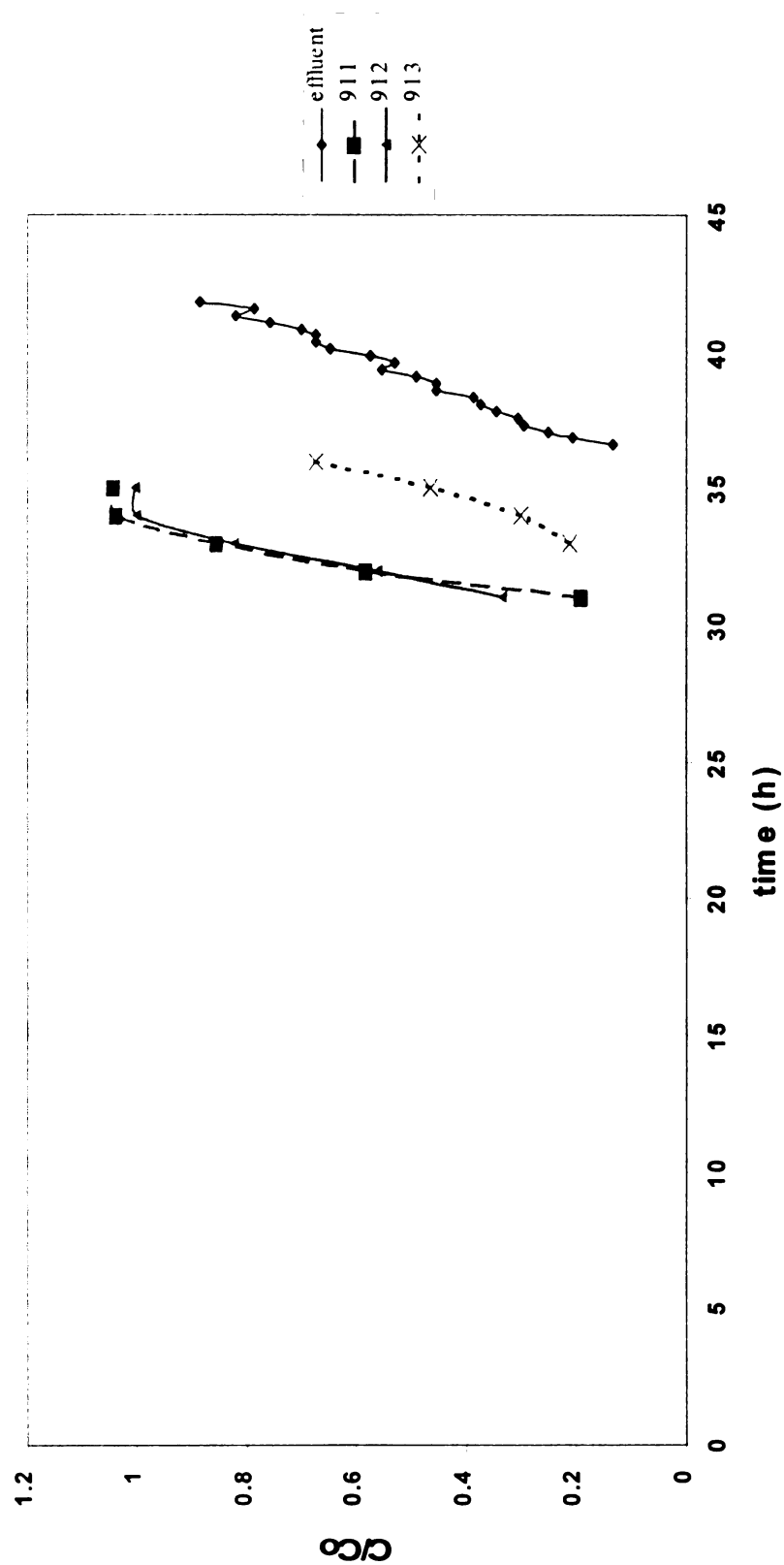


**Figure 11.** Bromide breakthrough at ports 911, 912, 913 and vertical-flow effluent.  
Vertical flow working at 33 ml/min. Samples measured by bromide electrode.



uses a weighted approach, in which the concentration at a given point is calculated from all the scattered data available and weighting their values proportional to the distance to the point. Thus, the farther the distance, the less the weight of its contributed concentration, a phenomena that results in a tendency to decrease the concentration at points of the numerical grid located far from any sampling port.

A second important factor to point out from Figure 10 is the decrease in bromide concentration that took place at the bottom of the tank hours after starting the vertical flow. As previously mentioned, this was originated by the problems experienced in both the mixing tank and the influent lines that caused the variation and decrease in the aquifer influent concentration.

When the bromide front reached the upper layer of the tank, sampling efforts were intensified to get a complete picture of the tracer breakthrough. Figure 11 shows the data obtained at 3 sampling ports of this layer (layer 9); effluent breakthrough has also been included for comparison. The average of bromide influent concentrations (71.3 ppm NaBr) was taken as  $C_0$  for computation objectives.

Almost all layer-9 sampling ports behaved similarly and showed 50% bromide breakthrough around 32 hours after starting the experiment (2.4 cm/hour linear velocity from the beginning of the experiment). Effluent breakthrough (an averaged effluent of ports 1, 2, 4, and 6 located at the top of the tank, 15 cm higher than layer 9) occurred 7 hours later (39 hours after the beginning of the experiment), giving an average linear velocity of 2.35 cm/hour. Note that some of the layer 9 ports showed a 3-hour delay on bromide breakthrough (913 and 921, see Figure 11 and Appendix B). This may have been caused by the different distance of the sampling ports to the influent and effluent points and the asymmetry of the flow lines. Groundwater enters the column through four ports (numbers 1, 2, 4 and 6) located at the bottom and leaves through four ports (1, 2, 4, and 6) at the top. Although heads are theoretically uniform within the same horizontal layer and decrease towards the top of the tank, providing a uniform flow velocity, some sort of non-uniform flow may exist. This could cause a difference on tracer breakthrough at



different points within the aquifer. On the other hand, ports at the top present a twist angle of 30 degrees with respect to the bottom. The asymmetry between influent and effluent ports, then, could also cause a variation in the flow paths in the vicinity of the ports and thus complicate the tracer breakthrough, creating non-ideal behavior.

### ***3.2 Breakthrough of CT***

Figure 12 shows the vertical profile of liquid-phase CT concentrations in the model aquifer at 24, 48, 72, 120 and 146 hours after starting the injection. Data points represent the average of carbon tetrachloride concentrations at the corresponding layer (9 sampling ports per layer); concentration standard deviations are given by the error bars.

When CT-spiked groundwater is injected into solid matrixes, the organic contaminant is sorbed onto the solid materials and thus the total amount of compound present is given by not only the aqueous phase but also by the solid-sorbed phase. (CT is also a volatile compound and would be also present in the gas phase if any air pocket were present). That causes a contaminant migration of CT different from an ideal or conservative one –such as bromide that does not interact with the solid materials present in the matrix. Hence, the bulk of CT concentration (given by 50% breakthrough) is retarded relative to bromide; the characteristics of this delayed response are given by the retardation factor ( $R$ ). On the other hand, the sorption of CT results in a second major difference between a conservative tracer and a reactive tracer: the spread of the breakthrough curve, which tends to be greater at a given position for the reactive (sorbed) compound. Hence, if we compare the breakthroughs of bromide and CT at one location of the tank, i.e. layer 6 (Figures 10.b. and 14.b.), the front of concentrations is more spread in the case of CT than in the case of bromide.

As shown in Figure 12, the CT front moves up with time, tending to homogenize the concentration along the column. The bulk of CT concentration (50% breakthrough) migrated up approximately 42 cm during the first 24 hours, 14 cm less than the bromide front. That represents

an average CT linear velocity of 1.75 cm/hr, whereas the groundwater average linear velocity (given by the bromide front) was 2.3 cm/hr for the same period of time. The retardation factor for CT in the column can be computed as follows:

$$(\bar{u} / \bar{u}_c) = R = 1 + (\rho_b/n)K_d \quad (2)$$

where  $\bar{u}$  is the average linear velocity of the groundwater and  $\bar{u}_c$  is the velocity of the  $C/C_0 = 0.5$  point on the concentration profile of the retarded constituent (Freeze *et. al.*, 1979). The bulk mass density is represented by  $\rho_b$ ,  $n$  is the matrix porosity and  $K_d$  the distribution coefficient. Therefore, in the case of the 3-dimensional model aquifer, the retardation of CT would be:

$$R = 2.3 / 1.75 = 1.3 \quad (3)$$

determined at 24 hours. According to this value, CT breakthrough at layer 9 should have taken place at around 42 hours (1.3 times later than bromide 50% breakthrough which occurred at around 32 hours). However, at 48 hours CT concentrations at layer 9 were still about 30% breakthrough (12.7 ppm as an average). This difference could have been caused again by the varying flow (which tended to slightly decrease with time) and the fluctuating influent concentration. The retardation factor for CT in 1-dimensional columns packed with this kind of aquifer material had been previously determined to be 1.2 (Witt, 1995).

The varying influent CT-concentration had a major effect on concentration profiles obtained at 120 and 146 hours (see Figure 12: vertical CT profile at 24, 48, 72, 120 and 146 hours). By day 4 after starting the tracer and sorption experiments, the problems in the mixing tank became significant and the influent concentration varied substantially. This caused a decrease in liquid phase concentrations and originated an arched curve when a straight line would be expected for fully saturated and constant influent concentration conditions. Figure 13 shows the 3D-tank influent and effluent CT concentrations versus time.

**Figure 12.** CT vertical profile. Nine readings per data point;  $\pm$  standard deviation.

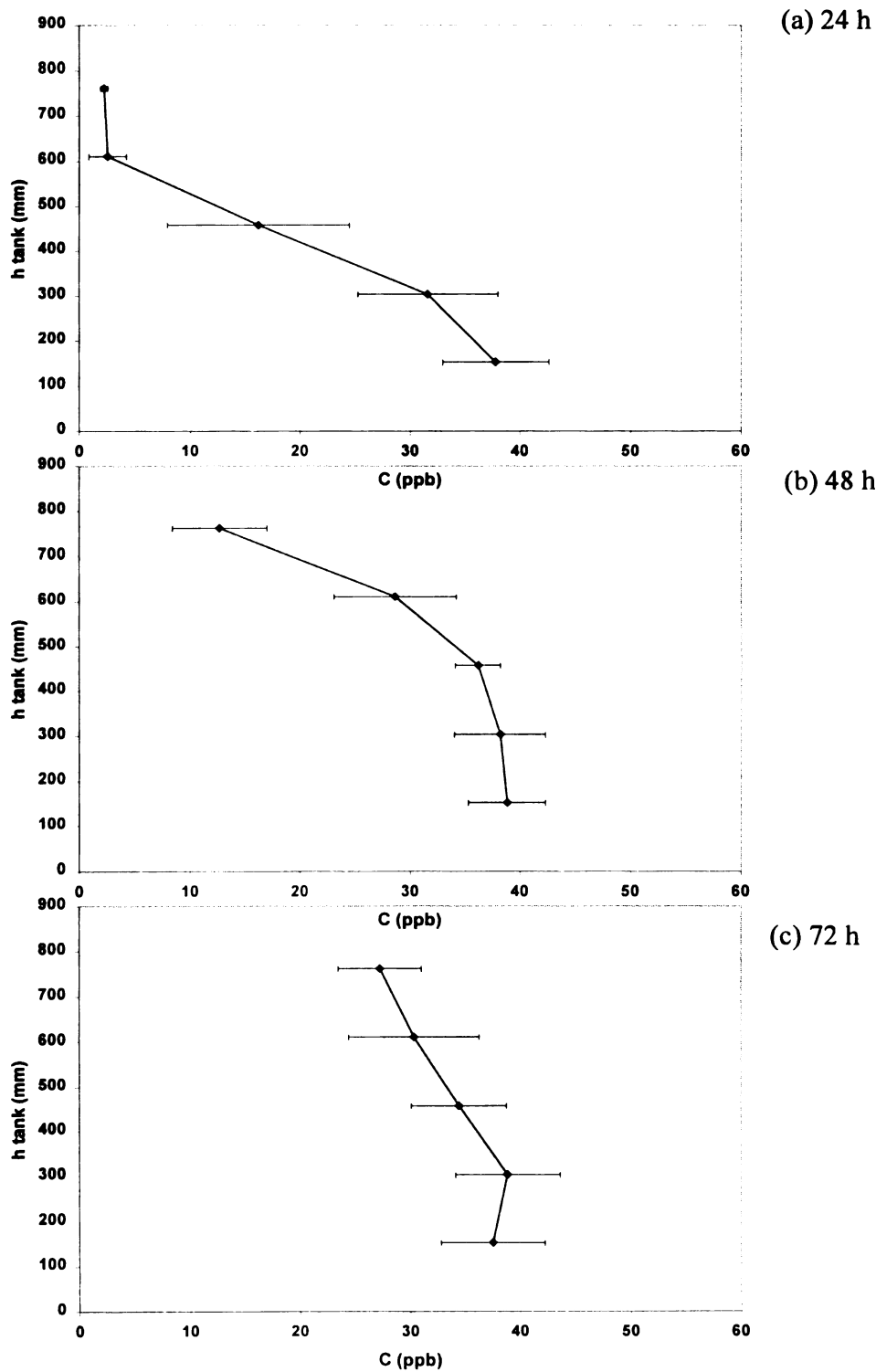


**Figure 12.** CT vertical profile. Nine readings per data point;  $\pm$  standard deviation.

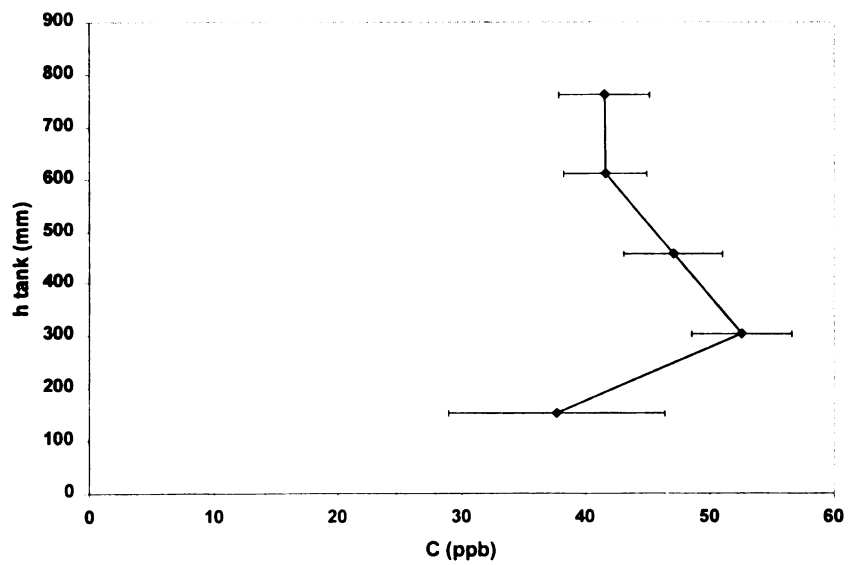
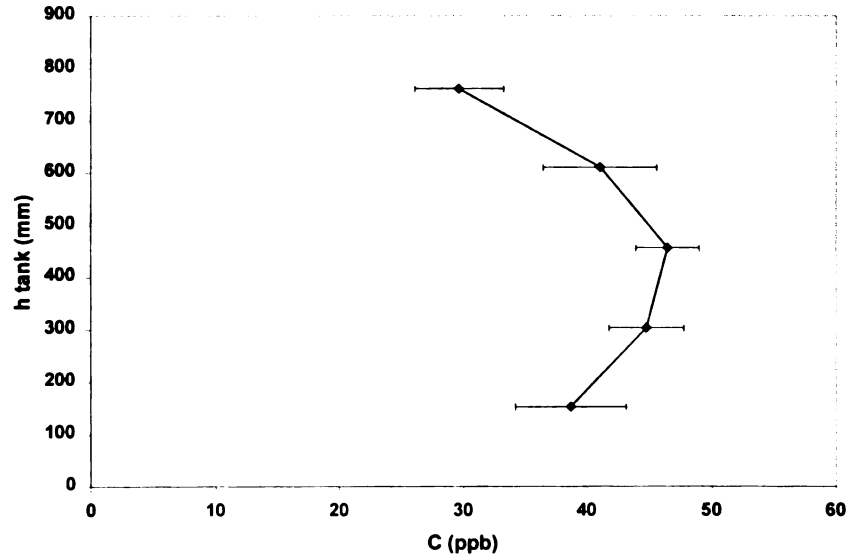


**Figure 13.** CT breakthrough in the 3D model aquifer.  
Vertical flow working at 33 ml/min (average). Samples taken at the mixing tank (influent) and tank vertical-flow effluent (constant head reservoir) and measured by GC.

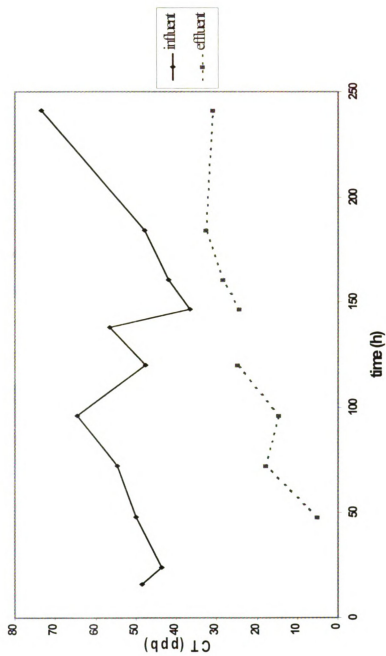
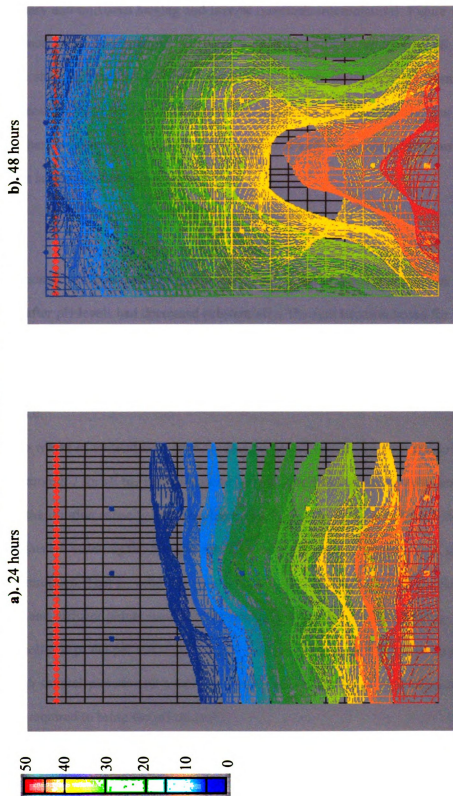


**Figure 14.** CT vertical 3D profile during vertical pumping, seen normal to the surface.  
Scattered data measured by GC and interpolation obtained by inverse quadratic statistics in GMS.



Point CT-data was obtained and interpolated in the 3-dimensional tank model grid. For interpolation purposes, the software package GMS was used and several interpolation parameters were tried (ordinary and universal kriging and inverse quadratic interpolation). Figure 14 shows the results obtained when interpolating the vertical profiles obtained at 24 and 48 hours by inverse quadratic statistical methods. There it can be seen how the 3-dimensional front migrates up through the column. Like the bromide front, CT moves up quite uniformly, but shows a tendency for higher concentrations in the center of the tank and lower concentrations near the walls, a trend that seems to increase with time.

### ***3.3 Soil titration***

As mentioned in Section 2.5, the 3-dimensional column was titrated twice: prior to inoculation, and after pH levels had decreased substantially. The first titration lasted for 16 hours, pumping at an average rate of 280 ml/min. Thus, approximately 288 L of 8.2-pH adjusted water were pumped cross the column without recirculation. At the end of the pumping, the effluent showed a pH of 8.0.

After two weeks of vertical flow (two feeding events at pH 8.2 had been conducted), pH had decreased to around 7 for all the sampling ports located within the bioactive zone (rows 3 and 5), showing that the titration capacity had been lost (alkalinity consumed). It was then decided to pump pH 8.2-adjusted water again through the cross-flow inoculation point, this time with groundwater recirculation. That is, water leaving the system through the cross-flow effluent point (vertical influent and effluent points were closed) was pumped back into the injection reservoir, where a pH-controller kept the pH at 8.2 (8.15-8.25) with the addition of base. The titration was conducted through several periods and a total estimated volume of 1,214 liters of groundwater ( $1.6 \times 10^{-6}$  M) was required to bring the pH up to 8.2.

### **3.4 Breakthrough and distribution of *P.KC***

*Pseudomonas* strain KC was aerobically grown for 24 hours to a final inoculum concentration of  $8.7 \times 10^7$  cfu/ml (average reading. See Appendix D). The 50-L inoculum fermenter was then attached to the cross-flow injection point to start pumping at an average 273-ml/min flow rate. Vertical flow influent and effluent ports were closed during the inoculation. The biomass breakthrough (liquid phase) at 4 sampling points (312, 322, 332 and cross-flow effluent, all located within the main direction of flow) can be seen in Figure 15. Influent biomass concentration has been also included as a reference.

At the end of the inoculation event, which lasted for 3 hours, 100% biomass breakthrough had been achieved at the 3 sampling points in the center of the column, whereas the effluent was still about two orders of magnitude lower ( $3.9 \times 10^6$  cfu/ml). This seems to agree with the bromide breakthrough results presented previously in Section 3.1 (Figure 7), that suggested that lower concentrations could occur at the far end of the cross-flow pathway.

Liquid samples for biomass determination were also analyzed for bromide, so the breakthrough at different points (312, 322, 332 and effluent) could be obtained, as can be seen in Figure 16. Again, lower concentrations are observed near the effluent port. Figure 17 shows the combined data for biomass and bromide breakthrough obtained during the inoculation at the 4 sampling ports. Data for both breakthroughs were determined from the same set of samples, that is, bromide readings were performed in the same liquid sample that had been used for plate counts. Data might thus differ from other results obtained from other samples. An average sodium bromide concentration of 100 ppm and biomass concentration of  $8.7 \times 10^7$  cfu/ml were used to determine  $C_0$ . If any  $C/C_0$  value was determined to be above 1, it was arbitrarily taken as 1 since it is assumed no mass generation occurred inside the aquifer. In the case of bromide, high  $C/C_0$  values ( $>1$ ) would have been caused by analytical errors; however, they were never found to be above 1.1. In the case of biomass, nevertheless, high  $C/C_0$  values (approaching 2) were determined for most liquid-phase samples after 100% breakthrough had occurred, due to either



**Figure 15.** Biomass breakthrough at ports 312, 322, 332, influent and effluent during inoculation. Liquid samples measured by plate counts.

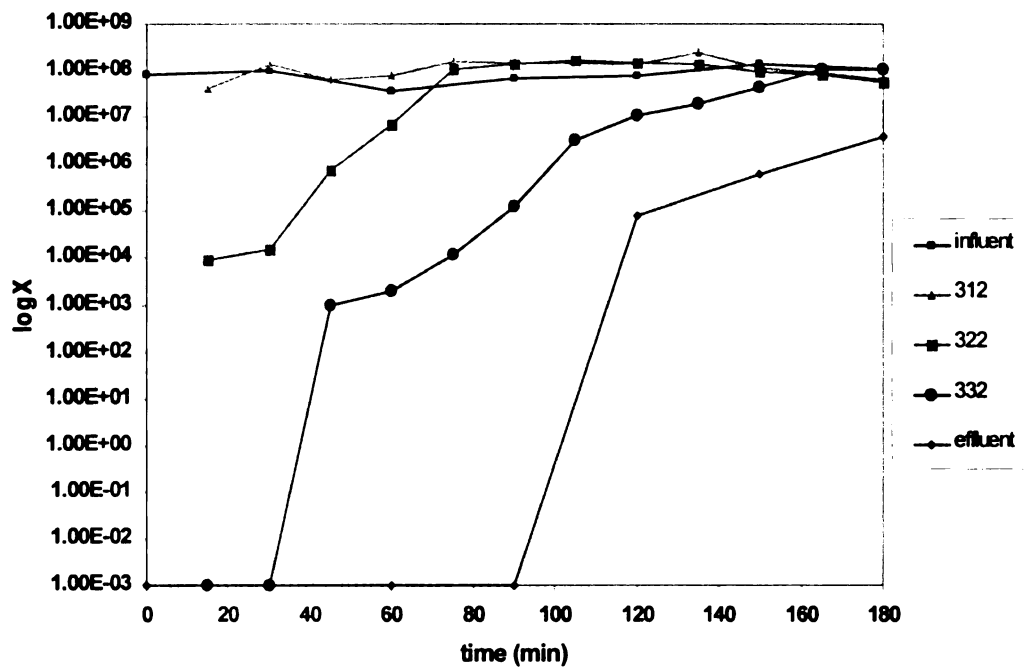


**Figure 16.** Bromide breakthrough at ports 312, 322, 332, influent and effluent during inoculation. Readings by bromide electrode.

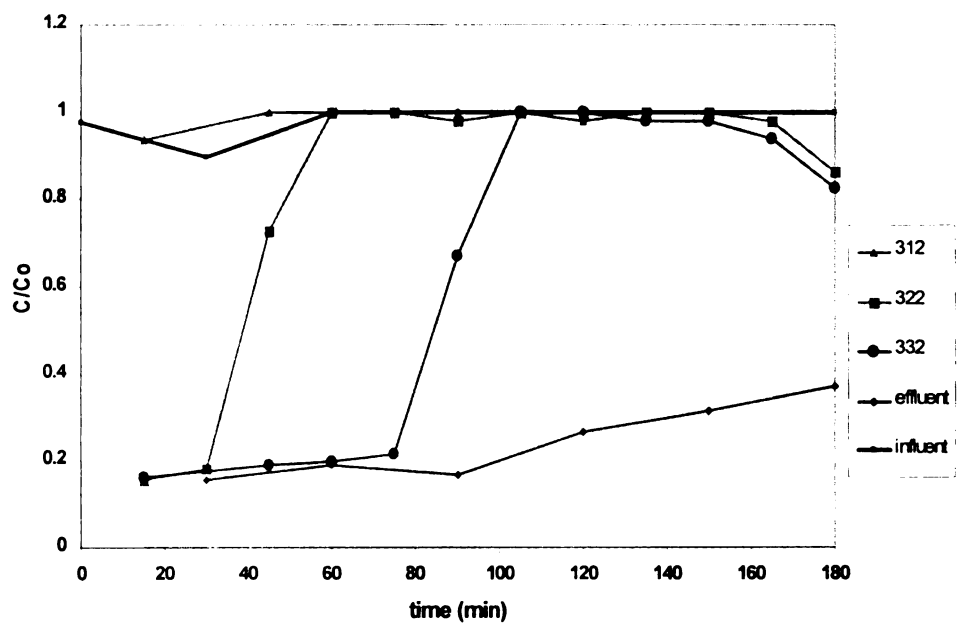


**Figure 17.** Bromide and biomass breakthrough during inoculation. Readings by bromide electrode and plate counts.

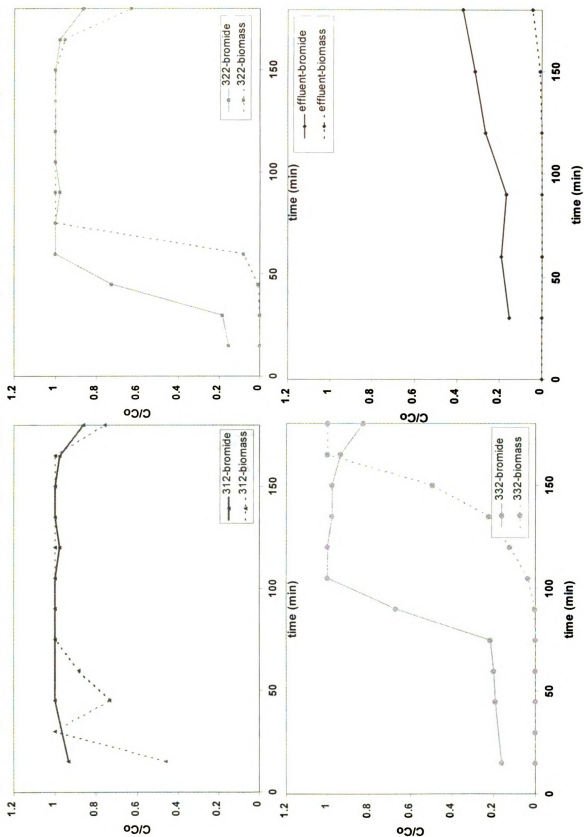
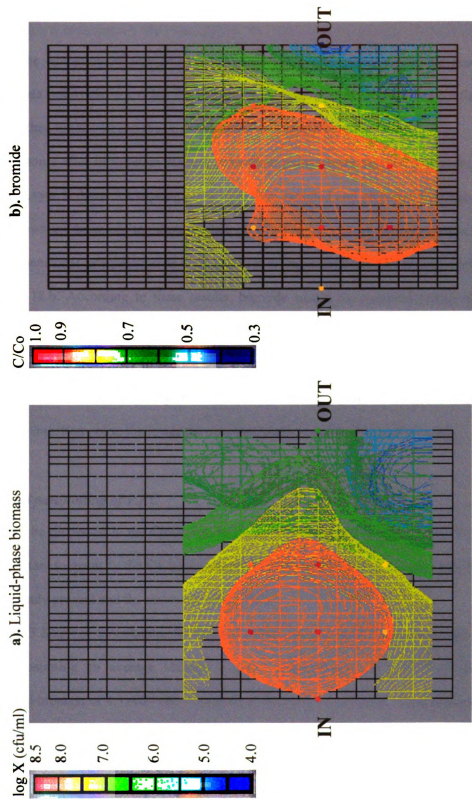


**Figure 18.** Biomass and bromide 3D distribution at the end of the inoculation, normal to surface. Interpolation by ordinary kriging.



growth of strain KC during the inoculation event or detachment of accumulated KC in the solid phase. At the same time, some error could have been introduced by the analytical procedure used (plate counts).

With the exception of port 312 at 30 minutes after the beginning of the inoculation pumping, all data points show a delay for biomass with respect to bromide. That confirms that biomass is attached to the soil and thus it may behave as a reactive tracer.

Three hours after inoculation started, cross-flow pumps were stopped and vertical flow was restarted. Layer 1, 3 and 5 sampling ports were then sampled and prepared for plate counts. Figure 18.a shows the biomass liquid-phase data obtained at the end of the inoculation and the results of 3-dimensional interpolation as well. Data for bromide distribution has been included as well in Figure 18.b. According to these results, bromide would have moved further than the biomass, thus confirming the biomass delay during the transport through the porous media. It can also be seen, as stated previously in section 3.1, that different vertical sampling columns would present different tracer and biomass profiles at the end of the 3-hour inoculation event. The farther from the injection point, the lower the concentrations of both tracer and biomass.

### ***3.5 Liquid-solid partitioning of P.KC***

As will be discussed in the Chapter 4, knowing the amount of biomass injected into the system is important to quantify the CT bioremediation performance, and the relationship between native flora already present and the newly introduced KC.

During 3 hours of inoculation, 49 liters of culture were injected into the model aquifer (cross-flow). Assuming an average influent biomass concentration of  $8.7 \times 10^7$  cfu/ml, that represents a total biomass of  $4.3 \times 10^{12}$  cfu. A portion of this biomass attached to the solid particles during its transport and thus never reached the exit point. It is the objective of the following discussion to estimate how much of the biomass remained in the soil (as no solid samples were taken to experimentally determine the values).

Biomass and bromide breakthroughs that took place during the inoculation event were presented and discussed in the Sections 3.1 and 3.4. Retardation of biomass with respect to the bromide front was experimentally observed (Figure 17). This delay on the biomass front was used to determine the amount of biomass that attached to the soil particles, and the results can be seen in Figure 19. Data points were obtained by multiplying the difference between  $C/C_0$  for bromide and biomass by the average influent biomass concentration at the 4 points sampled during the event (Equation 4).

$$\text{Attached biomass} = \left[ \left( \frac{C}{C_0} \right)_{\text{bromide}} - \left( \frac{C}{C_0} \right)_{\text{Kc}} \right] C_{0,Kc} \quad (4)$$

It must be pointed out, however, that these values do not represent the distribution of biomass in the soil fraction of the matrix, but the total amount of biomass left between the injection point and the sampling point. The area under the curve would represent the total amount of biomass attached per ml and during 180 minutes; the data is presented in Table 1.

**Table 1:** integration of curve in Figure 19.

Sampling port	Area under the curve (cfu/mL)
312	$2.56 \times 10^9$
322	$2.58 \times 10^9$
332	$6.38 \times 10^9$
effluent	$3.24 \times 10^9$

Since all four sampling ports were located within the same horizontal line in the main direction of the flow (line 32, Figure 3), it should be observed that the farther the sampling point from the influent point, the higher the biomass which is been left attached. Thus, the amount of biomass left on the soil particles should increase as sampling ports move farther from the injection point; theoretically, each sampling port includes information from upstream locations. According, then, to Table 1, that is true except for the effluent point. This point, however, never reached 100% breakthrough (as did all others) and thus biomass was still attaching to the soil. In addition, the effluent point represents the average concentration of all flow lines leaving the

system, some of which can be more diluted than the flow line projecting horizontally from the cross-flow influent to the effluent along ports 312, 322 and 332. Thus, direct comparison of data obtained at the mentioned ports with the data from cross-flow effluent may not be possible.

Assuming that the effluent flow is an average of all flow-lines that exit from the injection and move through the aquifer in different velocities and directions to later converge in the effluent, it can be said that the amount of strain KC that was deposited inside the aquifer is given by the total amount that was introduced ( $4.3 \times 10^{12}$  cfu as previously explained) minus the amount of biomass that left the tank ( $3.24 \times 10^9$  cfu, given by the effluent). Therefore, approximately  $4.3 \times 10^{12}$  cfu of *Pseudomonas stutzeri* st. KC were effectively retained in the model aquifer. Again, part of this biomass remained in the liquid phase and the rest was attached to the soil. The distribution of biomass within the model aquifer, though, is not uniform, but varies in a 3-dimensional way, given the 3-dimensional flow patterns. The distribution of biomass in the liquid phase has been presented above. The solid-phase biomass may be distributed in a similar fashion.

One way to estimate the biomass adhered to the soil during the inoculation can be based on the clean-bed filtration theory, in which the collision efficiency and the blocking factor determine the percentage of biomass effectively attached to the soil particles. These parameters are highly dependent on solid matrix characteristics, ionic strength of the solution, cell physiology and cell concentration. Radabaugh, 1998, determined the basic filtration parameters for strain KC in Schoolcraft material one-dimensional columns and determined its solid cell concentration at saturation (soil loading capacity). According to these results, obtained in similar conditions to the 3D tank inoculation, Schoolcraft soils become saturated at a biomass concentration of  $3 \times 10^7$  cfu/g soil. Once this concentration is achieved in the soils, 100% biomass breakthrough is observed in the liquid phase. Using, then, the 3-dimensional biomass distribution from the liquid phase obtained at the end of the inoculation (Figure 18.a), solid phase data can be derived by assuming that the concentration in the soil is proportional to the breakthrough in the

liquid phase. A linear relationship has been considered in order to compute the data; that is, at 100% breakthrough in the liquid phase, solids are at their loading capacity ( $3 \times 10^7$  cfu/g soil), whereas at 80% breakthrough in the liquid phase, solids present an 80% of saturation. By this methodology, solid-phase concentrations for the 3-dimensional aquifer have been obtained and the results can be seen in Figure 20. It should be pointed out, however, that the values obtained from the filtration theory are not applicable to all ranges of concentrations. The theory predicts removal of almost every particle from the liquid phase and thus the process would produce sterile groundwater. However, it is known that this does not occur in reality. At low concentrations, nevertheless, the blocking efficiency would be reduced and particles—that is, bacteria--would be transported farther than otherwise predicted.

Hence, the solid-phase biomass distribution is based on the assumption that it follows the same pattern as the liquid-phase distribution, decreasing as flow-lines move farther from the entrance point. Near the effluent solid-phase concentrations of  $1.35 \times 10^6$  cfu/g would be observed. See Appendix D for data.

**Figure 19.** Biomass remaining in the tank during inoculation, as determined by equation 4.

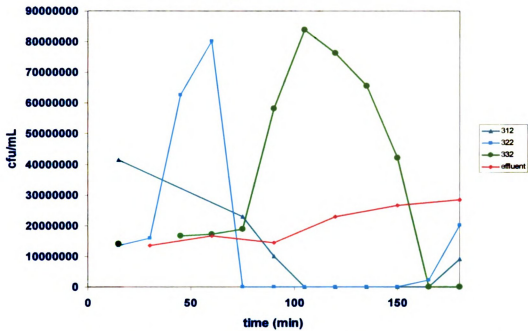
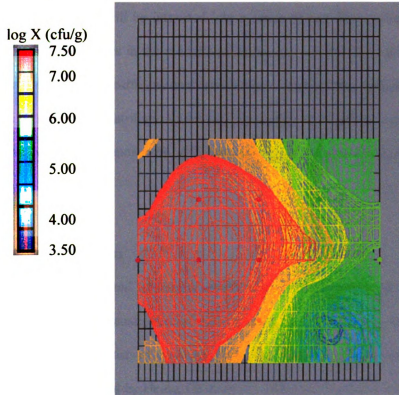


**Figure 20.** Solid-phase biomass distribution at the end of the inoculation.





## PREDICTION OF CT-REMOVAL EFFICIENCY

### ***4.1 Basis for competition between native flora and P.KC***

When nutrients are added into the aquifer, they can be used by many organisms present and thus sometimes depleted. Microorganisms will start a succession based on competition for resources and determined by the different kinetics that drives their activity. Not only the kinetics will determine the final output of the competition, but also the initial conditions, such as the ratio of flora to inoculum, will have an effect on microbial succession. This may in turn influence final levels of bioremediation activity. Hence, the objective of this chapter is to develop an understanding of the effect of biomass distribution (KC versus native flora ratio) upon the final performance of the bioremediation strategy and microbial community formed in the subsurface. Three-dimensional data will be imported into a series of one-dimensional numerical models to describe laminar flow lines in the model aquifer natural gradient flow after inoculation of strain KC. It is assumed that one-dimensional vertical flow patterns predominate in the aquifer. Given the gradient of biomass distribution after the inoculation, it is further expected that several one-dimensional vertical columns with different starting conditions (biomass ratio) could behave differently.

### ***4.2 Mass balance equations***

The one-dimensional numerical model used herein to simulate the establishment and maintenance of the CT transformation zone as well as understanding the microbial processes occurring in the zone, consists of a system of six mass balance equations derived from an original 5-equation model presented by Heine, (Witt. et al., 1995) and further developed by Kelly (Kelly,

1995). The original model considers only the presence of the newly introduced organism (strain KC) as a sink for both acetate and nitrate, and was presented as follows:

$$\frac{\partial C_{CT}}{\partial t} = \frac{D}{R_{CT}} \frac{\partial^2 C_{CT}}{\partial x^2} - \frac{U}{R_{CT}} \frac{\partial C_{CT}}{\partial x} - \frac{k' C_{CT}}{R_{CT}} (X_{KC} + X'_{KC}) \quad (5)$$

$$\frac{\partial X_{KC}}{\partial t} = D \frac{\partial^2 X_{KC}}{\partial x^2} - U \frac{\partial X_{KC}}{\partial x} + (\mu - b_{KC} - K_{CKC}) X_{KC} + K_{YKC} X'_{KC} \quad (6)$$

$$\frac{\partial X'_{KC}}{\partial t} = (\mu - b_{KC} - K_{YKC}) X'_{KC} + K_{CKC} X_{KC} \quad (7)$$

$$\frac{\partial C_A}{\partial t} = \frac{D}{R_A} \frac{\partial^2 C_A}{\partial x^2} - \frac{U}{R_A} \frac{\partial C_A}{\partial x} - \frac{\mu}{Y_A R_A} (X_{KC} + X'_{KC}) \quad (8)$$

$$\frac{\partial C_N}{\partial t} = \frac{D}{R_N} \frac{\partial^2 C_N}{\partial x^2} - \frac{U}{R_N} \frac{\partial C_N}{\partial x} - \frac{\mu}{Y_N R_N} (X_{KC} + X'_{KC}) \quad (9)$$

in which  $C_{CT}$  is the carbon tetrachloride concentration;  $X_{KC}$  and  $X'_{KC}$  are the concentrations of strain KC in the mobile and stationary phases respectively;  $C_A$  is the concentration of acetate, the electron donor for strain KC; and  $C_N$  is the concentration of nitrate, the electron acceptor for strain KC. Furthermore, the growth rate,  $\mu$ , is a function of both acetate and nitrate concentrations as follows:

$$\mu = \mu_{\max} \min \left[ \frac{C_A}{K_{SA} + C_A}, \frac{C_N}{K_{SN} + C_N} \right] \quad (10)$$

although in this work has been considered to be:

$$\mu = \mu_{\max} \frac{C_A}{K_{SA} + C_A} \frac{C_N}{K_{SN} + C_N} \quad (11)$$

These mass balance equations were derived to describe the change in concentration of each of the variables involved with CT degradation, including CT, acetate, nitrate, and strain KC in both the mobile and stationary phases (but no native flora). The assumptions underneath the model were the following: first, it was assumed that CT was transformed by both mobile and stationary cells, and that CT transformation was first order with respect to concentration of cells and first order with respect to CT concentrations. Secondly, it was assumed that a linear relationship existed between CT concentrations in the solid and liquid phases (assumption that was later modified by a two-site nonequilibrium model). Utilization kinetics for acetate, the electron donor, and nitrate, the electron acceptor, were assumed to obey Monod saturation kinetics. Finally, the attachment and detachment rates of bacterial cells were described by first order rate expressions.

The first and second order derivatives in equations 5, 6, 8, and 9 describe the advection and dispersion of CT, mobile cells, acetate, and nitrate respectively. Note that the dispersion,  $D$ , and the linear velocity,  $U$ , is constant for Eqs. 5, 6, 8, and 9. The remaining terms in these four equations are reaction terms. Equation 7 does not contain an advection or dispersion term since it models cells that attached to the soil particles. Equation 7 consists only of reaction terms describing growth, decay, and detachment of cells as well as the attachment of mobile cells onto the soil particles. The reaction term in Equation 5 describes the degradation of CT; in Eq. 6, the growth, decay and attachment of mobile (liquid phase) strain KC and the detachment of stationary (solid phase) strain KC cells; in Eqs. 8 and 9, the utilization of the electron donor and acceptor. Furthermore, an equation was added (Eq. 12, introduced by the Department of Geological Sciences) to describe the desorption of CT from the solid to the liquid phase according to a two-site nonequilibrium model (Lassey, 1988).

$$\frac{\partial S_{CT}}{\partial t} = \kappa((1-f)K_d C_{CT} - S_{CT}) \quad (12)$$

At the same time, equation (7) was modified to include sorption to the solid phase:

$$\frac{\partial C_{CT}}{\partial t} = \frac{D}{R_{CT}} \frac{\partial^2 C_{CT}}{\partial x^2} - \frac{U}{R_{CT}} \frac{\partial C_{CT}}{\partial x} - \frac{k' C_{CT}}{R_{CT}} (X_{KC} + X'_{KC}) - \frac{\rho \kappa}{R_{CT} \theta} ((1-f)K_d C_{CT} - S_{CT}) \quad (13)$$

The input parameters used in the 6-equation model are defined in Table 2 with their experimental and numerically optimized values.

**Table 2:** input parameters used in the mass balance equations

Input parameter	Definition	Experimental value	Optimized value (3)
D	dispersion, cm <sup>2</sup> /day		25
U	linear velocity, cm/day		14.8
R	retardation coefficient		
	CT	1.3 <sup>(1)</sup>	2.63
k'	second order rate coefficient, L/mg-day		0.039
μ <sub>max</sub>	growth rate, day <sup>-1</sup>		
	KC	3.12±0.69 <sup>(2)</sup>	3.1
	native denitrifiers	0.81±0.21 <sup>(2)</sup>	
b	decay, day <sup>-1</sup>		
	KC		0.1
	native denitrifiers	assumed 0.1	
K <sub>s</sub>	half-saturation coefficient, mg/L		
	acetate, KC		1.0
	nitrate, KC	11.97±1.34 <sup>(2)</sup>	12.0
	acetate, native denitrifiers	1.0 <sup>(2)</sup>	
	nitrate, native denitrifiers	9.40±0.32 <sup>(2)</sup>	
Y	Yield, mg cells/ mg substrate		
	acetate, KC		0.4
	nitrate, KC	0.4±0.04 <sup>(2)</sup>	2.001
	acetate, native denitrifiers		0.4
	nitrate, native denitrifiers	0.12±0.03 <sup>(2)</sup>	
K <sub>C</sub>	attachment rate, day <sup>-1</sup>		
	KC		2.175
	native denitrifiers	assumed 2.175	
K <sub>Y</sub>	detachment rate, day <sup>-1</sup>		
	KC		0.001
	native denitrifiers	assumed 0.001	

((1) Witt, 1995 (one-dimensional soil columns). (2) Knoll, 1994. (3) Dr. Hyndman and Dr. Phanikumar, personal communication. Data which was not available was assumed from previous sources to obtain a numerical values to use in the model).

Two sets of values were available for most parameters, derived each of them from experimental data in batch reactors (Knoll, 1994) and from an optimization of the 6-equation model derived by the Department of Geological Sciences at MSU (Dr. Hyndman, personal communication). In this work, the latest set has been used (optimized values) for numerical predictions. However, and based on the difference between these two sets of values, it should be pointed out that some of them may not be realistic but just a numerical match. On the other hand, batch-derived data also may not fit soil systems. Knowing that the values for the numerical coefficients used in the model can have a considerable effect on the output, it is therefore recommended to determine, when possible, experimental values under biofilm conditions and thus tend towards a more real numerical model.

#### 4.3 Competition equations

For the purpose of biomass competition, two new equations representing the liquid phase and solid phase native flora are herein added to the existing model. New reaction terms for acetate and nitrate have been introduced as well, so two kinds of organisms consume these resources at the same time. CT degradation, however, is still a function of KC activity. Finally, sorbed CT has also been included based on a two-site nonequilibrium model (Lassey, 1988). The eight-equation system is formulated as follows:

$$\frac{\partial C_{CT}}{\partial t} = \frac{D}{R_{CT}} \frac{\partial^2 C_{CT}}{\partial x^2} - \frac{U}{R_{CT}} \frac{\partial C_{CT}}{\partial x} - \frac{k' C_{CT}}{R_{CT}} (X_{KC} + X'_{KC}) - \frac{\rho \kappa}{R_{CT} \theta} ((1-f) K_d C_{CT} - S_{CT}) \quad (14)$$

$$\frac{\partial X_{KC}}{\partial t} = D \frac{\partial^2 X_{KC}}{\partial x^2} - U \frac{\partial X_{KC}}{\partial x} + (\mu - b_{KC} - K_{cKC}) X_{KC} + K_{yKC} X'_{KC} \quad (15)$$

$$\frac{\partial X'_{KC}}{\partial t} = (\mu - b_{KC} - K_{yKC}) X'_{KC} + K_{cKC} X_{KC} \quad (16)$$

$$\frac{\partial C_A}{\partial t} = \frac{D}{R_A} \frac{\partial^2 C_A}{\partial x^2} - \frac{U}{R_A} \frac{\partial C_A}{\partial x} - \frac{\mu}{Y_A R_A} (X_{KC} + X'_{KC}) - \frac{\mu_{NF}}{Y_{ANF} R_{ANF}} (X_{NF} + X'_{NF}) \quad (17)$$

$$\frac{\partial C_N}{\partial t} = \frac{D}{R_N} \frac{\partial^2 C_N}{\partial x^2} - \frac{U}{R_N} \frac{\partial C_N}{\partial x} - \frac{\mu}{Y_N R_N} (X_{KC} + X'_{KC}) - \frac{\mu_{NF}}{Y_{NNF} R_{NNF}} (X_{NF} + X'_{NF}) \quad (18)$$

$$\frac{\partial X_{NF}}{\partial t} = D \frac{\partial^2 X_{NF}}{\partial x^2} - U \frac{\partial X_{NF}}{\partial x} + (\mu_{NF} - b_{NF} - K_{CNF}) X_{NF} + K_{YNF} X'_{NF} \quad (19)$$

$$\frac{\partial X'_{NF}}{\partial t} = (\mu_{NF} - b_{NF} - K_{YNF}) X'_{NF} + K_{CNF} X_{NF} \quad (20)$$

$$\frac{\partial S_{CT}}{\partial t} = \kappa((1-f)K_d C_{CT} - S_{CT}) \quad (21)$$

where  $X_{NF}$  and  $X'_{NF}$  represent liquid-phase and solid-phase denitrifying native flora respectively, and its growth rate,  $\mu_{NF}$ , is described in Equation 22 as  $\mu$  for strain KC. The NF subscript designates the newly introduced terms regarding biomass competition. The sorbed CT is defined by  $S_{CT}$ ,  $\kappa$  is its first order kinetic (de)sorption rate,  $f$  is the fraction of exchange sites at equilibrium, and  $K_d$  the distribution coefficient. Finally,  $\rho$  defines the soil bulk density and  $\theta$  the porosity of the soil matrix.

$$\mu_{NF} = \mu_{NF \max} \frac{C_A}{K_{S_{NFA}} + C_A} \frac{C_N}{K_{S_{NFN}} + C_N} \quad (22)$$

The assumptions considered for this model were essentially the same as the ones in the previous model. The native flora is assumed to behave according to Monod kinetics, but with different parameters (growth rate,  $\mu$ , and saturation constant,  $K_s$ ) than KC, so competition will occur. Batch-derived parameters from Knoll, 1994, have been used for native flora numerical simulations, although it is expected that future optimization of the model will modify these values. Dispersion, advection, attachment and detachment terms have been considered to be the same as strain KC's.

An important aspect of biomass kinetics needs to be taken into account when modeling the system: the survival of biomass in the subsurface without addition of acetate, or after this carbon source has been depleted. Although no data is now available about the biomass kinetics under starving or low carbon-level conditions, it is known that biomass is present in the system prior to any addition of external carbon, and also remains after acetate is depleted. Native flora is believed to be present in the Schoolcraft soil at concentrations of  $10^4$ - $10^5$  cfu/ml in the liquid phase and about  $10^5$ - $10^6$  cfu/g of soil (Dybas, personal communication). A concentration of  $3 \times 10^6$  has been used in this work. It survives using other sources of organic carbon present in the system probably at low metabolic rates. Although one component of native flora are denitrifiers, activity under these low carbon conditions consumes very low levels of nitrogen (nitrate) and hence no major gradient of N is observed in the field prior to addition of acetate. In order to reproduce this behavior in the numerical model, the following conditions were introduced:

- A minimum level of native flora is always present in the system, regardless of the levels of acetate and nitrogen. That would account for the background levels of biomass that survive in the subsurface at a concentration of  $10^5$  cfu/ml and  $3 \times 10^6$  cfu/ g soil which may be able to grow if enough nutrients are added.
- Nitrate and acetate are not used by the biomass unless a minimum amount (of nitrate and/or acetate) is present. That is in agreement with the minimum resource level ( $S_{min}$ ) theory (Rittman and McCarty, 1980), according to which no biomass growth occurs unless a minimum amount of substrate is present to balance growth and decay. At the same time, this allows the numerical model to avoid creating a nitrogen gradient due to the presence of native flora, as it is known to occur in the field. However, nitrogen and acetate depletion will vary depending on the  $S_{min}$  used.

The indigenous microorganisms considered so far in this model represent several populations of denitrifiers living and acting in the soil matrix. They have been grouped into one single type of behavior as if they all belonged to the same population, or as if even by belonging

to different populations, they all presented the same kinetics. In reality, however, all these denitrifying populations could also compete among themselves and selection among succeeding populations after the addition of the acetate may change the bulk *native flora* behavior. Furthermore, other bacterial populations that do not use nitrate as an electron acceptor but do consume carbon, are also present in the system and interact with previously mentioned microorganisms. It is also known, nevertheless, that other electron acceptors are not used unless the more oxidized one has been depleted, thus creating normally a spatial separation in the soils that represents different redox conditions. In the case of Schoolcraft, sulfate-reducing populations are present in the soil to utilize any carbon left when all nitrate is depleted. If enough carbon is then added to the system to deplete all nitrate and still allow the sulfate-reducers to grow, these populations would develop, creating in this case a major problem: chloroform formation as a product of CT degradation (by sulfate-reducing activity). Although this factor has not yet been introduced in the model, it could be considered by incorporating a third group of microorganisms that consume not only the acetate (after nitrate depletion) but also the CT to produce another harmful chemical (chloroform).

#### ***4.4 Numerical simulation***

The six and eight coupled mass balance equations were solved numerically using the Quickest finite difference spatial discretization form combined with an Euler approximation in the time domain (Leonard, 1979, Chapra and Canale, 1988). The Quickest formulation is detailed in Appendix F. Its general form with reaction term  $\phi(C)$  is as follows:



$$\begin{aligned}
C_{k+1,i} = & \frac{CO}{R} \left( \alpha - \frac{1}{6} + \frac{CO^2}{6} \right) C_{k,i-2} + \frac{1}{R} \left( \alpha - 3\alpha CO + CO + \frac{CO^2}{2} - \frac{CO^3}{6} \right) C_{k,i-1} + \\
& \frac{1}{R} \left( R + 3\alpha CO - 2\alpha - CO^2 - \frac{CO}{2} + \frac{CO^3}{2} \right) C_{k,i} + \\
& \frac{1}{R} \left( \alpha - CO\alpha - 2\alpha - \frac{CO}{3} + \frac{CO^2}{2} - \frac{CO^3}{6} \right) C_{k,i+1} + \phi(C)
\end{aligned} \tag{23}$$

where  $i$  is the node position,  $k$  is the time step, CO is the Courant number and  $\alpha$  is the dispersion parameter.

$$CO = \frac{U\Delta t}{\Delta x} \tag{24}$$

$$\alpha = \frac{D\Delta t}{\Delta x^2} \tag{25}$$

The numerical solution incorporated initial and boundary conditions for each of the equations. The initial conditions specified that the concentration of each of the parameters along the length of the column was equivalent to the concentration in the experimental column: CT saturation, no gradient of nitrate, and a slug injection of acetate and strain KC. The shape of the slug injection is approximated as explained in section 4.5. A constant concentration along the column has also been considered as the starting condition for indigenous denitrifiers, at both solid and liquid phases. In addition to the initial conditions, boundary conditions were also specified in the numerical solution. At the entrance of the column, a Dirichlet boundary condition was used and at the end of the column, a Newman boundary condition was specified. These conditions are described by the following equations and are further detailed in Table 3:

$$C\{x,0\} = C_m \tag{26}$$

$$C\{0,t\} = C_m \tag{27}$$

$$\frac{\partial C_m}{\partial x} \{L,t\} = 0 \tag{27}$$

in which  $C_m$  represents each model variable.

**Table 3:** initial and boundary conditions.

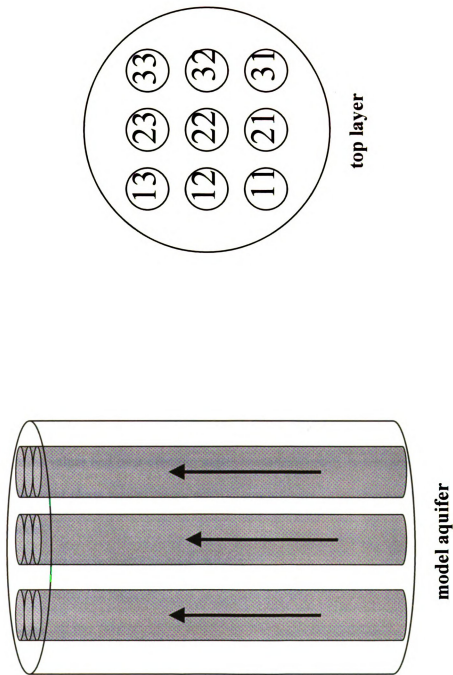
Model variable, $C_m$	Initial condition, $C_m$	$C_m$ at upstream boundary	$\frac{\delta C_m}{\delta x}$ at downstream boundary
$C_{CT}$	40 ppb	40 ppb	0
$C_N$	70 ppm	70 ppm	0
$C_A$	slug injection	0	0
$X_{KC}$	slug injection	0	0
$X'_{KC}$	slug injection	0	0
$X_{NF}$	$10^5$ cfu/mL	$10^5$ cfu/mL	0
$X'_{NF}$	$3 \times 10^6$ cfu/g	$3 \times 10^6$ cfu/g	0

The eight mass balance equations combined with the initial and boundary conditions made up the numerical model for predicting the eight model parameter concentrations, and was programmed using Mathcad. The computer program simulated the bioremediation processes at different locations within the 3-dimensional tank, representing each different KC-native flora ratio.

#### ***4.5 One-dimensional columns***

One-dimensional columns were (conceptually) placed in the 3-D tank to allow the prediction of CT-removal using the model presented in Sections 4.2 and 4.3. Nine columns were defined, each for every column of sampling ports, assuming that vertical flow in the 3D lab-scale model was mainly one-dimensional. Figure 21 is a schematic of the columns. They will be used to predict biological processes occurring in the matrix immediately after the inoculation event was finished and vertical flow, mimicking natural gradient flow, was restarted. Weekly feeding events could also be considered in the model if run for longer periods of time.

**Figure 21.** One-dimensional columns in the model aquifer.



In order to determine the starting conditions at each column to model the CT-removal, inoculation data for bromide and strain KC were used and the following assumptions and methodology were followed:

- Acetate is transported as a non-reactive tracer. Therefore, bromide data obtained at the end of the inoculation can be used for estimating acetate concentration at every sampling point. Since bromide data for layers 7 and 9 was not available, data from the first tracer study was considered. For each column a polynomial curve was fitted to the data to express the distribution of the chemical. Negative and high values ( $C/C_0 < 0$  and  $C/C_0 > 1$ ) were eliminated and changed for 0 and 100 ppm ( $C/C_0 = 1$ ) respectively.

- The liquid-phase KC profile obtained at the end of the inoculation was directly used as the starting conditions for each column, after addition of a trend line. Opposite to the approach used in Section 3.4, values of  $C/C_0 > 1$  were used. Biomass values for layers 7 and 9 were estimated from tracer and KC breakthroughs: bromide data was used as in the case of acetate, whereas KC was approximated using Figure 17. The ratio  $5.4 \times 10^9$  cfu/mg was used to convert plate counts data to ppm of biomass (as needed in the numerical model).

- The solid-phase KC distribution was determined from liquid-phase profiles and the soil loading capacity as explained in Section 3.5. Again, a best-fit equation was used to express this distribution. Negative values and over-capacity values were eliminated. A conversion factor was used to express the solid phase results (cfu/g soil) in liquid-phase concentration units (ppm) as required by the model.

Data for the nine columns are included in Appendix E.

#### ***4.6 Numerical results***

Figures 22 to 32 show the numerical results for columns 12, 21 and 33 (see Figure 21) using the six-equation numerical model. They were modeled using the tracer and biomass data obtained during the inoculation and considering both absence and presence of (denitrifying)

native flora. The three columns represent the range of conditions occurring in the 3D tank, from high concentrations of acetate and strain KC in columns 12 and 21, to low concentrations in column 33, the farthest from the injection point. The other columns (11, 13, 22, 23, 31 and 32, Figure 21) presented similar distributions.

#### 4.6.a. Initial conditions

Figures 22.a, 23.a and 24.a represent the starting conditions for the three columns modeled. The levels of starting biomass (KC transported) differ from one column to another. Whereas two of the columns, 12 and 21, show saturation of KC in the soil particles ( $3 \times 10^7$  cfu/g or 24 ppm expressed in liquid-phase units), column 33 presents KC concentrations in the soil one order of magnitude lower. At the same time, acetate levels also decrease from columns 12 and 21 to column 33, although less substantially.

#### 4.6.b. Growth substrate utilization

The differences in biomass distribution affect not only CT degradation but also nutrient consumption. As shown in figures 22, 23 and 24, graphs b and c, nitrate and acetate levels decrease much faster in columns 12 and 21 than in column 33. Twenty-four hours after the beginning of the simulation, after inoculation, acetate has been almost totally depleted in columns 12 and 21, while column 33 still has high acetate concentrations, even when the initial concentrations were lower in the latter column. In all columns acetate was consumed, as predicted by the numerical model, before 72 hours, and by the end of the week there is no acetate remaining in any column.

#### 4.6.c. CT degradation and biofilm establishment

On the other hand, CT degradation is also carried out at different rates in the several columns. By the end of the first week of biological activity, CT is totally degraded in the bioactive zone of columns 12 and 21, whereas noticeable amounts of CT still remain in column 33, which shows degradation efficiencies of about 75% (Figure 26.c).

**Figure 22.** Predictions for column 12 using the 6-equation model.  
Initial conditions and growth substrate utilization.

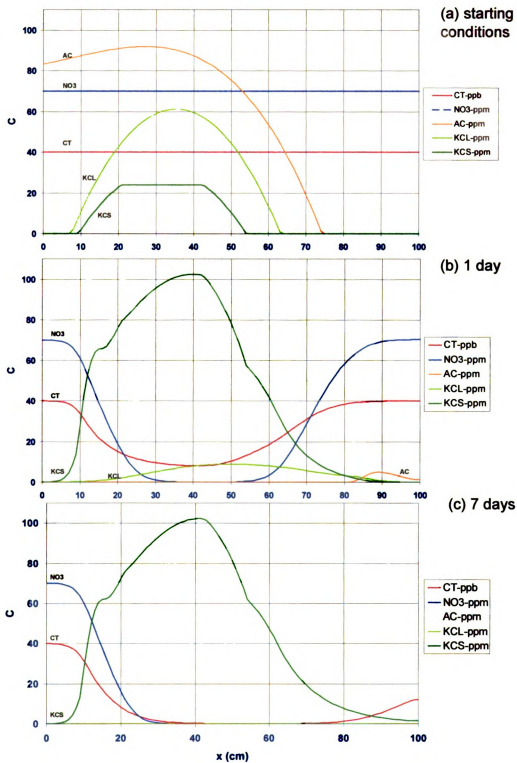


**Figure 23.** Prediction for column 21 using the 6-equation model.  
Starting conditions and growth substrate utilization.

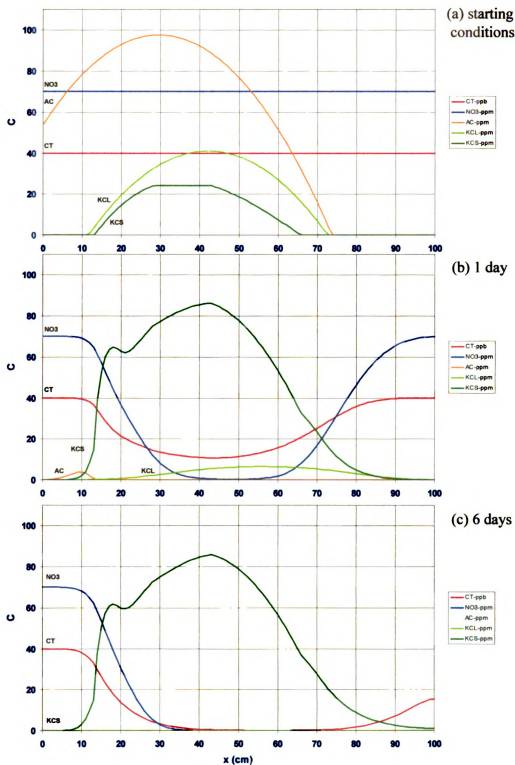


**Figure 24.** Predictions for column 33 using the 6-equation model.  
Starting conditions and growth substrate utilization.

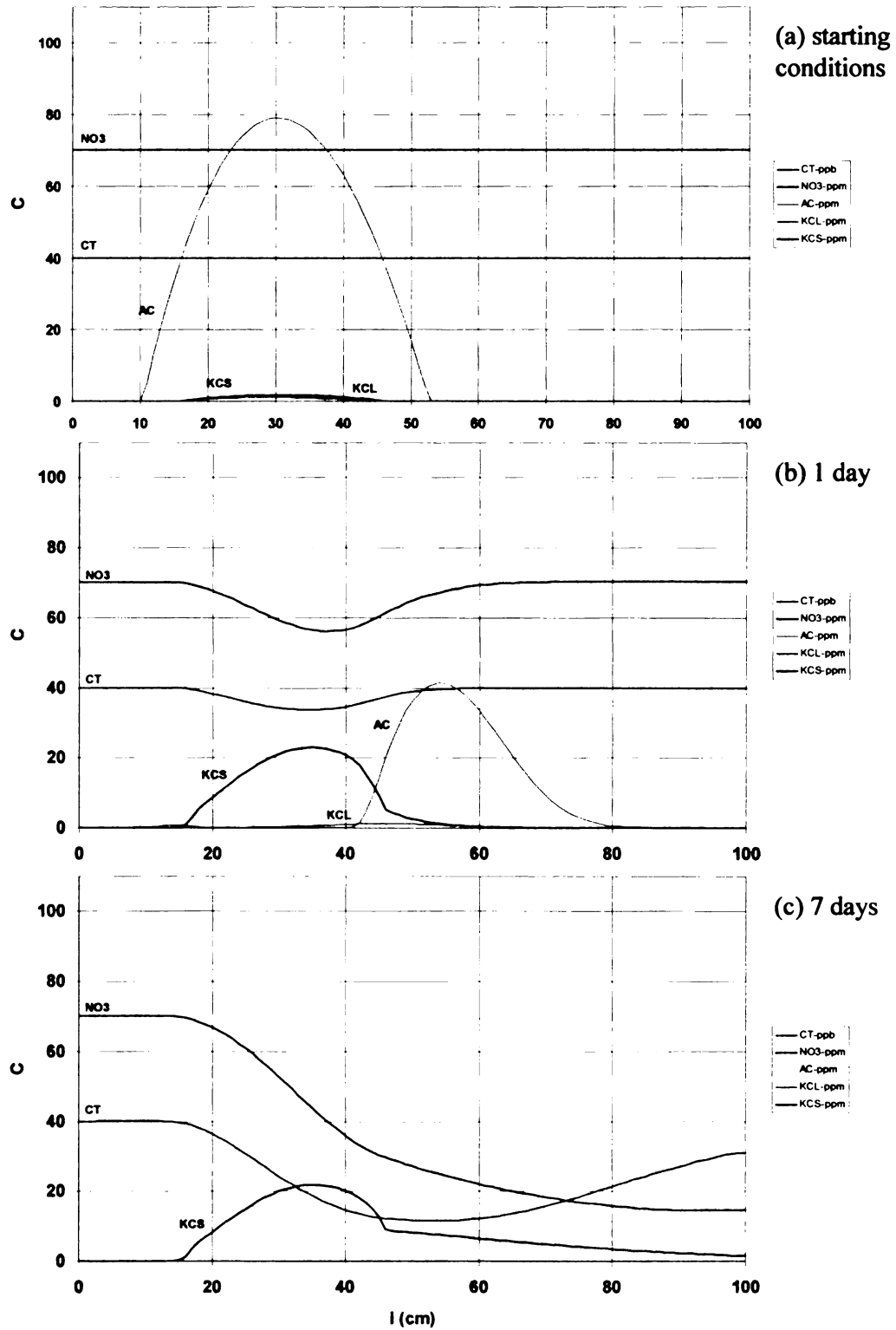




**Figure 25.** CT-removal and biofilm establishment in column 12 using the 6-equation model.

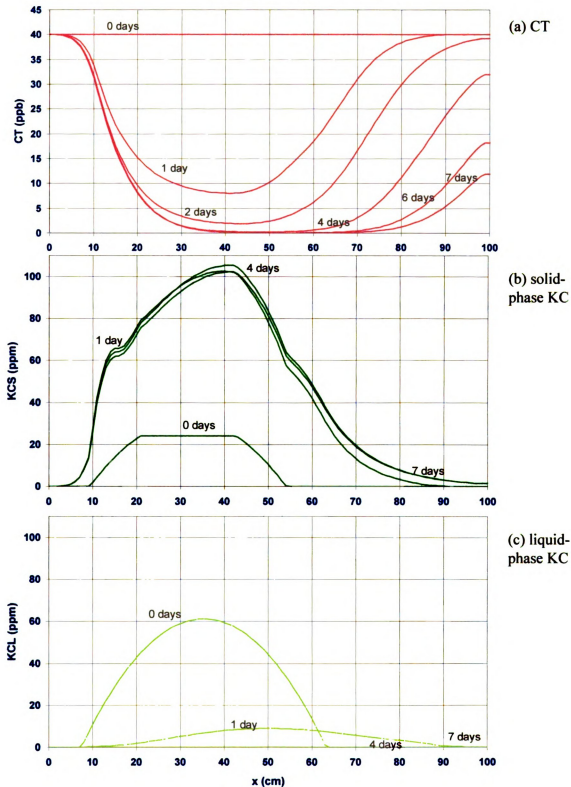


**Figure 26.** CT-removal and biofilm establishment for column 21 using the 6-equation model.

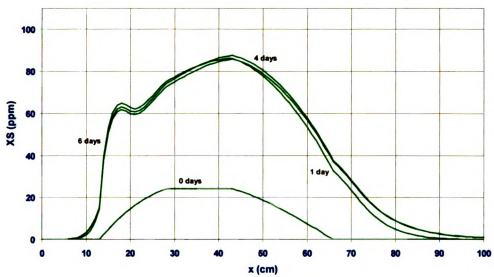
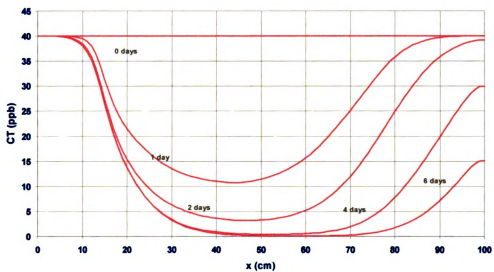
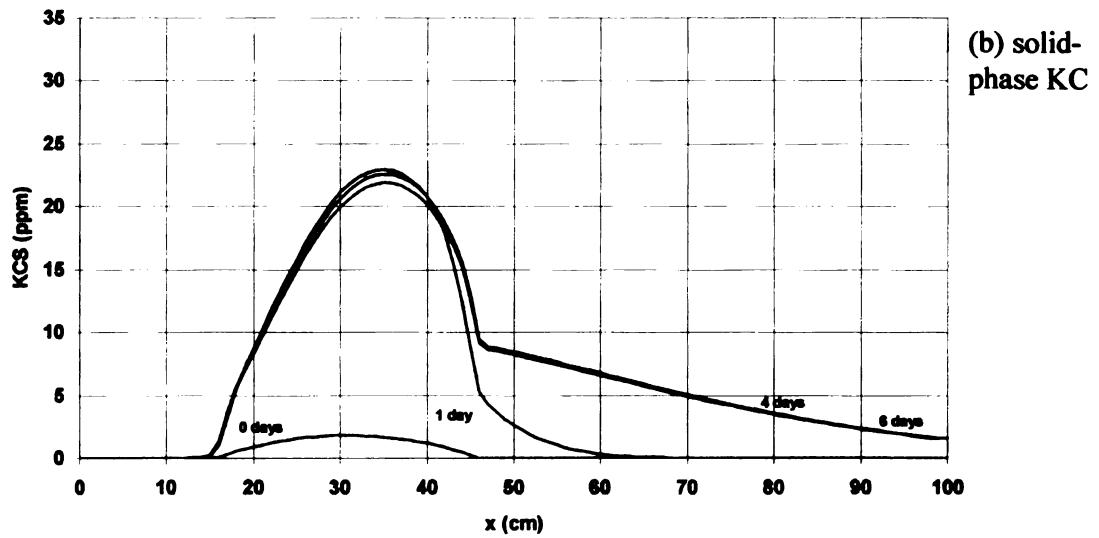
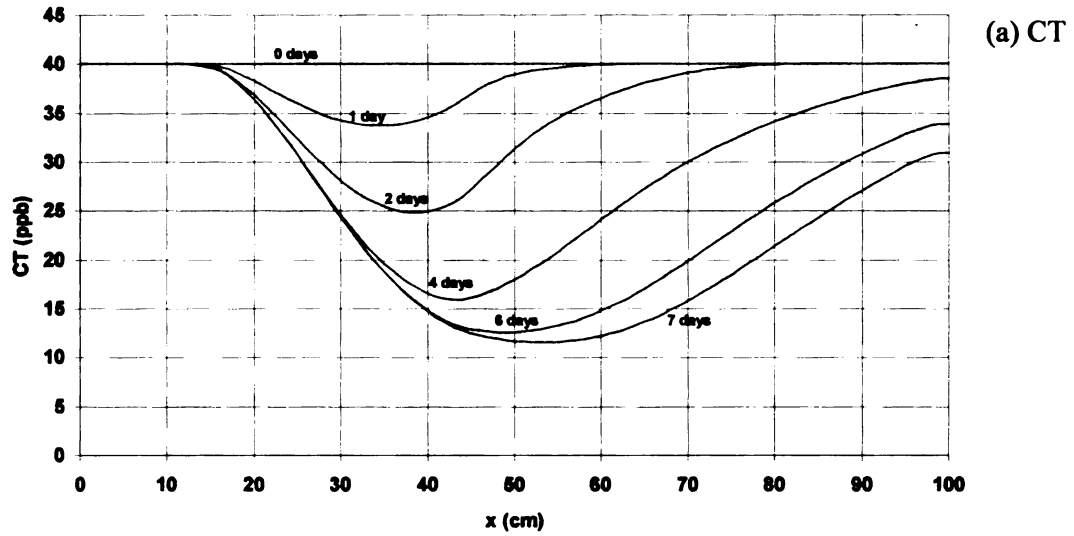


**Figure 27. CT-removal and biofilm establishment for column 33 using the 6-equation model.**



Figures 25, 26 and 27 show the CT-removal and the biofilm establishment during the first week, immediately after KC has been inoculated into the tank. In all cases (Fig. 25.a, 26.a, 27.a) CT is degraded as it enters the reactive zone from the influent point (0 cm). The concentrations of CT decrease over time as a result of both biological activity and advection. Furthermore, different removals are observed in the three columns modeled, as a result of the different amount of KC present. Column 12 (Fig. 25.a) shows degradation efficiencies approaching 99%, whereas column 33 (Fig. 27.a) does not degrade CT in more than 70% for the first week of biological activity. Finally, the remediated water moves towards the top of the tank causing the shift on CT curves.

Contrary to CT, solid-phase KC is not directly transported by advection, and thus remains approximately constant over time (Fig. 25.b, 26.b, and 27.b). During the first 24 hours, the biofilm grows significantly due to the added nutrients, although the biofilm in column 33 is not as robust as the others. As nutrients disappear, decay becomes greater than growth and the biofilm tends to decrease, but only slightly. Hence, the biofilm seems to remain almost unaltered even though there are no nutrients present. Detachment also causes a decrease in the biofilm biomass, delivering KC to the liquid phase. This would represent a constant source of liquid-phase KC; however, the low detachment rates used in the model seems to produce lower amounts of KC in the liquid than otherwise can be expected.

The transport and evolution of liquid-phase KC in column 12 can be observed in Figure 25.c. As inferred from Figures 25.b and 25.c, the initial biomass present in the liquid rapidly attaches to the soil and thus decreases its liquid-phase concentration substantially over the first 24 hours, even though it also grows based on the acetate and nitrate presents. With time, liquid-phase KC seems to disappear as it gets attached to the soil at faster rates than it is detached. At the same time, its peak is transported downstream of the inoculation zone by the advection. Similar results were obtained from columns 21 and 33.

Overall, these results indicate that, although steady-state conditions had not been reached and the biofilms were still developing, the lag time required to achieve above 99% CT-removal in

the aquifer is short, and low CT-concentrations, below regulatory limits, could be expected downstream of the reactive zone within a week. However, this time increases as less KC is transported. That is, lower CT levels will be expected close to the injection point than far from it, where initial levels of strain KC were smaller.

#### ***4.7 Feeding events***

A first feeding event, one week after the inoculation, was simulated for columns 12 and 33, the last one with presence of native flora. In order to determine the chemical distribution along each column at the end of the feeding event and thus the starting conditions for the second week of biological activity, bromide inoculation data was used again. Acetate, added to the feeding solution to a concentration of 100 ppm, and nitrate, present in the Schoolcraft groundwater used for the feeding solution at 70 ppm, were assumed to follow bromide distribution (Witt, 1998). On the other hand, CT, which was added to the solution to obtain aquifer conditions, was assumed to be retarded with respect to the tracer transport. Since three hours of cross-flow pumping do not allow for complete saturation of CT, low concentrations are expected in leading edges of the cross-flow influence zone. Outside of the cross-flow inoculation zone, where the polynomial lines representing tracer distribution present negative values, the concentrations at the end of the first week of vertical-flow were considered to remain constant during the feeding event and thus used as initial conditions for the second week. At the same time, KC in the liquid phase was assumed zero across the cross-flow pumping influence zone, since the feeding did not incorporate KC, and the modeled concentrations of day 7, prior to the feeding event, were kept as the initial conditions for the second week for the rest of the column (outside the cross-flow zone of influence). Finally, solid-phase KC was assumed to remain the same as prior to the feeding event.

Figures 28 and 29 show the initial conditions for the two columns modeled, 12 and 33. It seems that the assumption adopted to represent the flow behavior occurred during the inoculation

does not reflect a realistic situation, since it allows null values to exist next to high concentration values. According to these results, flow during the inoculation would have occurred only in the central zone affected by the feeding polynomial line and the rest of the column would have remained stagnant. However, this is not believed to be an accurate assumption. It also assumes that any previous chemical present in the liquid phase in the zone of influence would be flushed out.

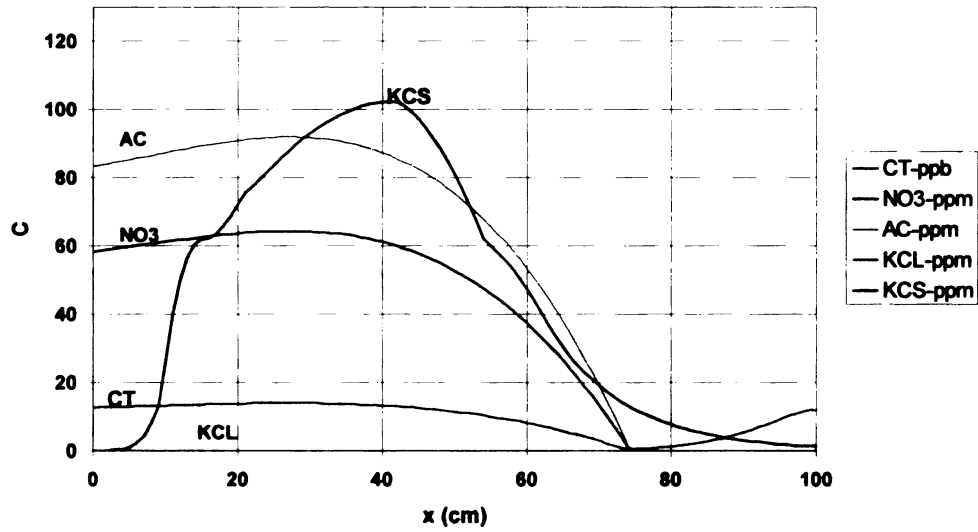
If a feeding event was conducted one week after the inoculation without recirculation of water and assuming modeled conditions exist in the tank, the sequence of events schematized in Figure 30 could represent the movement of water and chemicals across the tank. At the beginning of the pumping, high concentrated groundwater would enter the tank through the influent point. Inside the tank, and according to the previously presented results, low concentration zones of nitrate and CT would occur near the injection point, whereas higher concentrations would be expected far from it and near column 33. Acetate would be depleted everywhere. Finally, small quantities of liquid-phase KC would be present everywhere in the tank where an active biofilm is present.

As feeding groundwater enters the tank, the old water is displaced towards the effluent varying in a 3-dimensional sense. Hence, low-concentration water from columns 12 and 21 would be transported to column 33 and its vicinity, whereas water from column 33 is flushed out as effluent. This would originate a decrease in both nitrate and CT in column 33 since clean water is entering the region. As the feeding event progresses, the new feed water, with high concentrations of nitrate, CT and acetate, reaches more distant points and approaches the effluent port, displacing the clean water that had arrived there from columns 12 and 21.

Figures 28 and 29 present the numerical results at the end of the second week of activity, one week after the first feeding event was carried out. Both biofilms increased over the second week as a result of the new nutrients added into the system. Nevertheless, column 33 still shows CT-removal efficiencies lower than 99%, whereas CT-degradation in column 12 is complete.

**Figure 28.** Predictions for the first feeding event in column 12 using the 6-equation model.

(a) distribution of chemicals at the end of the feeding event



(b) 7 days after the feeding event

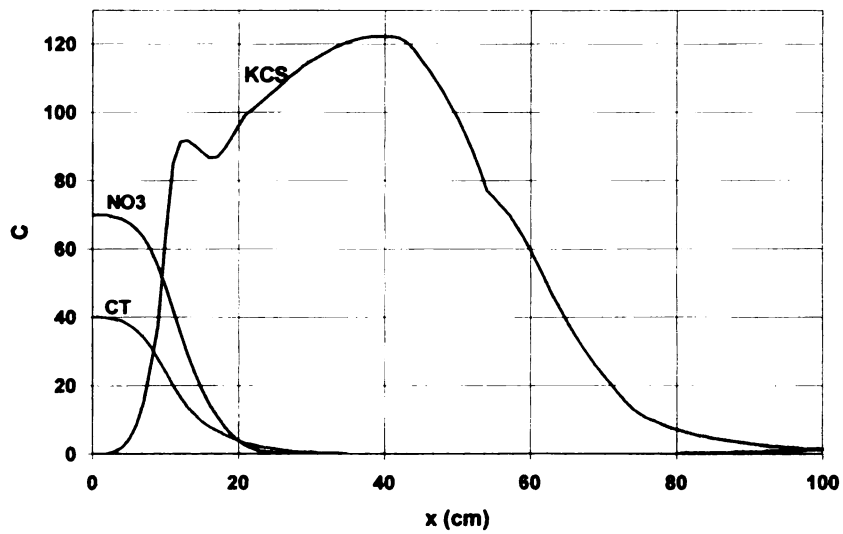
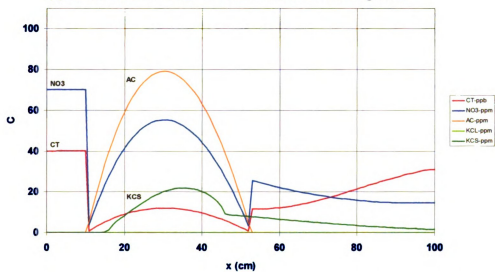


**Figure 29.** Predictions for column 33 after the first feeding event using the 6-equation model.

(a) distribution of chemicals at the end of the feeding event



(b) 7 days after the feeding event

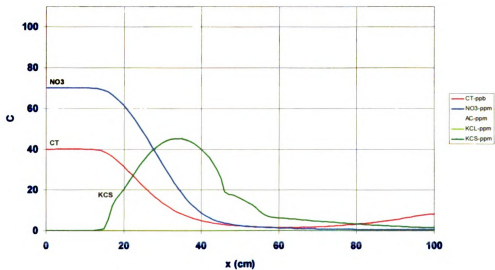
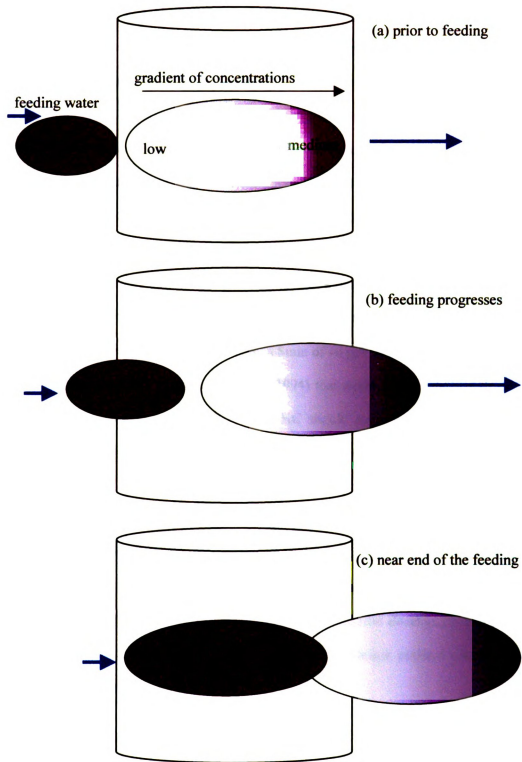




**Figure 30.** Schematics of a 3-hour feeding event.



#### **4.8 Competition**

Columns 12, 21 and 33 (Fig. 21), were modeled again using the eight-equation model that incorporates competition with native denitrifiers. The initial and boundary conditions are specified in Table 3. Figures 31, 32 and 33 graph the numerical results of these simulations.

The main effect of incorporating the native flora is observed on the nutrient profiles. As both strain KC and native denitrifiers consume the same electron donor, acetate, and acceptor, nitrate, it is expected that these substrates would be depleted faster than just considering the presence of KC, regardless of the succession they may have. That is, even when KC overcomes the native flora at all times, acetate and nitrate profiles along the column decrease faster than with the 6-equation model, simply because the presence of native flora introduces new sinks for them. However, the consumption of chemicals will vary depending on the  $S_{min}$  considered as explained in Section 4.3. For the predictions presented here, a  $S_{min}$  of 10 ppb of acetate was used.

It was experimentally determined (Knoll, 1994) that strain KC grows at 4-times faster rate than native denitrifiers. As a result of this, KC should overcome native flora in most scenarios. The numerical model used in this work predicts that native denitrifiers will be able to compete and grow over their survival limits only if low levels of KC are present and still some nutrients are available. The higher the concentration of KC, the lower the growth of native flora. Thus, the growth of native flora is only observed in early stages of the biofilm formation, in low KC sections of columns 12 and 21, and in most locations of column 33, where KC and native flora levels are comparable (see Fig. 31, 32 and 33). As the biofilm develops, however, native flora becomes less competitive and is displaced due to insufficient nutrient consumption to generate additional biomass.

**Figure 31.** Predictions for column 12 using the 8-equation competition model. Starting conditions and growth substrate utilization.

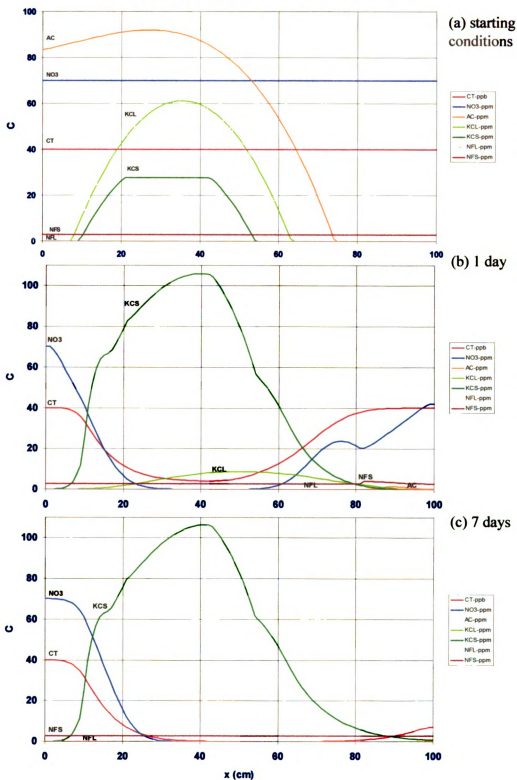


**Figure 32.** Predictions for column 21 using the 8-equation competition model.  
Starting conditions and growth substrate utilization.

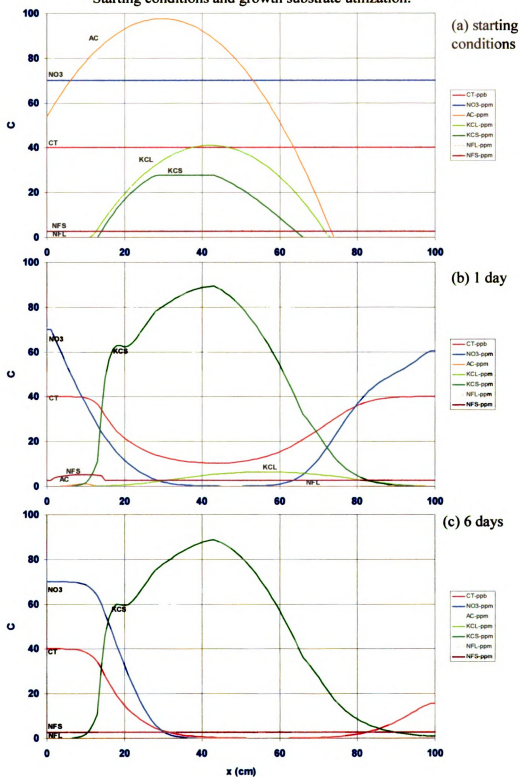
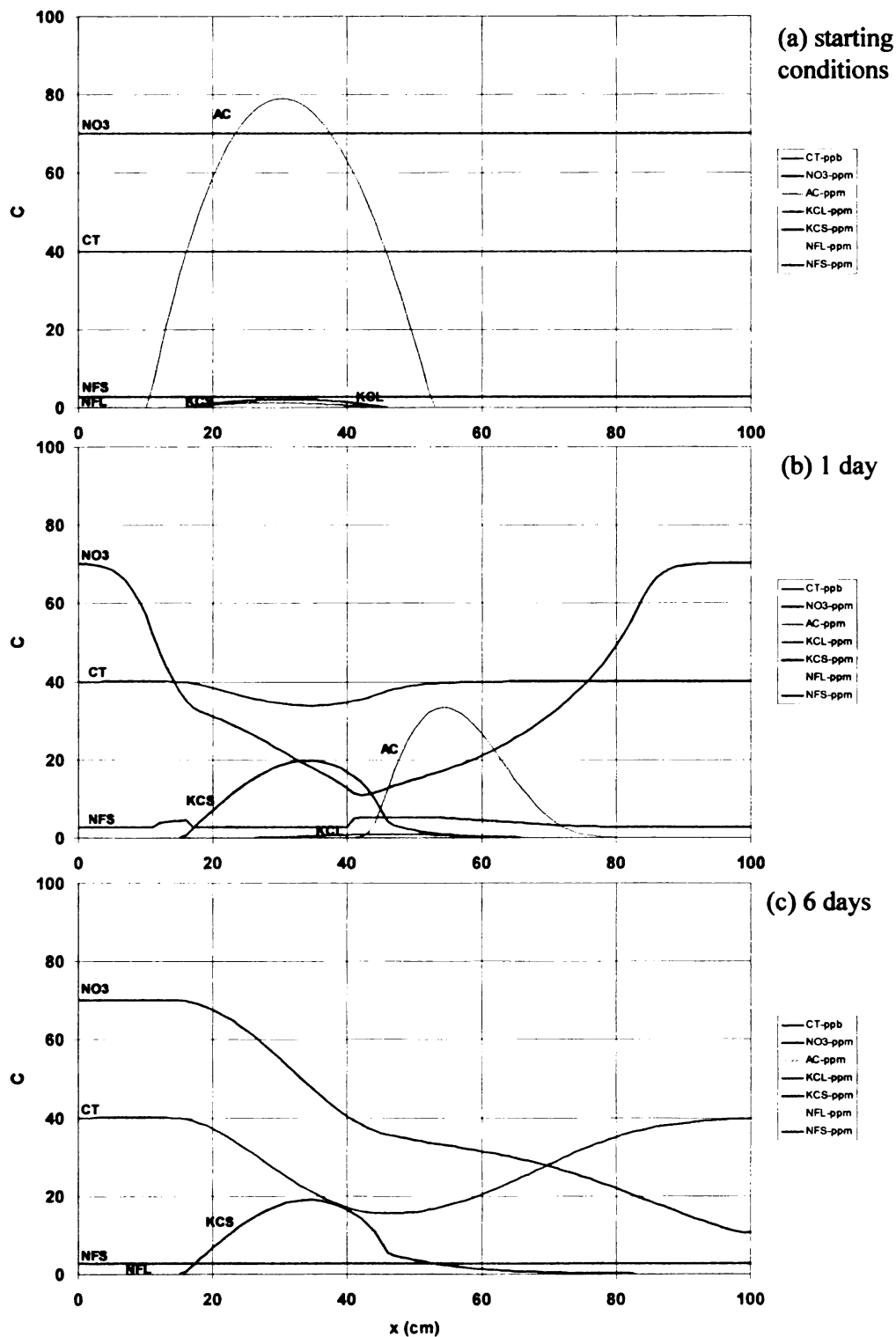


**Figure 33.** Predictions for column 33 using the 8-equation competition model.



#### ***4.9 Varying groundwater linear velocity and KC's yield for nitrate***

A simple analysis of input parameters was performed for the 6 and 8-equation models to observe the effect of changing some variables. Columns 12 and 33 were modeled again varying the linear velocity,  $U$ , and the strain KC's yield for nitrate,  $Y_{\text{KCNI}}$ . Decreasing the linear velocity would allow the rough estimation of the biological behavior if a hypothetical scenario with groundwater recirculation was considered; that is, if clean water downstream of the treatment zone is extracted and reinjected into the bioactive zone to increase the mixing in the aquifer. In the case of KC's yield for nitrate, the simulation was performed again using the (liquid batch) experimentally-derived value (0.4 g cell/g nitrate, Knoll, 1994), since the value previously used (2.001) had been derived from a model optimization (Hyndman, personal communication) and differed from the experimental one by an order of magnitude.

Figures 34 and 35 shows the numerical prediction for column 33 (with and without competition with native flora) when the linear velocity is reduced to one-third its original value (14.8/3). An important effect is observed on the nitrate profile with respect to previous predictions (Fig. 27), which decreases at a faster rate when less nitrogen is available (when advection is slower). In the 8-equation model, with presence of native denitrifiers, it can even become depleted prior to total consumption of acetate. Hence, extra carbon would be available for other populations using another electron acceptor, such as sulfate. In the case of Schoolcraft, this would be a major concern, since the sulfate-reducing activity promotes the formation of chloroform as a result of CT degradation. When high levels of KC were present (columns 12 and 21), nevertheless, this situation was not observed, and acetate would be depleted faster than nitrate.

Similar results are obtained when  $Y_{\text{KCNI}}$  is reduced from 2.001 to 0.4, the value experimentally determined by Knoll, 1994. These results can be seen in Figure 36, representing column 33 one day after the inoculation. Again, major effects are observed in the nitrate profile,

**Figure 34.** Predictions for column 33 using the 6-equation model and one-third of the linear groundwater velocity.

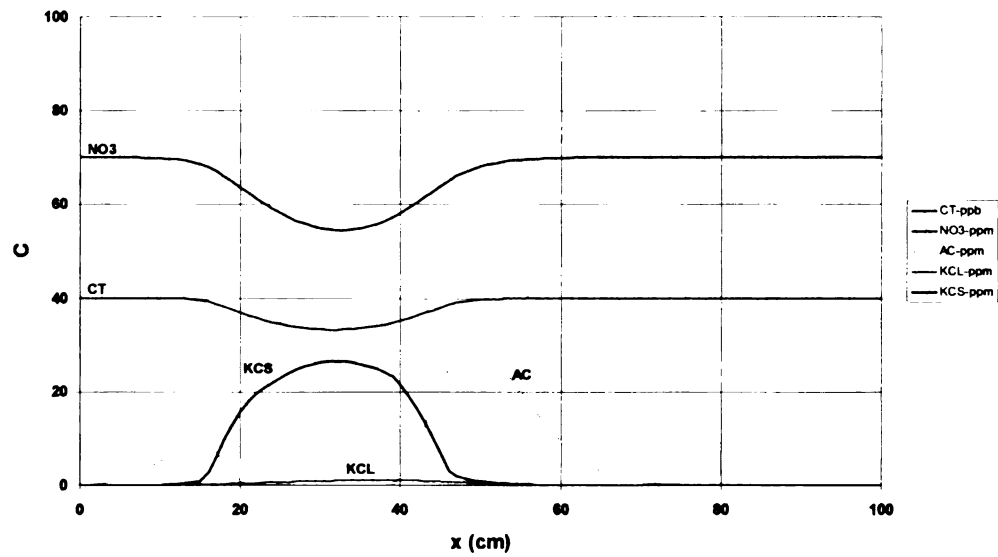


**Figure 35.** Prediction for column 33 using the 8-equation model and one-third of the linear groundwater velocity.

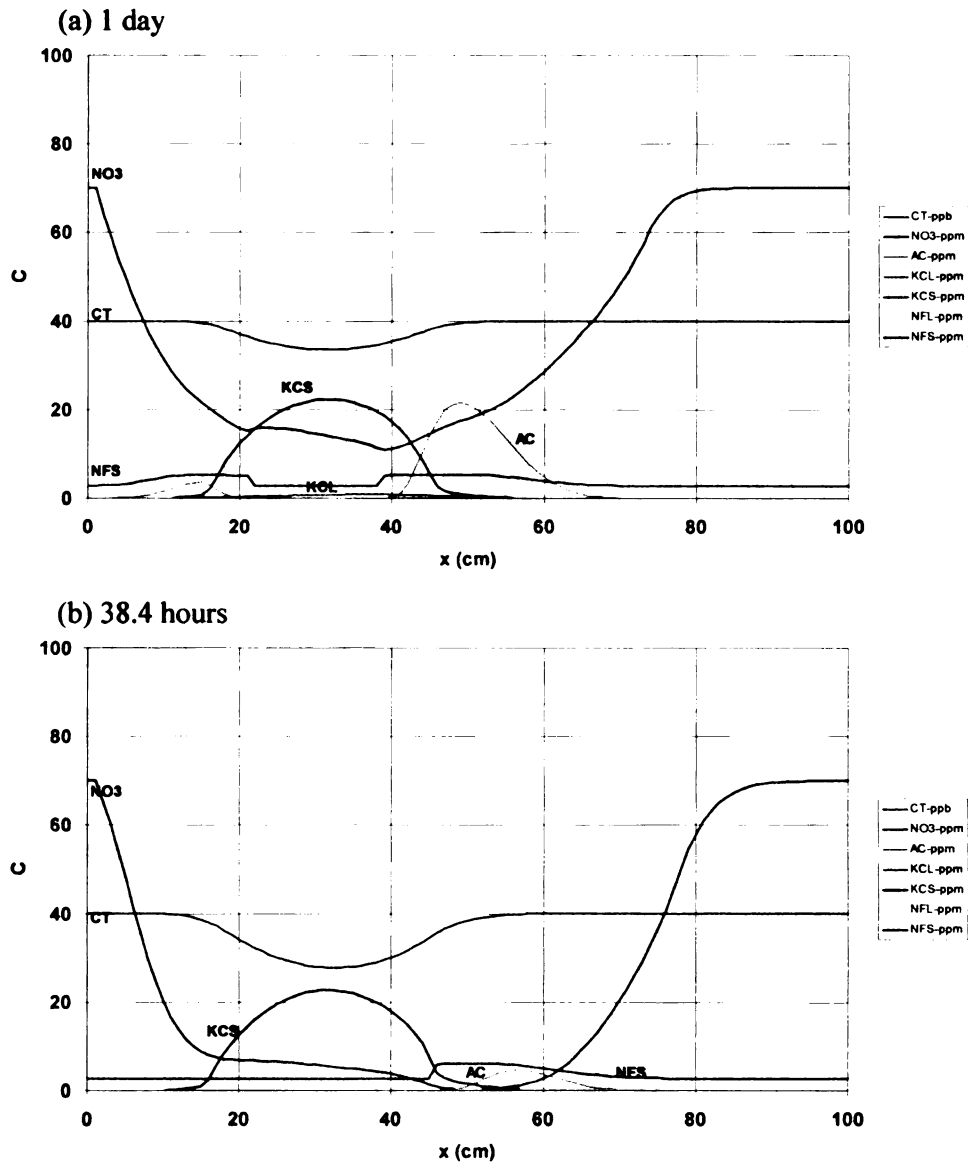
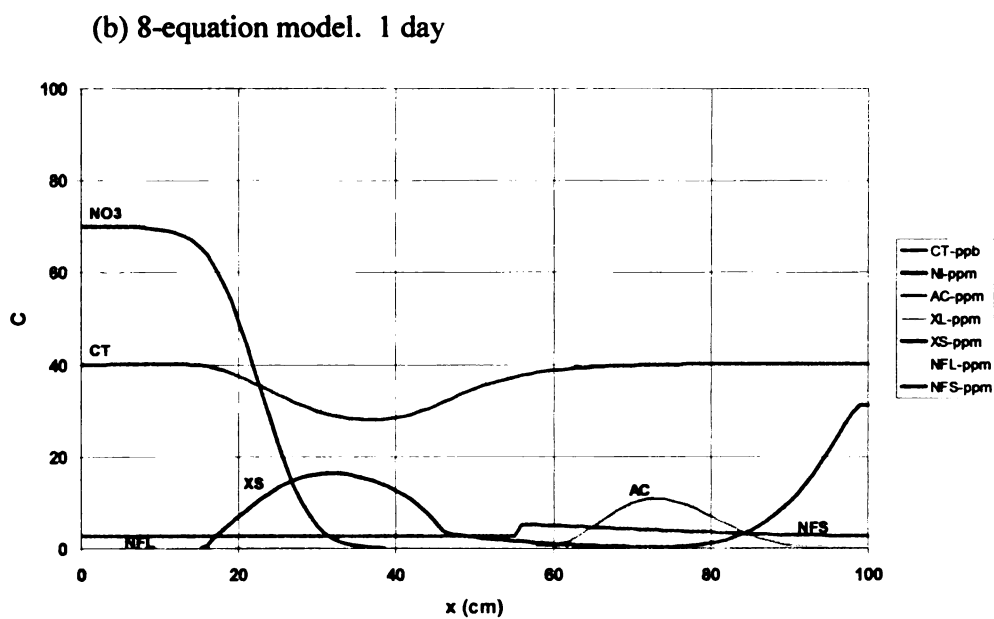
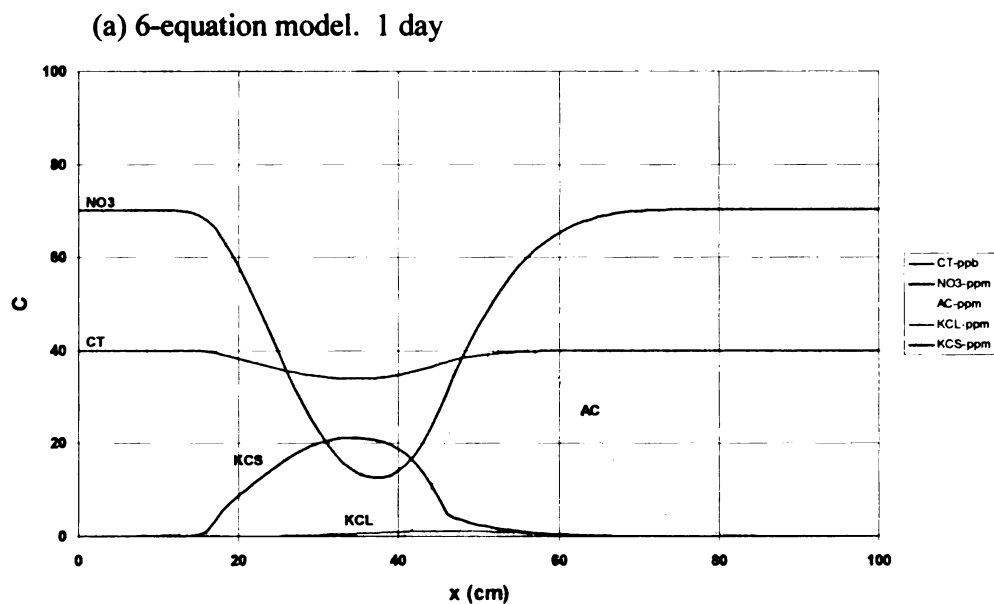




**Figure 36.** Predictions for column 33 using the 6 and 8-equation models and low  $Y_{NI}$ .



which decreases faster since there is a bigger need for nitrogen uptake by KC. This may lead to situations of sulfate-reducing activity due to the extra carbon present in the system.

#### **4.10 Numerical stability**

Numerical stability for the Quickest solution is based on two parameters: the Courant number, CO, and the diffusion parameter,  $\alpha$ . Following Leonard, 1979, the criteria are:

$$CO \leq 1 \quad (29)$$

$$\left[ \alpha \leq \frac{(3 - 2 \cdot CO) \cdot (1 - CO^2)}{6 \cdot (1 - 2 \cdot CO)} \right] \text{ if } CO < \frac{1}{2} \quad (30)$$

$$\left[ \alpha \leq \frac{(3 - 2 \cdot CO) \cdot (CO^2 - 1)}{6 \cdot (2 \cdot CO - 1)} \right] \text{ if } CO > \frac{1}{2} \quad (31)$$

All criteria were met for the numerical model used to predict CT biodegradation. The model was programmed in Mathcad, using a time step,  $\Delta t$ , for the time derivative and a distance step,  $\Delta x$ , for the spatial derivatives, of 0.002 day and 1 cm respectively. That is, the computer program simulated concentrations of the eight variables at one hundred positions along the column and for five hundred time increments each day. Larger time steps could have been used to decrease computational efforts, but some instability was observed in this case. These values define a CO of 0.03 and an  $\alpha$  of 0.05, meeting the requirements presented above in Equations 29 and 30.

#### **4.11 Model Limitations**

As a simplification of the biological process, the numerical model has some limitations to represent the variety of biological phenomena taking place in the soil matrix. Both the 6 and 8-equation models presented in this thesis could be further developed to include situations so far not

considered. Particularly, some of the considerations that would improve the model focus on the kinetics of both strain KC and native flora under high and low nutrient conditions:

- The current model predicts constant kinetics for KC regardless the levels of nutrients present. That is, KC wouldn't grow when one of the two substrates is depleted, but the consumption of nutrients remain the same as when exponential growth occurs. However, it is known that under starving conditions, this kinetics may change considerably and maintenance and decay can be a major sink for nutrients present in the aquifer. At the same time, attachment and detachment rates could also be modified when lower substrate levels dominate the system.

- CT-degradation rates, which are assumed to be first order with respect to the levels of KC present and second order with respect to CT concentrations, also decrease under low metabolic rates. If according to the predictions starving conditions prevail in the system for long periods of time during feeding events, this change on degradation rates could have a significant effect of remediation performance. Thus, longer times would be needed to achieve high CT-removal efficiencies than predicted in this work.

- In a similar manner to strain KC, native flora also changes its kinetics from growing to starving conditions. Although no data for kinetic coefficients are now available, it is believed that native denitrifiers are much better competitors than KC under starving conditions. This could in turn affect the biofilm formation and the final output for competition presented here, which predict KC overcoming native flora in all scenarios. Although the 8-equation model used here considered the survival of native flora when no nutrients are available in an effort to account for the slow kinetics under starving conditions, further development is needed towards more realistic approaches.

Despite microbial kinetics, there are other aspects of this model that should be addressed in future studies. First, the utilization of the biomolecule by other microbes present should be considered. It is known that once secreted to the environment by KC, the biomolecule could undergo reaction with CT under the reducing agent of other bacteria. Hence, CT-degradation

would depend not only on KC and CT but also on other microbes. Second, model development in three dimensions could help explain the feeding events that occur in the cross-flow mode, and that are difficult to introduce into the one-dimensional vertical flow model as discussed in Section 4.7. The approach used here assumed a stagnant region to exist in the 3D model aquifer, a complete flushing out of chemicals and liquid-phase KC during cross-flow pumping, and no detachment from solid to liquid phase KC, assumptions that seem to contradict experimental observations. At the same time, 3D models could improve the analysis of biomass distribution that occurs during the inoculation. Finally, other aspects could be considered, such as microbial kinetics at pH not optimal for KC growth, iron availability, or sulfate-reducing activity and chloroform production, but it should be pointed out that the more the aspects introduced, the more the complexity of the model.

## ENGINEERING APPLICATION

In-situ bioremediation of Schoolcraft Plume A, contaminated with carbon tetrachloride and nitrate, has been the objective of study for several years at both the lab and the field. Results obtained over the past twelve years suggested that the remediation by bioaugmentation with *Pseudomonas stutzeri* strain KC by of creating a bioactive zone or biocurtain in the subsurface is an effective and feasible alternative for decontaminating the plume, a process that should soon be implemented by the MDEQ.

Working in the lab, with smaller reactors than the site itself, allows for testing of operations with reduced times, high control and lower costs. Although the information derived from lab experiments is not exactly representative of field conditions, its validity is often high. In this thesis, a complex model was able to provide unique 3-dimensional data. This microcosm was an extension of the traditional 1-dimensional soil columns. Soil columns (1-dimensional) provide useful data with the advantage of an easier analysis; a single space dimension facilitates numerical manipulation and study of the data. This data may be later applied to more complicated systems. However, working in a 3-dimensional lab-scale reactor may reproduce field conditions more closely and thus produce data directly related to the field. The data for chemicals and biomass transport occurring during injection events at the model aquifer has been presented and commented in this report. The ultimate goal is to provide information on how these processes take place in the field and use the findings to optimize the delivery of the system.

An important aspect of the reactor used for this work is not only the data it provided about Schoolcraft Plume A but also the experience obtained for future applications. That is, other conditions, or even other microcosms (with different soil matrix and/or different contaminants)

could be tested using the 3-dimensional model aquifer. Hence, it would be only a question of replacing the matrix and adapting the system to reproduce other conditions and other remediation strategies, thus allowing predicting the behavior once in the field. An interesting future application could be performed by repeating the experiment presented in this document under improved conditions, allowing for a better sampling and control of the biological process, and thus obtaining more information to complete the understanding of both the inoculation and the bioremediation processes. In the same Schoolcraft project framework, on the other hand, the system could be used to assess the bioremediation of Plume G, contaminated mainly with PCE and TCE and their degradation daughter-products. Again, simpler systems (one-dimensional columns, liquid microcosms, etc.) would still provide useful information about the process.

It should be mentioned, nevertheless, that running such a complicated system is not an easy task. Running a reactor always means periodic care; the system needs to be checked daily because something may get disconnected, clogged, etc. That is, there is always a necessity for checking proper functioning. When the reactor is much bigger than the commonly used one-dimensional columns, incorporates more connections and side-systems, and uses a soil matrix, the disruptions and complications multiply. During our first experiment, we learned valuable lessons for future runs. In order to improve these future experiments in the 3D tank, the following suggestions are made:

- Develop a consistent experimental design that allows maximizing the information obtained from the 3D experiment and prevents data gaps which limit interpretation.
- Measure volumes, flow rates, etc. periodically and completely so mass balances can be conducted on the data.
- Store all samples until all needed information has been obtained.
- Use a more stable method of tracer analysis. Do not use the bromide probe in line.

- Improve the mixing tank configuration to avoid variation in the influent rate. Pumps could be used for both influent (to the mixing tank) and effluent (from the mixing tank and to the 3D model aquifer), and an open line could be placed for any overflow.
- Place screens in influent and effluent points to reduce the clogging. Measure pressures at several points.
- Check and control the system periodically, for both physical and biological processes.
- If less concentration gradients are required, feedings (and inoculation) should be carried out in a close-loop manner to avoid new water entering the tank and thus tend to homogenize concentrations in the delivery zone.

#### ***Future aspects of the model***

A second important contribution of this thesis is the incorporation of the biomass competition aspects into the already existing modeling for KC's CT-remediation activity at Schoolcraft. Knoll, 1994, determined the basic kinetic parameters for two kinds of microorganisms present at the site: indigenous denitrifiers and introduced strain KC. These parameters have been used in the present study to incorporate the competition between the two kinds of microorganism into the 5-equation model originally created by Heine, (Witt, et al., 1995). The main aspect of this contribution, besides extending the microbial kinetic formulation of Schoolcraft Plume A, is the application of the approach to other systems and modeling efforts that numerically conceptualize biological activities in soil matrixes. Other scenarios, like Schoolcraft Plume G in which biostimulation of indigenous flora or bioaugmentation with new organisms will be explored, could be conceptualized in a similar manner. Hence, the same basic modeling ideas could be used although proper changes should be incorporated to adapt to each case.

Despite competition and chloroform production, a variety of other aspects could be incorporated into the existing model to improve its performance and thus make its predictions

more precise. Some of them are discussed in Section 4.11, like changes in microbial kinetics or pH-rate-dependence. It has been previously explained that pH plays a major role on KC activity through metals availability. Furthermore, it has been experimentally seen in the 3-dimensional cell how a failure in pH control can originate a major change in biomass competition, reducing strain KC' activity. The effect of pH is not only on metals availability and CT-degradation activity but on microbial kinetics as well: at different pH levels, microorganisms change their growing parameters, and species that would out compete at pH 8.2 could die out at pH 7. All these processes could be introduced into the model to increase its application to different scenarios. However, the level of complexity would increase substantially.



## CONCLUSIONS

This thesis presented the very first 3-dimensional experiment conducted in a lab-model aquifer under the Schoolcraft project framework. It was designed to mimic the remediation of Plume A, contaminated with CT, by bioaugmentation of *Pseudomonas stutzeri* strain KC in the soil matrix. Tracer tests were performed to study the flow characteristics in the reactor and, furthermore, an inoculation event was carried out to study the distribution of strain KC during and after an inoculation event. Data from the transport of species was used to predict the behavior of the remediation activity using previously developed one-dimensional models and furthermore incorporating new terms to account for the presence of native flora in the system.

The main findings of this work are as follows:

- Transport of a tracer in a 3D model aquifer was characterized during a three-hour cross-flow pumping event. These pumping conditions resulted in a zone of influence across the cell, achieving over 70% breakthrough at the effluent.
- The injection of chemicals through the cross-flow injection point creates a 3D gradient of concentrations, which decrease as distance from the injection point increases. An interpolation of the tracer data using GMS was performed.
- A conservative tracer is transported (vertically) asymmetrically with respect to the injection point due the model aquifer boundaries, thus showing an asymmetry of flow lines.
- Strain KC attaches to the soil particles during transport and hence behaves as a reactive chemical, showing retardation with respect of the movement of tracer. Attachment of bacteria to the soil particles is influenced by the collision efficiency and the blocking factor, and dependent on physiological characteristics of the cells, as well as ionic strength of the solution.

- An estimate of the amount of KC attached to the soil during an inoculation event is based on the soil loading capacity, a solid cell concentration at saturation derived from the clean-bed filtration theory.

- A numerical simulation of growth, substrate utilization and CT degradation was performed. This model included liquid and solid phase CT, liquid and solid phase strain KC, acetate and nitrate.

- The consumption of nutrients, as well as the CT-removal efficiencies, depends on the amount of KC present, which decreases at farther distances from the injection point.

- The one-dimensional model cannot accurately predict three-dimensional feeding delivery.

- The numerical simulation was modified incorporating the presence of native denitrifiers. Predictions of growth and CT-removal were obtained with and without the presence of this native flora.

- Strain KC overcomes native denitrifiers present in the aquifer, as predicted by the modified numerical model. However, the competition affects the availability of nutrients.

- The variation of the yield of KC for nitrate noticeably affects the numerical simulation, causing the depletion of nitrate before acetate when low yields are considered.

## RECOMMENDATIONS FOR FUTURE WORK

This thesis helped to answer some questions about the distribution of strain KC in the subsurface after an inoculation event and the possible effects of this distribution upon the bioremediation activity. However, and mainly because this has been the first work conducted in the 3-dimensional tank, some aspects remain unsolved and thus should be addressed in future studies to complete the knowledge of the process and also optimize the control over the system. The following work is recommended:

- Analyze existing tracer data and use it to refine a flow model for the cross and vertical flow patterns, incorporating flow streams, movement of solutes, and movement of particles. Develop a 3D-streamline model.

- Carry out a characterization of biomass distribution during an inoculation event, for liquid and solid phases. Include both strain KC and native flora.

- Carry out a characterization of biomass distribution after the formation of a biofilm and follow the degradation of CT.

- Experimentally determine the yield of KC for nitrate, as well as other kinetic parameters, in the 3D model aquifer to obtain the basic information of biofilm succession in soil matrixes. Use the experimental values to optimize a numerical model.

- Obtain experimental data of the feeding events in the 3D cell and model the delivery, transport and mixing of chemicals that takes place. Use the data to optimize the 3D cross-flow model.

- Address the model limitations stated in Section 4.11 to develop more realistic models that account for a wider spectrum of biological and physical phenomena.

## **APPENDIX A**

Appendix A.

First cross-flow bromide tracer study

Table A.1: 1st cross-flow tracer study. Liquid samples (bromide).

port #	location			C/Co					
	x (m)	y (m)	z (m)	30 min	60 min	90 min	120 min	150min	180 min
300	0.0001	0.3048	0.3048	1.00	1.00	1.00	1.00	1.00	1.00
3000	0.6096	0.3048	0.3048	0.02	0.02	0.09	0.28	0.41	0.67
111	0.1524	0.1524	0.1524				0.77	0.80	0.97
112	0.1524	0.3048	0.1524				0.79	0.80	1.0(*)
113	0.1524	0.4572	0.1524				0.79	0.87	1.0(*)
121	0.3048	0.1524	0.1524				0.77	0.84	0.86
123							0.74		0.96
131	0.4572	0.1524	0.1524					0.10	0.45
132							0.09		0.66
212	0.1524	0.3048	0.2286	0.80	0.67	0.66	0.77	0.87	1.0(*)
222	0.3048	0.3048	0.2286		0.57	0.59	0.83	0.80	1.0(*)
232	0.4572	0.3048	0.2286				0.77	0.93	0.96
311	0.1524	0.1524	0.3048	0.90	0.80	0.66	0.77	0.91	1.0(*)
312	0.1524	0.3048	0.3048	0.96	0.70	0.75	0.83	0.91	0.97
313	0.1524	0.4572	0.3048	0.78	0.78	0.72	0.77	0.84	1.0(*)
321	0.3048	0.1524	0.3048		0.20	0.61	0.79	0.84	1.0(*)
322					0.75	0.69	0.77		1.0(*)
331	0.4572	0.1524	0.3048				0.19	0.93	0.96
332	0.4572	0.3048	0.3048				0.86	1.01	0.96
412	0.1524	0.3048	0.381	0.78	0.78	0.66	0.83	0.91	0.93
422	0.3048	0.3048	0.381		0.78	0.72		0.80	1.0(*)
432									1.0(*)
511	0.1524	0.1524	0.4572				0.77	0.87	0.86
512	0.1524	0.3048	0.4572				0.79	0.84	0.93
513	0.1524	0.4572	0.4572				0.86	0.77	1.0(*)
521	0.3048	0.1524	0.4572					0.83	
522	0.3048	0.3048	0.4572				0.86	0.93	1.00
523	0.3048	0.4572	0.4572				0.83	0.97	0.89
612	0.1524	0.3048	0.5334					0.84	1.0(*)
622	0.3048	0.3048	0.5334					0.90	
711	0.1524	0.1524	0.6096					0.37	1.0(*)
712	0.1524	0.3048	0.6096					0.73	0.93
713	0.1524	0.4572	0.6096					0.80	1.0(*)
721	0.3048	0.1524	0.6096					0.05	0.09
722	0.3048	0.3048	0.6096					0.10	0.34
723	0.3048	0.4572	0.6096					0.09	0.09
731	0.4572	0.1524	0.6096					0.06	0.05
732	0.4572	0.3048	0.6096					0.05	0.04
812									0.96

port #	location			C/Co					
	x (m)	y (m)	z (m)	30 min	60 min	90 min	120 min	150min	180 min
822									0.04
832									0.03
911									0.10
913									0.03
921									0.03
922									0.02

**Table A.2:** 1st crosflow tracer study. Flow rates.

time (min)	flow rate (ml/min)
0	276
30	280
60	286
90	300
120	286
150	266
180	260
average	279.14

## **APPENDIX B**

Appendix B.

Vertical-flow bromide tracer study

**Table B.1:** Vertical-flow tracer study. Liquid samples.

port #	ppm NaBr									
	0 h	16 h	24 h	30 h	31 h	32 h	33 h	34 h	35 h	36 h
1	74.63	67.70	62.04	71.33						
2	74.63	67.70	62.04	71.33						
4	74.63	67.70	62.04	71.33						
6	74.63	67.70	62.04	71.33						
111		69.65	69.53							
112		74.77	62.04							
113		74.77	66.94							
121		75.54	64.45							
122		70.18	62.04							
123		70.18	64.45							
131		80.30	67.87							
132		70.06	67.87							
133		67.72	64.73							
311		72.16	66.94							
312		72.16	69.53							
313		35.51	64.45							
321		60.56	64.45							
322		70.18	62.04							
323		72.81	66.94							
331		67.72	64.73							
332		63.26	64.73							
333		65.45	64.73							
511		15.16	69.53							
512		9.91	66.94							
513		6.25	51.31							
521		14.39	55.36							
522		50.37	66.94							
523		56.26	64.45							
531		21.99	67.87							
532		9.38	64.73							
533		8.19	64.73							
711		0.00	9.64							
712		0.00	11.66							
713		0.00	7.97							
721		10.72	8.94							
722		5.95	39.33							
723		4.59	57.50							
731		0.00	34.94							
732		0.00	14.88							
733		0.00	6.96							
812					48.12	66.16	76.30	79.91	74.44	
822				54.87	65.36	77.23	79.21	76.97	74.44	
832				35.42	50.27	68.77	70.78	71.40	77.36	



port #	0 h	16 h	24 h	30 h	31 h	32 h	33 h	34 h	35 h	36 h
911		0.00	6.35		13.53	41.59	60.91	74.13	74.44	
912		0.00	6.11		23.89	40.01	58.67	71.40	71.63	
913		0.00					15.19	21.48	33.20	48.03
921		0.00	8.94	3.64	3.64	9.56	17.65	26.91	40.23	56.22
922		0.00	4.87	12.95	37.01	58.91	70.78	71.40	71.63	
923		0.00	5.45	29.74	52.52	74.30	76.30	74.13	77.36	
931		0.00	4.33	8.00	23.89	52.46	65.66	71.40	74.44	
932		0.00	4.77	2.15	2.15	13.55	36.02	40.66	56.87	71.20
933		0.00	4.77	3.06	12.40	30.52	48.63	57.00	66.33	71.20
1000		0.00	1.53							

## **APPENDIX C**

Appendix C.

CT-sorption study

Table C.1: Ct sorption study. Liquid samples (ppb).

port #	ppb CT								
	16 h	24 h	48 h	72 h	96 h	120 h	138 h	146 h	161 h
1	48.54	43.65	49.92	54.67	64.51	47.64	56.57	36.71	42.00
2	48.54	43.65	49.92	54.67	64.51	47.64	56.57	36.71	42.00
4	48.54	43.65	49.92	54.67	64.51	47.64	56.57	36.71	42.00
6	48.54	43.65	49.92	54.67	64.51	47.64	56.57	36.71	42.00
111		31.90	37.78	34.71		39.61		33.79	
112		45.59	37.46	41.81		41.82		39.23	
113		41.33	36.95	44.27		38.09		54.56	
121		34.09	37.77	40.11		39.07		51.77	
122		38.80	43.13	40.94		45.78		35.38	
123		43.83	44.91			39.09		34.12	
131		34.91	34.13	37.24		33.02		27.56	
132		34.28	36.57	30.12		32.54		41.94	
133		35.37	35.34	43.16		44.27		42.01	
311		26.54		44.92		40.28		54.40	
312		37.70	36.79	43.39		43.50		53.30	
313		18.34	35.52	37.68		47.93		48.12	
321		30.70	42.61	36.23		50.46		43.73	
322		37.64	43.55	31.06		45.14		55.51	
323		37.83		35.89		44.49		56.03	
331		33.29	35.99	42.06		45.52		53.79	
332		29.73	32.02	38.47		44.25		51.49	
333		32.76	35.92	32.44		42.11		54.41	
511		12.54	37.10	36.68		48.15		46.89	
512		9.90	37.52	35.90		46.84		49.18	
513		3.42		40.04		44.83		45.66	
521		6.17	34.60	31.49		42.76		43.85	
522		26.49	33.03	35.84		44.55		49.22	
523		27.34	36.70	27.79		45.83		40.81	
531		18.51	37.74	33.43		45.45		51.38	
532		14.16	36.64	40.11		51.66		48.14	
533		17.20	32.69	40.69		45.15		54.08	
711		1.68	29.51	36.71		39.16		44.85	
712		1.69	23.00	29.35		39.42		43.54	
713		0.29	15.36	22.85		31.12		39.77	
721		4.55	31.87	31.06		42.24		43.49	
722		2.22		26.70		39.06		42.21	
723		1.86	32.08	18.96		46.80		44.14	
731		5.92	29.78	36.01		44.53		37.33	

port #	16 h	24 h	48 h	72 h	96 h	120 h	138 h	146 h	161 h
732		2.62	25.56	33.49		36.10		35.68	
733		2.04	27.66	32.41		38.92		38.13	
911		1.95	12.64	23.43		32.37		34.52	38.51
912		1.97	11.66	24.18		30.54		43.63	38.79
913			4.42	22.58		24.79		39.63	37.54
921		2.15	11.83	21.94		24.03		43.17	28.78
922		2.15	6.33	30.73		33.77		44.16	39.93
923		2.22	17.23	31.55		30.75		45.99	42.22
931		2.76	17.48	28.78		25.54		42.18	40.77
932		2.44	11.56	30.37		30.75		37.00	34.88
933			12.52	26.64		26.71		40.96	37.24
1000			4.98	17.85	14.67	24.67		24.44	28.35

**Table C.2:** CT sorption study. Flow rates.

time (h)	flow rate (ml/min)
0	31.5
16	35.5
24	36
30	34
48	34
72	32
96	32
120	32
138	25
146.5	33.5
160.75	33
184.25	33
241	33
260	22

## **APPENDIX D**

*Appendix D.*

**Inoculation of KC: biomass (strain KC) data**

**Table D.1:** Inoculation of KC. Biomass liquid samples (cfu/ml) taken during the inoculation event.

time (min)	influent (300)	ports			effluent (3000)	Qh (ml/min)
		312	322	332		
0	8.10E+07				0.00E+00	235
5						280
15		4.00E+07	9.00E+03	0.00E+00		
30	1.03E+08	1.37E+08	1.50E+04	0.00E+00	0.00E+00	
35						270
45		6.40E+07	7.30E+05	1.00E+03		
60	3.60E+07	7.70E+07	6.80E+06	2.00E+03	0.00E+00	285
75		1.60E+08	1.05E+08	1.20E+04		
90	6.70E+07	1.43E+08	1.35E+08	1.20E+05	0.00E+00	277
105		1.83E+09	1.71E+08	3.15E+06		
115						280
120	8.00E+07	1.37E+08	1.50E+08	1.06E+07	8.00E+04	
135		2.41E+08	1.39E+08	1.96E+07		275
150	1.36E+08	1.11E+08	9.50E+07	4.30E+07	6.20E+05	275
165		8.90E+07	8.30E+07	1.09E+08		275
180	1.06E+08	6.60E+07	5.50E+07	1.04E+08	3.90E+06	

**Table D.2:** Inoculation. Biomass liquid-phase samples (log cfu/ml) taken at the end of the inoculation event.

port #	x (m)	y (m)	z (m)	log X
300	0	0.3048	0.3048	8.03
3000	0.6096	0.3048	0.3048	6.59
111	0.1524	0.1524	0.1524	7.63
112	0.1524	0.3048	0.1524	8.15
113	0.1524	0.4572	0.1524	7.99
121	0.3048	0.1524	0.1524	7.37
122	0.3048	0.3048	0.1524	7.56
123	0.3048	0.4572	0.1524	7.41
131	0.4572	0.1524	0.1524	6.37
132	0.4572	0.3048	0.1524	5.38
133	0.4572	0.4572	0.1524	4.3
311	0.1524	0.1524	0.3048	8.18
312	0.1524	0.3048	0.3048	8.43
313	0.1524	0.4572	0.3048	8.05
321	0.3048	0.1524	0.3048	8.25
322	0.3048	0.3048	0.3048	8.35
323	0.3048	0.4572	0.3048	7.98
331	0.4572	0.1524	0.3048	6.37
332	0.4572	0.3048	0.3048	7.88
333	0.4572	0.4572	0.3048	6.84
511	0.1524	0.1524	0.4572	8.4
512	0.1524	0.3048	0.4572	8.43
513	0.1524	0.4572	0.4572	8.33
521	0.3048	0.1524	0.4572	7.83
522	0.3048	0.3048	0.4572	7.91
523	0.3048	0.4572	0.4572	7.89
531	0.4572	0.1524	0.4572	5.88
532	0.4572	0.3048	0.4572	7.14
533	0.4572	0.4572	0.4572	5.85

### Inoculation: bromide (tracer) data

**Table D.3:** Inoculation. Tracer samples taken during the inoculation event (vertical flow stopped). C/Co. See Table D.5 for complete effluent data.

time (min)	influent	312	322	332	effluent	Qh (ml/min)
0	0.98					235
5						280
15		0.94	0.15	0.16		
30	0.90		0.18		0.15	
35						270
45		1.06	0.73	0.19		
60	1.02		1.06	0.20	0.19	285
75		1.06	1.11	0.22		
90	1.06	1.15	0.98	0.67	0.17	277
105		1.07	1.11	1.07		
115						280
120	1.11	0.98	1.02	1.07	0.27	
135		1.02	1.02	0.98		275
150	1.11	1.07	1.02	0.98	0.31	275
165		0.98	0.98	0.94		275
180	0.83	0.86	0.86	0.83	0.37	



**Table D.4:** Inoculation. Tracer samples taken at the end of the inoculation event (vertical flow restarted). C/Co.

port #	x (m)	y (m)	z (m)	C/Co
111	0.1524	0.1524	0.1524	0.94
113	0.1524	0.4572	0.1524	0.90
121	0.3048	0.1524	0.1524	0.90
122	0.3048	0.3048	0.1524	0.94
123	0.3048	0.4572	0.1524	0.90
131	0.4572	0.1524	0.1524	0.64
132	0.4572	0.3048	0.1524	0.79
133	0.4572	0.4572	0.1524	0.36
311	0.1524	0.1524	0.3048	0.90
312	0.1524	0.3048	0.3048	0.94
313	0.1524	0.4572	0.3048	0.90
321	0.3048	0.1524	0.3048	0.94
322	0.3048	0.3048	0.3048	0.90
323	0.3048	0.4572	0.3048	0.90
331	0.4572	0.1524	0.3048	0.79
332	0.4572	0.3048	0.3048	0.86
333	0.4572	0.4572	0.3048	0.86
511	0.1524	0.1524	0.4572	0.83
512	0.1524	0.3048	0.4572	0.86
513	0.1524	0.4572	0.4572	0.90
521	0.3048	0.1524	0.4572	0.94
522	0.3048	0.3048	0.4572	0.90
523	0.3048	0.4572	0.4572	0.86
531	0.4572	0.1524	0.4572	0.86
532	0.4572	0.3048	0.4572	0.90
533	0.4572	0.4572	0.4572	0.67

**Table D.5:** Inoculation. Tracer samples taken at the effluent (port 3000) during the inoculation

time (min)	C/Co (cal3)	time (min)	C/Co (cal3)	time (min)	C/Co (cal3)	time (min)	C/Co (cal3)	time (min)	C/Co (cal3)
0	0.109	36	0.136	74	0.169	112	0.189	150	0.389
2	0.179	38	0.169	76	0.152	114	0.236	152	0.435
4	0.224	40	0.136	78	0.136	116	0.066	154	0.460
6	0.279	42	0.169	80	0.143	118	0.250	156	0.412
8	0.115	44	0.143	82	0.169	120	0.236	158	0.460
10	0.169	46	0.152	84	0.143	122	0.312	160	0.389
12	0.143	48	0.160	86	0.152	124	0.264	162	0.543
14	0.179	50	0.143	88	0.152	126	0.295	164	0.460
16	0.179	52	0.136	90	0.045	128	0.312	166	0.460
18	0.152	54	0.128	92	0.169	130	0.264	168	0.607
20	0.136	56	0.136	94	0.152	132	0.295	170	0.574
22	0.143	58	0.160	96	0.143	134	0.330	172	0.607
24	0.143	60	0.160	98	0.143	136	0.348	174	0.642
26	0.169	62	0.160	100	0.189	138	0.330	176	0.295
28	0.143	64	0.160	102	0.152	140	0.348	178	0.642
30	0.160	66	0.169	104	0.160	142	0.330	180	0.678
32	0.169	68	0.169	106	0.189	144	0.389	182	0.607
34	0.160	70	0.143	108	0.169	146	0.389	184	0.678
		72	0.160	110	0.224	148	0.435		

# Appendix E.

## Initial conditions for modeling one-dimensional columns

**Table E.1:** Initial conditions: column 11.

port	Z (cm)	bromide C/Co	liquid KC (cfu/ml)	solid KC (cfu/g)
111	15.24	0.938592	4.30E+07	8068966
311	30.48	0.899864	1.53E+08	30000000
511	45.72	0.827136	2.70E+08	23103448
911	76.2	0.02	0.1	0.1

**Table E.2:** Initial conditions: column 12.

port	Z (cm)	bromide C/Co	liquid KC (cfu/ml)	solid KC (cfu/g)
112	15.24	0.899864	1.40E+08	30000000
312	30.48	0.938592	2.68E+08	30000000
512	45.72	0.862734	2.67E+08	30000000
912	76.2	0.02	0.1	0.1

**Table E.3:** Initial conditions: column 13.

port	Z (cm)	bromide C/Co	liquid KC (cfu/ml)	solid KC (cfu/g)
113	15.24	0.899864	9.80E+07	30000000
313	30.48	0.899864	1.12E+08	30000000
513	45.72	0.899864	2.16E+08	30000000
913	76.2	0.02	0.1	0.1

**Table E.4:** Initial conditions: column 21.

port	Z (cm)	bromide C/Co	liquid KC (cfu/ml)	solid KC (cfu/g)
121	15.24	0.899864	2.34E+07	8068966
321	30.48	0.938592	1.77E+08	30000000
521	45.72	0.938592	6.70E+07	23103448
721	60.96	0.08	0.1	0.1

**Table E.5:** Initial conditions: column 22.

port	Z (cm)	bromide C/Co	liquid KC (cfu/ml)	solid KC (cfu/g)
122	15.24	0.938592	3.60E+07	12413793
322	30.48	0.899864	2.26E+08	30000000
522	45.72	0.899864	8.10E+07	27931034
722	60.96	0.3	4.35E+06	1500000

**Table E.6:** Initial conditions: column 23.

port	Z (cm)	bromide C/Co	liquid KC (cfu/ml)	solid KC (cfu/g)
123	15.24	0.899864	2.56E+07	8827586
323	30.48	0.899864	9.60E+07	30000000
523	45.72	0.862734	7.70E+07	26551724
723	60.96	0.08	0.1	0.1

**Table E.7:** Initial conditions: column 31.

port	Z (cm)	bromide C/Co	liquid KC (cfu/ml)	solid KC (cfu/g)
131	15.24	0.642357	2.35E+06	810344.8
331	30.48	0.793006	2.35E+06	810344.8
531	45.72	0.862734	7.60E+05	262069
731	60.96	0.05	0.1	0.1

**Table E.8:** Initial conditions: column 32.

port	Z (cm)	bromide C/Co	liquid KC (cfu/ml)	solid KC (cfu/g)
132	15.24	0.793006	2.40E+05	82758.62
332	30.48	0.862734	7.60E+07	26206897
532	45.72	0.899864	1.39E+07	4793103
732	60.96	0.04	0.1	0.1

**Table E.9:** Initial conditions: column 33.

port	Z (cm)	bromide C/Co	liquid KC (cfu/ml)	solid KC (cfu/g)
133	15.24	0.356104	2.00E+04	6896.552
333	30.48	0.862734	6.90E+06	2379310
533	45.72	0.670003	7.00E+05	241379.3
733	60.96	0.06	0.1	0.1

Note that only columns 12, 21 and 33 were modeled using the one-dimensional 6 and 8-equation models.

## Estimation of KC in the solid phase

The following equation has been used to determine the solid-phase KC from the liquid-phase scattered data:

$$\text{liquid-phase breakthrough } (C/C_0) \times \text{saturation in the solid phase } (3 \times 10^7 \text{ cfu/g}) = \text{cfu/g solids}$$

The scattered data was interpolated into the numerical 3D grid by using ordinary kriging statistical methods in GMS. To obtain the distribution in 1D columns, a second-order polyline was added to the scattered data. Finally, cfu/g calculations were converted into ppm in the liquid phase to be used in the model by using the soil bulk density and the matrix porosity.

## **APPENDIX F**

## Appendix F.

### Quickest solution

The general Mathcad code form of the one-dimensional advective-dispersive equation for one variable,  $C$ , with reaction term  $\phi(C)$  is as follows:

$$\frac{\delta c}{\delta t} := D \cdot \frac{\delta^2 c}{\delta x^2} - U \cdot \frac{\delta c}{\delta x} + \phi(c)$$

The Quickest formulation for the dispersion term is expressed as:

$$D \cdot \frac{\delta^2 c_i}{\delta x^2} := \frac{D}{\Delta x^2} \left[ c_{i+1} - 2 \cdot c_i + c_{i-1} - \frac{CO}{2} \cdot (c_{i-1} + c_{i+1} - 2 \cdot c_i) + \frac{CO}{2} \cdot (c_{i-2} + c_i - 2 \cdot c_{i-1}) \right]$$

whereas the advection term can be approximated as:

$$U \cdot \frac{\delta c_i}{\delta x} := \frac{U}{\Delta x} \left[ \frac{1}{2} \cdot (c_{i+1} - c_{i-1}) + \frac{CO}{2} \cdot (-c_{i+1} + 2 \cdot c_i - c_{i-1}) + \frac{q}{6} \cdot (c_{i-2} - 3 \cdot c_{i-1} + 3 \cdot c_i - c_{i+1}) \right]$$

in which  $i$  is the node position, CO the Courant number and  $\alpha$  the dispersion parameter, as defined in the *Numerical Simulation* section. The parameter  $q$  is defined by:

$$q := 1 - CO^2 - 3 \cdot \alpha$$

The Euler approximation for the time derivative is given as:

$$\frac{\partial c_i}{\partial t} = \frac{c_{k+1,i} - c_{k,i}}{\Delta t}$$

in which  $k$  designates the current time,  $t = k \Delta t$ .

Combining all these terms and substituting  $q$ , results in the following Quickest solution:

$$c_{k+1,i} := \frac{CO}{R} \cdot \alpha - \frac{1}{6} + \frac{CO^2}{6} \cdot c_{k,i-2} + \frac{1}{R} \cdot \alpha - 3 \cdot \alpha \cdot CO + CO + \frac{CO^2}{2} - \frac{CO^3}{6} \cdot c_{k,i-1} + \quad$$

$$\frac{1}{R} \cdot R + 3 \cdot \alpha \cdot CO - 2 \cdot \alpha - CO^2 - \frac{CO}{2} + \frac{CO^3}{2} \cdot C_{k,i} + \quad$$

$$\frac{1}{R} \cdot \alpha - CO \cdot \alpha - 2 \cdot \alpha - \frac{CO}{3} + \frac{CO^2}{2} - \frac{CO^3}{6} \cdot C_{k,i+1} + \phi(C)$$

which can be written for each of the seven mass balance equations from the numerical model.

The next pages show the actual formulation used in Mathcad, together with the boundary and initial conditions and all input parameters.





**INITIALIZE VARIABLES:**

(ppb)

$$i := 0 \dots N$$

$$k := 0 \dots k_{\max}$$

**CT:**

$$CT_{0,i} := 40$$

**ACETATE:**

$$AC_{0,i} := 0$$

**NITRATE:**

$$NI_{0,i} := 70000$$

**SORBED CT:**

$$\kappa := 0.96 \quad (\text{day}^{-1})$$

$$f := 0.437$$

$$K_d := 2.6 \cdot 10^{-11} \quad (\text{L}/\mu\text{g})$$

$$SCT_{0,i} := (1 - f) \cdot K_d \cdot CT_{0,i}$$

**TRACER:**

$$Br_{0,i} := 0$$

**NATIVE FLORA:**

$$NFL_{0,i} := \frac{10^5}{5.4 \cdot 10^3}$$

$$NFL_{0,8} = 18.519$$

$$NFS_{0,i} := \frac{3 \cdot 10^6}{54 \cdot 10^8} \cdot 10^6 \cdot \frac{1.6}{\Theta}$$

$$NFS_{0,7} = 2.778 \times 10^3$$

**SLUG INJECTION:**

$$\text{CalcAC} := \left| \begin{array}{l} AC \leftarrow AC \\ \text{for } i \in 0 \dots N \\ \left| \begin{array}{l} AC_{0,i} \leftarrow (1 \cdot 10^{-5} \cdot i^3 - 0.0027 \cdot i^2 + 0.136 \cdot i - 1.13) \cdot 100000 \\ AC_{0,i} \leftarrow 0 \text{ if } AC_{0,i} < 0 \\ AC_{0,i} \text{ otherwise} \end{array} \right. \\ AC \end{array} \right.$$

$$\text{CalcAC} = \begin{array}{|c|c|c|c|c|} \hline & 0 & 1 & 2 & 3 & 4 \\ \hline 0 & 0 & 0 & 0 & 0 & 0 \\ \hline \end{array} \quad (\text{ppb})$$

$$AC := \text{CalcAC}$$

LIQUID-PHASE KC:

$XL_{0,i} := 0$

$CalcXL := \begin{cases} XL \leftarrow XL \\ \text{for } i \in 0..N \\ \left| \begin{array}{l} XL_{0,i} \leftarrow \frac{874.86i^3 - 108156i^2 + 4 \cdot 10^6 \cdot i - 4 \cdot 10^7}{5.4 \cdot 10^3} \text{ if} \\ 0 \text{ otherwise} \\ XL_{0,i} \leftarrow 0 \text{ if } XL_{0,i} < 0 \\ XL_{0,i} \text{ otherwise} \end{array} \right. \\ XL \end{cases}$

$CalcXL = \begin{array}{|c|c|c|c|} \hline & 0 & 1 & 2 \\ \hline 0 & & 0 & 0 \\ \hline \end{array}$   
(ppb)

$XL := CalcXL$

SOLID-PHASE KC:

$XS_{0,i} := 0$

$CalcXS := \begin{cases} XS \leftarrow XS \\ \text{for } i \in 0..N \\ \left| \begin{array}{l} XS_{0,i} \leftarrow \frac{-9709.8i^2 + 599602i - 7 \cdot 10^6}{54 \cdot 10^8} \cdot 10^6 \cdot \frac{1.6}{\ominus} \\ XS_{0,i} \leftarrow 0 \text{ if } XS_{0,i} < 0 \\ XS_{0,i} \text{ otherwise} \\ XS_{0,i} \leftarrow \frac{3 \cdot 10^7}{54 \cdot 10^2} \cdot \frac{1.6}{\ominus} \text{ if } XS_{0,i} > \frac{3 \cdot 10^7}{54 \cdot 10^2} \cdot \frac{1.6}{\ominus} \\ XS_{0,i} \text{ otherwise} \end{array} \right. \\ XS \end{cases}$

$CalcXS = \begin{array}{|c|c|c|c|c|c|} \hline & 0 & -1 & 2 & 3 & 4 \\ \hline 0 & 0 & 0 & 0 & 0 & 0 \\ \hline \end{array}$   
 $XS := CalcXS$   
(ppb)

**FUNCTION:**

```
Calc := CT ← CT
        NI ← NI
        AC ← AC
        XL ← XL
        XS ← XS
        NFL ← NFL
        NFS ← NFS
        SCT ← SCT
        for k ∈ 1 .. kmax
            for i ∈ 2.. N - 1
                CTk,0 ← 40
                NIk,0 ← 70000
                ACk,0 ← 0
                XLk,0 ← 0
                XSk,0 ← 0
                NFLk,0 ←  $\frac{10^5}{5.4 \cdot 10^3}$ 
                NFSk,0 ←  $\frac{3 \cdot 10^6}{54 \cdot 10^8} \cdot 10^6 \cdot \frac{1.6}{\Theta}$ 
                SCTk,0 ← (1 - f) · Kd · CTk,0
                CTk,1 ← 40
```

$NI_{k,1} \leftarrow 70000$	
$AC_{k,1} \leftarrow 0$	
$XL_{k,1} \leftarrow 0$	
$XS_{k,1} \leftarrow 0$	
$NFL_{k,1} \leftarrow \frac{10^5}{5.4 \cdot 10^3}$	
$NFS_{k,1} \leftarrow \frac{3 \cdot 10^6}{54 \cdot 10^8} \cdot 10^6 \cdot \frac{1.6}{\Theta}$	
$SCT_{k,1} \leftarrow (1 - f) \cdot Kd \cdot CT_{k,1}$	
$CT_{k,i} \leftarrow \left[ \frac{CO}{R} \cdot \left( \alpha - \frac{1}{6} + \frac{CO^2}{6} \right) \cdot CT_{k-1,i-2} \right] + \left[ \frac{1}{R} \cdot \left( \alpha - 3 \cdot \alpha \cdot CO + CO + \frac{CO^2}{2} - \frac{CO^3}{6} \right) \cdot CT_{k-1,i-1} \right] + \left[ \frac{1}{R} \cdot \left( R + 3 \cdot \alpha \cdot CO - 2 \cdot \alpha - CO^2 - \frac{CO^3}{6} \right) \right]$	
$CT_{k,i} \leftarrow \begin{cases} 0 & \text{if } CT_{k,i} < 0 \\ CT_{k,i} & \text{otherwise} \end{cases}$	
$NI_{k,i} \leftarrow \left[ CO \cdot \left( \alpha - \frac{1}{6} + \frac{CO^2}{6} \right) \cdot NI_{k-1,i-2} \right] + \left( \alpha - 3 \cdot \alpha \cdot CO + CO + \frac{CO^2}{2} - \frac{CO^3}{6} \right) \cdot NI_{k-1,i-1} + \left[ \left( 1 + 3 \cdot \alpha \cdot CO - 2 \cdot \alpha - CO^2 - \frac{CO^3}{6} \right) \right]$	
$NI_{k,i} \leftarrow \left[ CO \cdot \left( \alpha - \frac{1}{6} + \frac{CO^2}{6} \right) \cdot NI_{k-1,i-2} \right] + \left( \alpha - 3 \cdot \alpha \cdot CO + CO + \frac{CO^2}{2} - \frac{CO^3}{6} \right) \cdot NI_{k-1,i-1} + \left[ \left( 1 + 3 \cdot \alpha \cdot CO - 2 \cdot \alpha - CO^2 - \frac{CO^3}{6} \right) \right]$	
$NI_{k,i} \leftarrow \begin{cases} 0 & \text{if } NI_{k,i} < 0 \\ NI_{k,i} & \text{otherwise} \end{cases}$	
$AC_{k,i} \leftarrow \left[ CO \cdot \left( \alpha - \frac{1}{6} + \frac{CO^2}{6} \right) \cdot AC_{k-1,i-2} \right] + \left( \alpha - 3 \cdot \alpha \cdot CO + CO + \frac{CO^2}{2} - \frac{CO^3}{6} \right) \cdot AC_{k-1,i-1} + \left[ \left( 1 + 3 \cdot \alpha \cdot CO - 2 \cdot \alpha - CO^2 - \frac{CO^3}{6} \right) \right]$	
$AC_{k,i} \leftarrow \begin{cases} 0 & \text{if } AC_{k,i} < 0 \\ AC_{k,i} & \text{otherwise} \end{cases}$	

$$\frac{CO}{2} + \frac{CO^3}{2} - \frac{\text{deg} \cdot \Delta t}{R} \cdot (XL_{k-1,i} + XS_{k-1,i}) \cdot CT_{k-1,i} - \frac{\kappa \cdot \rho}{R \cdot \Theta} \cdot \Delta t \cdot [(1 - \theta) \cdot K_d \cdot CT_{k-1,i} - SCT_{k-1,i}] + \frac{1}{R} \cdot \left( \alpha - CO \cdot \alpha - \frac{1}{3} \cdot CO + \frac{CO^2}{2} - \frac{CO^3}{6} \right) \cdot CT_{k-1,i+1}$$

116

$$\begin{aligned} & - \frac{\mu_{\max} \cdot \Delta t}{Y_{KCNF} \cdot (K_{SKNF} + NI_{k-1,i})} \cdot (XL_{k-1,i} + XS_{k-1,i}) \cdot NI_{k-1,i} \left[ \alpha - CO \cdot \alpha - \frac{1}{3} \cdot CO + \frac{CO^2}{2} - \frac{CO^3}{6} \right] \cdot NI_{k-1,i+1} \text{ if } AC_{k-1,i} \leq 10 \\ & - \frac{\mu_{\max} \cdot \Delta t}{Y_{KCNF} \cdot (K_{SKNF} + NI_{k-1,i})} \cdot (XL_{k-1,i} + XS_{k-1,i}) - \frac{\mu_{\max NF} \cdot \Delta t}{Y_{NFNF} \cdot (K_{SNFNF} + NI_{k-1,i})} \cdot (NFL_{k-1,i} + NFS_{k-1,i}) \cdot NI_{k-1,i} + \left( \alpha - CO \cdot \alpha - \frac{1}{3} \cdot CO + \frac{CO^2}{2} - \frac{CO^3}{6} \right) \cdot NI_{k-1,i} \\ & - \frac{\mu_{\max} \cdot \Delta t}{Y_{KCAC} \cdot (K_{SKCAC} + AC_{k-1,i})} \cdot (XL_{k-1,i} + XS_{k-1,i}) - \frac{\mu_{\max NF} \cdot \Delta t}{Y_{NFAC} \cdot (K_{SNFAC} + AC_{k-1,i})} \cdot (NFL_{k-1,i} + NFS_{k-1,i}) \cdot AC_{k-1,i} + \left( \alpha - CO \cdot \alpha - \frac{1}{3} \cdot CO + \frac{CO^2}{2} - \frac{CO^3}{6} \right) \cdot AC_{k-1,i} \end{aligned}$$

$$\begin{aligned}
XL_{k,i} &\leftarrow \left[ CO \cdot \left( \alpha - \frac{1}{6} + \frac{CU^-}{6} \right) \cdot XL_{k-1,i-2} \right] + \left[ \alpha - 3 \cdot \alpha \cdot CO + CO + \frac{CU^-}{2} - \frac{CO^-}{6} \right] \cdot XL_{k-1,i-1} + \left[ 1 + 3 \cdot \alpha \cdot CO - 2 \cdot \alpha - CO^2 - \frac{CU}{2} + \frac{CO^-}{2} \right] \\
XL_{k,i} &\leftarrow \begin{cases} 0 & \text{if } XL_{k,i} < 0 \\ XL_{k,i} & \text{otherwise} \end{cases} \\
XS_{k,i} &\leftarrow \left[ \left( \mu_{\max} \cdot \frac{AC_{k-1,i}}{K_{SKCAC} + AC_{k-1,i}} \cdot \frac{NI_{k-1,i}}{K_{SKCNI} + NI_{k-1,i}} - b_{KC} - K_{yKC} \right) \cdot \Delta t + 1 \right] \cdot XS_{k-1,i} + K_{CKC} \cdot \Delta t \cdot XL_{k-1,i} \\
XS_{k,i} &\leftarrow \begin{cases} 0 & \text{if } XS_{k,i} < 0 \\ XS_{k,i} & \text{otherwise} \end{cases} \\
NFL_{k,i} &\leftarrow \left[ CO \cdot \left( \alpha - \frac{1}{6} + \frac{CO^2}{6} \right) \cdot NFL_{k-1,i-2} \right] + \left( \alpha - 3 \cdot \alpha \cdot CO + CO + \frac{CO^2}{2} - \frac{CO^3}{6} \right) \cdot NFL_{k-1,i-1} + \left[ 1 + 3 \cdot \alpha \cdot CO - 2 \cdot \alpha - CO^2 - \frac{CO}{2} + \frac{CO^-}{2} \right] \\
NFL_{k,i} &\leftarrow \begin{cases} \frac{10^5}{5.4 \cdot 10^3} & \text{if } AC_{k,i} \leq 10 \\ NFL_{k,i} & \text{otherwise} \end{cases} \\
NFS_{k,i} &\leftarrow \left[ \left( \mu_{\max NF} \cdot \frac{AC_{k-1,i}}{K_{SNFAC} + AC_{k-1,i}} \cdot \frac{NI_{k-1,i}}{K_{SNFNI} + NI_{k-1,i}} - b_{NF} - K_{yNF} \right) \cdot \Delta t + 1 \right] \cdot NFS_{k-1,i} + K_{CNF} \cdot \Delta t \cdot NFL_{k-1,i} \\
NFS_{k,i} &\leftarrow \begin{cases} \frac{3 \cdot 10^6}{54 \cdot 10^8} \cdot 10^6 \cdot \frac{1.6}{\Theta} & \text{if } AC_{k,i} \leq 10 \\ NFS_{k,i} & \text{otherwise} \end{cases} \\
SCT_{k,i} &\leftarrow SCT_{k-1,i} + \Delta t \cdot \kappa \cdot [(1 - \vartheta) \cdot Kd \cdot CT_{k-1,i} - SCT_{k-1,i}] \\
CT_{k,N} &\leftarrow CT_{k,N-1} \\
NI_{k,N} &\leftarrow NI_{k,N-1} \\
AC_{k,N} &\leftarrow AC_{k,N-1} \\
XL_{k,N} &\leftarrow XL_{k,N-1} \\
XS_{k,N} &\leftarrow XS_{k,N-1}
\end{aligned}$$

$$\left( \mu_{\max} \cdot \frac{AC_{k-1,i}}{Ks_{KCAC} + AC_{k-1,i}} \cdot \frac{NI_{k-1,i}}{Ks_{KCNI} + NI_{k-1,i}} - b_{KC} - K_{CKC} \right) \cdot \Delta t \cdot \left[ XL_{k-1,i} + K_{yKC} \cdot \Delta t \cdot XS_{k-1,i} + \left( \alpha - CO \cdot \alpha - \frac{1}{3} \cdot CO + \frac{CO^*}{2} - \frac{CO^*}{6} \right) \cdot XL_{k-1,i+1} \right]$$

$$^3 - + \left( \mu_{\max NF} \cdot \frac{AC_{k-1,i}}{Ks_{NFAC} + AC_{k-1,i}} \cdot \frac{NI_{k-1,i}}{Ks_{NFNI} + NI_{k-1,i}} - b_{NF} - K_{CNF} \right) \cdot \Delta t \cdot \left[ NF_{k-1,i} + \left[ K_{yNF} \cdot \Delta t \cdot NFS_{k-1,i} + \left( \alpha - CO \cdot \alpha - \frac{1}{3} \cdot CO + \frac{CO^2}{2} - \frac{CO^3}{6} \right) \cdot NF_{k-1,i+1} \right] \right]$$



$NFL_{k,N} \leftarrow NFL_{k,N-1}$
$NFS_{k,N} \leftarrow NFS_{k,N-1}$
$SCT_{k,N} \leftarrow SCT_{k,N-1}$
<div> <div>CT</div> <div>NI</div> <div>AC</div> <div>XL</div> <div>XS</div> <div>NFL</div> <div>NFS</div> <div>SCT</div> </div>

	0	1	2	3	4	5	6
0	0	0	0	0	0	0	0
1	0	0	0	0	0	0	0
2	0	0	0	0	0	0	0
3	0	0	0	0	0	0	0
4	0	0	0	0	0	0	0
5	0	0	0	0	0	0	$4.8 \cdot 10^{-4}$
6	0	0	0	0	0	$1.878 \cdot 10^{-5}$	$2.579 \cdot 10^{-3}$
7	0	0	0	0	$7.333 \cdot 10^{-7}$	$1.173 \cdot 10^{-4}$	$8.098 \cdot 10^{-3}$
8	0	0	0	$2.866 \cdot 10^{-8}$	$5.228 \cdot 10^{-6}$	$4.195 \cdot 10^{-4}$	0.019
9	0	0	$1.12 \cdot 10^{-8}$	$2.295 \cdot 10^{-7}$	$2.099 \cdot 10^{-5}$	$1.127 \cdot 10^{-3}$	0.039
10	0	0	$9.954 \cdot 10^{-9}$	$1.022 \cdot 10^{-6}$	$6.248 \cdot 10^{-5}$	$2.525 \cdot 10^{-3}$	0.071

Calc2 =

CT := Calc0

NI := Calc1

AC := Calc2

XL := Calc3

XS := Calc4

NFL := Calc5

NFS := Calc6

SCT := Calc7

## **APPENDIX H**

## Appendix H.

### Ports locations.

**Figure H.1:** reference system used.

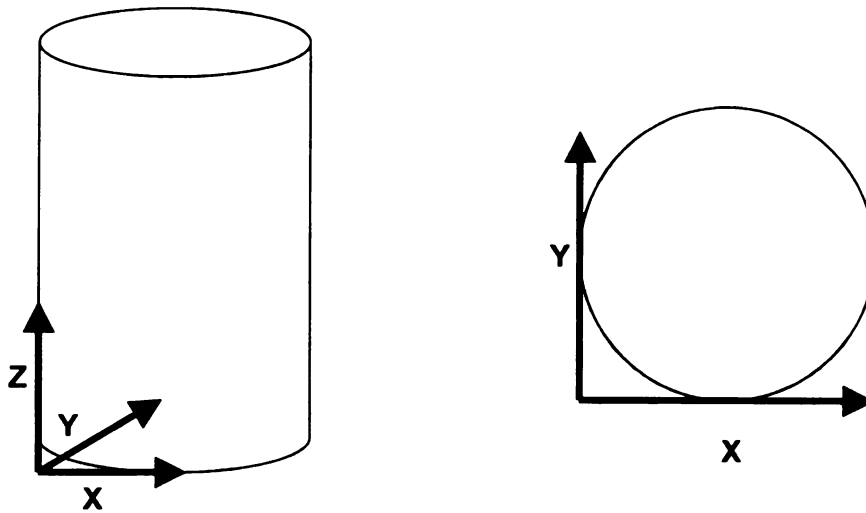


**Table H.1:** bottom influent ports (mm).

port #	X (horizontal)	Y (horizontal)	Z (vertical)
1	304.8	304.8	0
7	482.6	406.4	0
6	304.8	508	0
5	127	406.4	0
4	127	203.2	0
3	304.8	101.6	0
2	482.6	203.2	0

**Table H.2:** top effluent ports (mm).

port #	X (horizontal)	Y (horizontal)	Z (vertical)
1	304.8	304.8	914.4
4	406.4	482.6	914.4
3	508	304.8	914.4
2	406.4	127	914.4
7	203.2	127	914.4
6	101.6	304.8	914.4
5	203.2	482.6	914.4

**Table H.3:** cross-flow influent and effluent points (mm).

port	X (horizontal)	Y (horizontal)	Z (vertical)
in=300	0	304.8	304.8
out=3000	609.6	304.8	304.8

**Table H.4:** sampling ports (mm).

port #	X (horizontal)	Y (horizontal)	Z (vertical)
111	152.4	152.4	152.4
112	152.4	304.8	152.4
113	152.4	457.2	152.4
121	304.8	152.4	152.4
122	304.8	304.8	152.4
123	304.8	457.2	152.4
131	457.2	152.4	152.4
132	457.2	304.8	152.4
133	457.2	457.2	152.4
212	152.4	304.8	228.6
222	304.8	304.8	228.6
232	457.2	304.8	228.6
311	152.4	152.4	304.8
312	152.4	304.8	304.8
313	152.4	457.2	304.8
321	304.8	152.4	304.8
322	304.8	304.8	304.8
323	304.8	457.2	304.8
331	457.2	152.4	304.8
332	457.2	304.8	304.8
333	457.2	457.2	304.8
412	152.4	304.8	381
422	304.8	304.8	381
432	457.2	304.8	381
511	152.4	152.4	457.2
512	152.4	304.8	457.2
513	152.4	457.2	457.2
521	304.8	152.4	457.2
522	304.8	304.8	457.2
523	304.8	457.2	457.2
531	457.2	152.4	457.2
532	457.2	304.8	457.2
533	457.2	457.2	457.2
612	152.4	304.8	533.4
622	304.8	304.8	533.4
632	457.2	304.8	533.4
711	152.4	152.4	609.6
712	152.4	304.8	609.6
713	152.4	457.2	609.6
721	304.8	152.4	609.6

port #	X (horizontal)	Y (horizontal)	Z (vertical)
722	304.8	304.8	609.6
723	304.8	457.2	609.6
731	457.2	152.4	609.6
732	457.2	304.8	609.6
733	457.2	457.2	609.6
812	152.4	304.8	685.8
822	304.8	304.8	685.8
832	457.2	304.8	685.8
911	152.4	152.4	762
912	152.4	304.8	762
913	152.4	457.2	762
921	304.8	152.4	762
922	304.8	304.8	762
923	304.8	457.2	762
931	457.2	152.4	762
932	457.2	304.8	762
933	457.2	457.2	762

## **LIST OF REFERENCES**

## REFERENCES

- Chapra, S.C., and Canale, R.P. *Numerical Methods for Engineers*. McGraw-Hill, Inc., 1988.
- Criddle, C.S.; DeWitt, J.T.; Grbic-Galic, D.; McCarty, P.L. *Transformation of Carbon Tetrachloride by Pseudomonas sp. strain KC under denitrifying conditions*. Appl. Environ. Microbiol., 1990, 56: 3240-3246.
- Dybas, M.J., Hyndman, D.W., Heine, R., Phanikumar, M.S., Tiedje, J., Voice, T., Wallace, R., Wiggert, D.C., Zhao, X., Artuz, R., Criddle, C.S. *Operation and Long-term Performance of a Full-Scale Biocurtain*. Manuscript in preparation, 2000.
- Dybas, M.J.; Barcelona, M.; Bezborodnikov, S.; Davies, S.; Forney, L.; Heuer, H.; Kawka, O.; Mayotte, T.; Sepúlveda-Torres, L.; Smalla, K.; Sneathen, M.; Tiedje, J.; Voice, T.; Wiggert, D.C.; Witt, M.E.; and Criddle, C.S. *Pilot-Scale Evaluation of Bioaugmentation for In-situ Remediation of a Carbon Tetrachloride-Contaminated Aquifer*. Environ. Sci. Technol., 1998, 32 (22): 3598-3611.
- Dybas, M.J.; Tatara, G.; Knoll, W.; Mayotte, T.; Criddle, C.S. *Niche Adjustment for Bioaugmentation with Pseudomonas sp. strain KC* In Bioaugmentation for Site Remediation. Hinchee, R.E., Frederickson, J., Alleman, B.C., Eds. Bioremediation Series. Batelle Press: Columbus, OH, 1995. Vol. 3, pp 77-84.
- Freeze, R.A., and Cherry, J.A. *Groundwater*. Prentice-Hall, Inc. 1979.
- Halliburton NUS Environmental Corporation (1991). *Remedial Investigation and Feasibility Study of Remedial Alternatives, Plume A and Plume F*, Village of Schoolcraft, Kalamazoo County, Michigan.
- Hansen, S.R.; and Hubbel, S.P. *Single-nutrient microbial competition: qualitative agreement between experimental and theoretically forecast outcomes*. Science, 1980, 207: 1491-1493.

- Harvey, R.W. *Parameters Involved in Modeling Movement of Bacteria in Groundwater*. In *Modeling the Environmental Fate of Microorganisms*, American Society for Microbiology, 1991.
- Hyndman, D.W., Dybas, M.J., Forney, L., Heine, R., Mayotte, T., Phanikumar, M.S., Tata, G., Voice, T., Wallace, R., Wiggert, D., Zhao, X., and Criddle, C.S. Hydraulic characterization and design of a full-scale biocurtain. *Groundwater*, 2000, 38:3, 462-474.
- Kelly, K.C. *Numerical Simulation of Bioaugmentation with Uncertainty Analysis: Removal of Carbon Tetrachloride Using Pseudomonas stutzeri strain KC in Porous Media*. Master's Project at MSU. 1995.
- Knoll, W.H. *Factors Influencing the Competitive Advantage of Pseudomonas sp. strain KC for Subsequent Remediation of a Carbon Tetrachloride Impacted Aquifer*. Master Thesis, Michigan State University, 1994.
- Lassey, K.R. *Unidimensional Solute Transport Incorporating Equilibrium and Rate-Limited Isotherms With 1st-Order Loss. 1, Model Conceptualizations and Analytic Solutions*. *Water Resour Res*, 1988, 24(3): 343-350.
- Leonard, B.P. *A Stable Accurate Convective Modeling Procedure Based on Quadratic Upstream Interpolation*. *Computer Methods in Applied Mechanics and Engineering*, 1979, 19: 59-98.
- Lewis, T.A.; and Crawford, R.L. *Physiological Factors Affecting Carbon Tetrachloride Dehalogenation by the Denitrifying Bacterium Pseudomonas sp. strain KC*. *Appl. Environ. Microbiol.*, 1993, 59: 1635-1641.
- Martin, R.E., Bouwer, E.J., Hanna, L.M. *Application of Clean-Bed Filtration Theory to Bacterial Deposition in Porous Media*. *Environ. Sci. Technol.*, 1992, 26(5): 1053-1058.



- Mayotte, T.J.; Dybas, M.J.; and Criddle, C.S. *Bench-Scale Evaluation of Bioaugmentation to Remediate Carbon Tetrachloride-Contaminated Aquifer Materials*. Ground Water, 1996, 34 (2): 358-367.
- Radabaugh, P.D. *Factors Influencing Transport of Pseudomonas stutzeri KC*. Master Thesis, Michigan State University, 1995.
- Rijnaarts, H.H.M., Norde, W., Bouwer, E.J., Lyklema, J., Zehnder, A.J.B. *Bacterial Deposition in Porous Media Related to the Clean Bed Collision Efficiency and to Substratum Blocking by Attached Cells*. Environ. Sci. Technol., 1996, 30(10): 2869-2876.
- Rijnaarts, H.H.M., Norde, W., Bouwer, E.J., Lyklema, J., Zehnder, A.J.B. *Bacterial Deposition in Porous Media: Effects of Cell-Coating, Substratum Hydrophobicity, and electrolyte concentration*. Environ. Sci. Technol., 1996, 30(10): 2877-2883.
- Rittman, B.E.; and McCarty, P.L. Model of steady-state biofilm kinetics. Biotechnology and Bioengineering, 1980, 22: 2343-2357.
- Schwarzenbach, R.P. and Westall, J. Transport of nonpolar organic compounds from surface water to groundwater. Laboratory studies. Environ. Sci. Technol., 1981, 15: 1300-1367.
- Stumm, W.; and Morgan, J.J. *Aquatic Chemistry*, 2<sup>nd</sup> Ed, 1981. John Wiley & Sons, New York, New York.
- Tatara, G.M.; Dybas, M.J.; and Criddle, C.S. *Effects of Medium and Trace Metals on Kinetics of Carbon Tetrachloride Transformation by Pseudomonas sp. strain KC*. Appl. Environ. Microbiol., 1993, 59: 2126-2131.
- Tilman, D. *Tests of Resource Competition Theory Using Four Species of Lake Michigan Algae*. Ecology, 1981, 62(3): 802-815.
- Witt, M.E. *Development of a Laboratory-Scale Model Aquifer System to Monitor a Carbon Tetrachloride Transforming Zone by Pseudomonas sp. strain KC*. Master Thesis, Michigan State University, 1995.

- Witt, M.E. *Transformation of a Carbon Tetrachloride by Mobile and Stationary Phase Bacteria in Porous Media*. Ph.D. Dissertation, Michigan State University, 1998.
- Witt, M.E., Dybas, M.J., Heine, R.L., Nair, S., Criddle, C.S. *Bioaugmentation and Transformation of Carbon Tetrachloride in a Model Aquifer*. Bioremediation 3, Battelle Press, Columbus, 1995, pp 221-227.

MICHIGAN STATE LIBRARIES



3 1293 02208 6783